Stony Brook University

OFFICIAL COPY

Tungstate Sorption Mechanisms on Various Mineral Surfaces:

Systematic Batch Uptake Experiments and Spectroscopic Studies

A Dissertation Presented

by

Hyuck Hur

to

The Graduate School

in Partial Fulfillment of the

Requirements

for the Degree of

Doctor of Philosophy

in

Chemistry

Stony Brook University

August 2014

Stony Brook University

The Graduate School

Hyuck Hur

We, the dissertation committee for the above candidate for the

Doctor of Philosophy degree, hereby recommend

acceptance of this dissertation.

Clare P. Grey – Dissertation Advisor
Professor, Department of Chemistry

Stephen A. Koch - Chairperson of Defense
Professor, Department of Chemistry

Benjamin Hsiao
Professor, Department of Chemistry

Evert J. Elzinga – Outside Member of Defense
Professor, Department of Earth & Environmental Science, Rutgers University

Richard J. Reeder – Dissertation co-Advisor
Professor, Department of Geoscience

This dissertation is accepted by the Graduate School

Charles Taber

Dean of the Graduate School

Abstract of the Dissertation

Tungstate Sorption Mechanisms on Various Mineral Surfaces:

Systematic Batch Uptake Experiments and Spectroscopic Studies

by

Hyuck Hur

Doctor of Philosophy

in

Chemistry

Stony Brook University

2014

The importance of this study is related to releases of tungsten to environment as a result of its widespread used in industrial, civil, and military applications. Recent studies have reported the oxidative dissolution of tungsten metal or alloy under appropriate pH and redox conditions resulting in the formation of tungstate, W(VI), which occurs mainly as oxyanions—some of which have a high solubility in aquatic and soil systems. Therefore, the environmental fate of W ultimately depends on an understanding of tungstate geochemistry.

We will discuss the role of tungstate speciation on its sorption mechanism on environmentally relevant mineral surfaces, including aluminum oxyhydroxide, hydroxyapatite (HAP), and layered double hydroxide (LDH). Tungstate speciation in aqueous systems is strongly related to its mobility, toxicity, and bioavailability. Tungstate speciation in aqueous solution was investigated using reported stability constants of known tungstates, combined with characterization by X-ray absorption spectroscopy (XAS) and electrospray ionization mass spectroscopy (ESI-MS). Batch uptake experiments were carried out to investigate tungstate sorption behavior on boehmite over a range of environmentally relevant conditions such as pH, tungstate concentration, and ionic strength. Tungsten L_1- and L_3-edge XANES was used to distinguish coordination environment around W atoms. The local structure and coordination of tungsten at the surface were determined using tungsten L_3-edge EXAFS, which allowed us to

further characterize the binding mechanisms. Various sorption mechanisms such as the surface polymerization (aluminum oxide), the intercalation reaction (LDH), and coprecipitation (HAP) were suggested depending on the properties of mineral surfaces in this study. This work will provide a foundation for subsequent studies of tungstate sorption on other solids. The findings also have possible implications for tungsten toxicity in natural environments.

Dedicated to my family.

Table of Contents

List of Figures

List of Figures

Acknowledgments

I would like to take this opportunity to express my thanks to those who helped me with various aspects of conducting research and the writing of this thesis. First and foremost, Dr. Richard J. Reeder and Dr. Clare P. Grey, as my advisors, for his and her academic advice and guidance, patience and support throughout the whole research works and the writing of this thesis. His and her insights and words of encouragement have often raised me up, so I renewed my hopes and tided over big adversity for completing my graduate education.

I would like to deeply appreciate to Dr. Stephen A. Koch, Dr. Benjamin Hsiao, Dr. Evert J. Elzinga for their efforts to be my dissertation committee members.

I would like to give a special thanks to my group members in environmental geochemistry lab and all of my friends. Especailly, I owe special thanks to my two best friends in Korea, Gyeongchun Park and Youngboo Park.

Finally, I am forever indebted to my dad, mom, sister's family (Jaewon Shim, Taeseo, Hyuckjun, Jiyul), and my aunt.

Chapter 1. Introduction: Environmental Chemistry of Tungstate

1.1 Overview

The focus of this thesis is the investigation of tungstate sorption mechanisms on various mineral surfaces, including aluminum oxyhydroxide, hydroxyapatite, and layered double hydroxide. The importance of this study is related to releases of tungsten to the environment as a result of its widespread uses in industrial, civil, and military applications. Despite its broad applications and extensive uses, tungsten is one of the least studied transition metals in the environment, partly because it has been considered as being non-toxic in its metal and alloy forms.[1-3] However, recent studies have reported the oxidative dissolution of tungsten metal or alloy under appropriate pH and redox conditions[4] resulting in the formation of tungstate, W(VI), which occurs mainly as oxyanions—some of which have a high solubility in aquatic and soil systems. Therefore, the environmental fate of W ultimately depends on an understanding of tungstate geochemistry.

The toxicity, mobility, and bioavailability of tungstate are dependent on its chemical speciation. Tungstate speciation in solution is somewhat more complicated than other oxyanions owing to its strong tendency to polymerize at low pH conditions. Furthermore, polymerization kinetics can be sluggish, resulting in the appearance of intermediate species in the laboratory time scale, as we demonstrate using electrospray ionization mass spectroscopy (ESI-MS) in Chapter 2.[1, 5] The most important factors influencing tungstate speciation are pH and concentration in solution.

In this thesis, I have focused on the role of tungstate speciation on its sorption mechanisms on environmentally relevant mineral surfaces. The studies are briefly summarized in section 1.6, and the following chapters will describe detailed experimental procedures and results.

1.2 Introduction of tungsten and tungstate

1.2.1 Tungsten

Tungsten is an economically important transition metal with noteworthy chemical and physical properties. It has the highest melting point of all elements, a boiling point of 5660 ℃, high electrical and thermal conductivity, and the lowest vapor pressure and expansion coefficient of all metals.[6] Tungsten belongs to the VIB group along with Cr and Mo, and exists in a variety of oxidation states (-2, -1, 0, +2, +3, +4, +5, +6). In nature, tungsten is found dominantly associated with oxygen. Common forms include the minerals scheelite ($CaWO_4$) and wolframite [$(Fe, Mn)WO_4$].

The unique chemical and physical properties of tungsten are used to advantage in a wide range of applications. The industrial uses of tungsten include construction industries, electrical/electronic applications, heavy metal alloys and super alloys, and wear-resistant mechanical parts and specialized tools. The chemical uses of tungsten vary from catalysts to inorganic pigments. In civil life, it is used in lamp filaments, electrical consumer products, tires, and outdoor activities such as golf, fishing, and hunting ammunition.[2] Recently, tungsten has replaced lead in many military applications because of the adverse effects of lead in environments and related public health concerns.
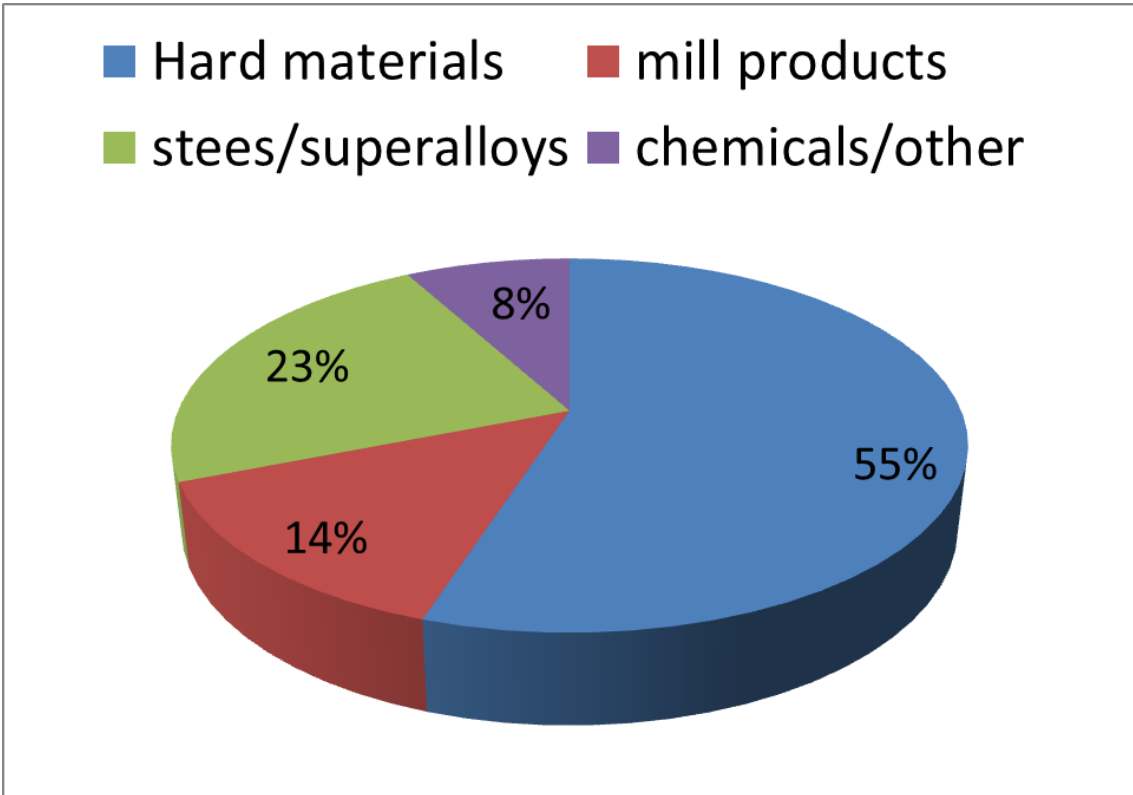
Figure 1. 1. World consumption of tungsten by end-use (2010). Graphic taken from Minor Metals Trade Association (http://www.mmta.co.uk/tungsten-market-overview)

With the increasing uses of tungsten, its toxicological and environmental effects have begun to receive new attention over the last decade. In the U.S. workplace exposure to soluble and insoluble tungsten compounds is regulated[7, 8], although there are no drinking water standards or discharge limits for air, surface water, groundwater or soils. An intensive tungsten eco-toxicological research program was conducted in Russia. As the results of this study, the Russian Federation limits tungsten levels in drinking water (0.05 mg/l) and in fishing lakes and rivers (0.0008 mg/l).[2] Intensive investigations of tungsten, including its fate and transport, as well as toxicological and ecotoxicology studies, have been conducted in connection with the U.S. Army's Green Ammunition Program.[3, 9-14] Biomedical researches have also examined potential applications of tungsten for implants and drugs.[15-17] A possible connection of tungsten to the childhood leukemia cluster in Fallon, NV, has also been studied extensively.[18-22]

Whereas tungsten has long been considered as nontoxic or environmentally inert in its metallic or alloyed forms, recent studies have focused on the toxicological aspects of tungstate.[1-4] Recent studies have also identified the occurrence of monomeric and polymeric tungstate species in soils.[3, 10, 11, 13, 22] For example, Clausen et al. reported monotungstate, polytungstate, and polyoxometallate species in firing range soils.[13] The study using size exclusion chromatography (SEC) Inductively Coupled Plasma Mass Spectrometry (ICP-MS) by Bednar et al. found several tungstate species which showed different mobilities.[11]
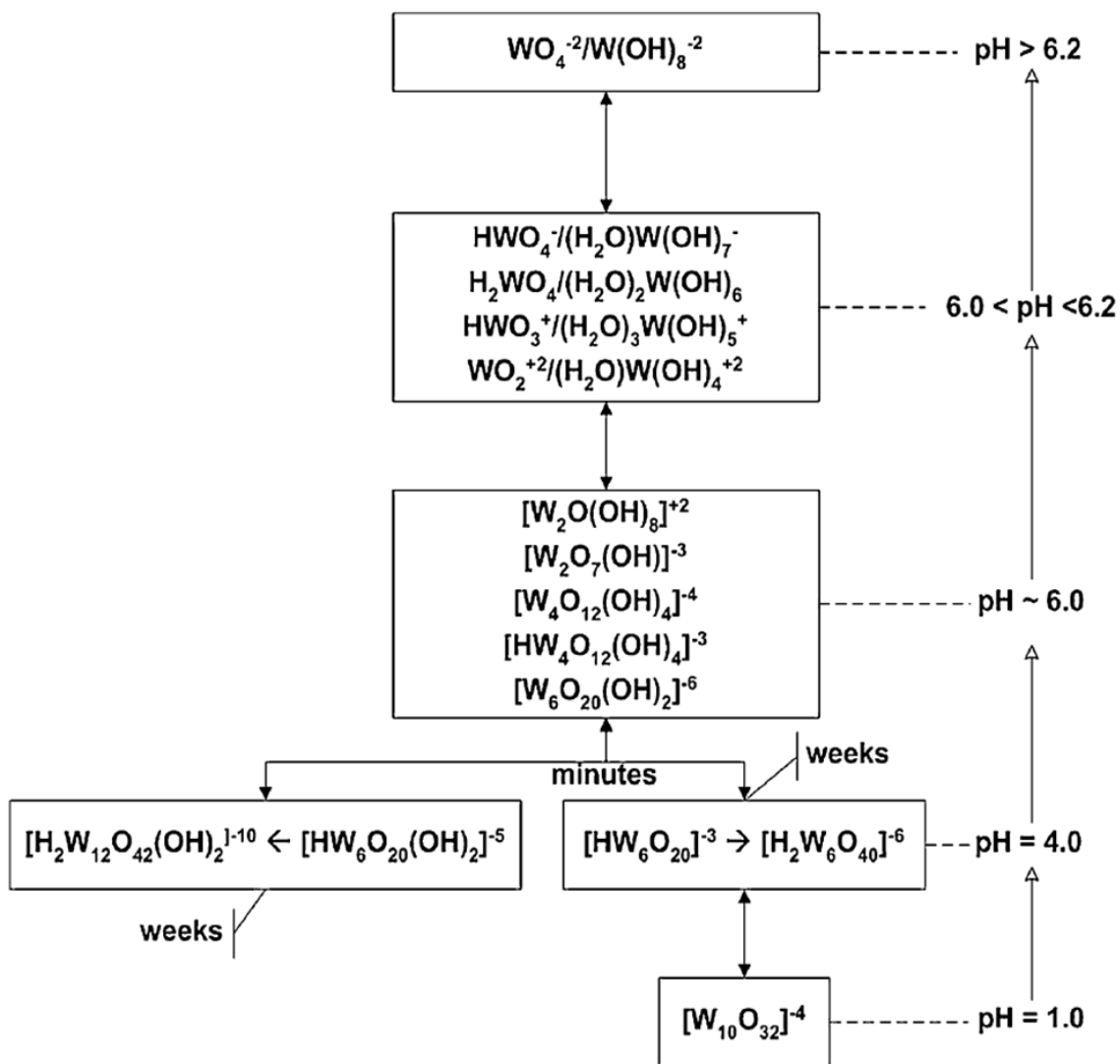
Figure 1. 2. Tungstate speciation in solution as a function of pH.[2] Tungstate favors formation of polymeric tungstate under acidic condition, while monotungstate is dominant above neutral pH. Some polytungstates in the diagram are intermediate species, and the time-scale of conversion kinetics is indicated. Graphic taken from reference 2.

1.2.3 Tungstate species

Chromium and molybdenum share the VIB group with tungsten. In their highest common oxidation state (VI), these elements form oxyanions, including dimeric or polymeric species in solution under appropriate conditions.[23] The two most important oxidation states of Cr in solution are Cr(VI) with mostly tetrahedral coordination and Cr(III) with octahedral coordination.[24] Chromium(VI) forms monomeric and polymeric species such as chromate (CrO_4^{2-}), dichromate ($Cr_2O_7^{2-}$), and less commonly trichromate ($Cr_3O_{10}^{2-}$) and tetrachromate ($Cr_4O_{13}^{2-}$), depending on pH and concentration in the solution. Although tungsten and molybdenum can exist in several oxidation states, hexavalent is the most important oxidation state in solution.[2] In contrast to mineral forms of W or Mo, the solution chemistry of tungsten(VI), tungstate, and molybdenum(VI), molybdate, is complicated. The dominant oxyanion species of tungstate and molybdate at basic pH are monomeric forms with tetrahedral coordination, WO_4^{2-} and MoO_4^{2-}. Tungstate and molybdate can also form polymeric species depending on pH and concentration in solution. The tendency for polymerization in the VIB group increases with increasing atomic number.[23] Tungstate has generally seen less study than molybdate and chromate regarding its aqueous chemistry.

ESI-MS was utilized to determine tungstate species in several tungstate salt solutions.[25] Walanda et al. reported the formation of polytungstates in freshly prepared aqueous tungstate solutions under acidic condition, and observed cation effects on tungstate species.[25] This study suggested a mechanism of tungstate polymerization via formation of open chain structures consisting of octahedral units that are edge shared with terminating tetrahedral units.
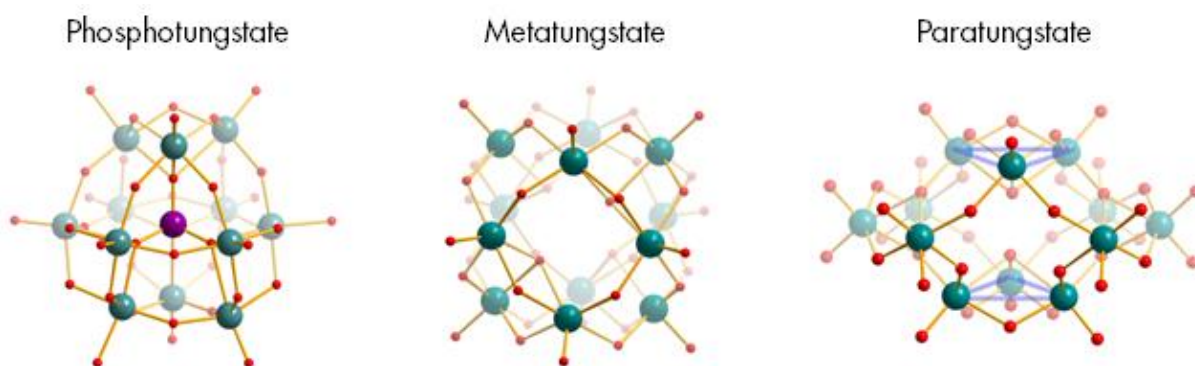
Figure 1. 3. Structures of some common polytungstates. Polytungstates are formed by condensation of simple tungsten anions WO_4^{2-} by protonation and release of water molecules. These polytungstates were included for the tungstate speciation calculation in Chapter 2. Image taken from Jena Bioscience (http://www.jenabioscience.com)

Tungsten can also form a variety of polyoxometallates (POMs) in solution and in soil systems.[29, 30] Tungsten-containing POMs can be considered a subset of polymeric tungstates, and may be difficult to distinguish because of structural similarities. Tungsten POMs consist of WO_6 octahedra and a central MO_4 tetrahedron. Phosphotungstic acid ($H_3PW_{12}O_{40}$), which has the Keggin structure, is the best known example (Figure 1.3).[1] Although previous studies reported their occurrence in environmental samples, few studies have examined their fate in soil or aquatic systems.[31-33] Given the large molecular size of POMs, their mobility is expected to be low and thus would likely be retained in soils. Therefore, tungsten POMs, along with other polymeric species, deserve greater investigation from a geochemical perspective.

1.2.4 Speciation and toxicity, mobility, and bioavailability

Tungstate speciation is relevant for understanding its toxicity, mobility, and bioavailability. The toxicological and biological effects of tungsten have been studied through experiments with monotungstate.[2, 17, 34, 35] Polytungstates have unique physical and chemical properties in comparison to monotungstate, and therefore can be expected to have different biological and toxicological properties. This is supported by recent discoveries indicating that tungsten speciation may be important to ecotoxicology, with polymeric tungstates differing from monotungstate with respect to toxicity.[1]

Different effects of polytungstate on porcine sperm activity compared to monotungstate were observed by Tajima et al.[36] In further studies, polymeric tungstate compounds enhanced antibacterial activity of β-lactam antibiotics on methicillin-resistant *Staphylococcus aureus*, while monotungstate showed no influence.[37-39] This led to further studies showing different effects on genes for tungsten POMs compared with monomeric tungstate.[16,40]

Different levels of toxicity depending on tungstate species were observed in experiments with plants and fish.[1, 40, 41] In toxicological experiments involving fish, sodium metatungstate ($3Na_2WO_4 \cdot 9WO_3$), a representative polytungstate, showed significantly greater toxicity than sodium tungstate, Na_2WO_4.[40, 41] A similar toxicity of phosphotungstic acid, silicotungstate acids, and sodium metatungstate was also observed in studies by Strigul.[1, 40, 41] These polytungstate have unique properties from an environmental toxicology point of view; they behave as oxidation agents and have acidic properties.[42-44]

1.2.5 Previous sorption studies

As mentioned above, the fate of tungstate in aquatic and soil systems is controlled by its speciation. For elements present in trace or minor concentrations, sorption on mineral surfaces represents a primary control on their mobility and bioavailability in natural environments. Relatively few studies have investigated tungstate sorption mechanism on mineral surfaces.[9, 18, 45-47] Laboratory experiments and modeling of tungstate sorption on ferrihydrite were conducted by Gustafsson.[45] The experimental results showed that tungstate strongly adsorbed on the ferrihydrite surface, showing pH dependence typical for anions. The Diffuse Layer Model (DLM) and CD-MUSIC Model (CDM) were used to fit the data with both mono- and polytungstate species. Competition between anions with strong affinity to form inner-sphere complexes is largely dependent on the relative sorption capabilities at the specific conditions. Xu et al. examined the competition of tungstate with other anions, including molybdate, phosphate, sulfate, and silicate, on the goethite surface.[46] This study reported that the affinity of anions for the goethite surface follows the order phosphate $\cong$ tungstate > molybdate > silicate > sulfate. Tungstate sorption on a biosorbent-coated clay was also investigated by Gecol et al.[47] Whereas all of these earlier studies found that tungstate interacts strongly with mineral surfaces, none has

focused on tungstate speciation and its role in sorption behavior. Therefore, the focus of this thesis is to highlight that aspect of tungstate geochemistry in order to gain a better understanding of mechanisms associated with the behavior of tungstate in natural systems.

1.3. Sorbents

1.3.1 Boehmite (γ-AlOOH)

Aluminum-containing minerals are abundant in soils and other environmental systems. Boehmite has been widely studied as a model sorbent, representing solids containing octahedrally coordinated aluminum. Boehmite is isomorphous with lepidocrocite (γ-FeOOH). Boehmite occurs naturally as a common weathering product. Boehmite has a simple and well-characterized structure.[48] Boehmite is also known as an effective sorbent for anionic and cationic contaminants in solution with its typically high surface area and basic point of zero charge (PZC, 8.7).[49-52]

The structure of boehmite is shown in Figure 1.4. It consists of layers of edge-shared aluminum octahedra linked by hydrogen bonding. Nordin et. al distinguished different oxygen sites in the structure (Figure 1.4).[48] η^i sites indicate terminal (nonbridging) sites, with 'i' ligand atoms bonding to the metal, and μ^i sites are ligand atoms that bridge 'i' metals. Boehmite consists of sheets containing 2 octahedral layers, giving the mineral a pronounced (010) cleavage that exposes 2 and 4 coordinated oxo groups (μ_2-OH, μ_4-OH) on basal planes and μ_2-OH, μ_3-O and η_1-OH sites at the sheet steps and edges.[48]
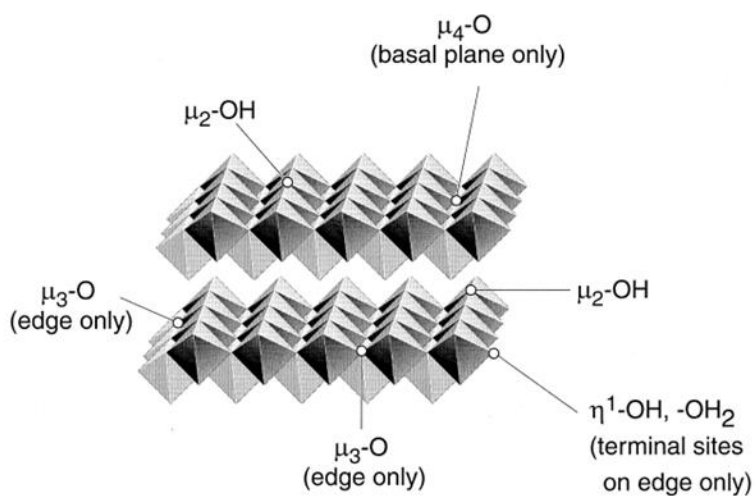
Figure 1. 4. Idealized AlO_6 polyhedral model for boehmite. Different oxygen sites are labeled with η and μ for terminal and bridging oxygen atoms, respectively.[48] Graphic taken from reference 48.

1.3.2 Layered double hydroxide (LDH)

Layered double hydroxides have been investigated for many years as possible host materials for anion exchange reactions. In this role they have been used extensively as ion-exchange materials, catalysts, and sorbents. The structure of LDHs (Figure 1.5) consists of layers of positively charged brucite-like sheets, where the positive charge is balanced by intercalation of anions in the hydrated interlayer regions. LDHs have relatively weak interlayer bonding and, as a consequence, exhibit excellent ability to capture various anions. The most interesting properties of LDHs include large surface area, high anion exchange capacity, and good thermal stability.[53]

The structure of LDHs can be described as a layered hydroxide (e.g. brucite, $Mg(OH)_2$), where a fraction of the divalent cations coordinated octahedrally by hydroxyl groups have been isomorphously replaced by trivalent cations, giving positively charged sheets.[54] The $^{2+}$ and M^{3+} octahedra share edges to form infinite sheets. These sheets are stacked on top of each other and are held together by hydrogen bonding. The general formula of an LDH is $[M_{1-x}^{2+}M_x^{3+}(OH)_2]^{x+}(A^{n-})_{x/n} \cdot mH_2O$, where M^{2+} and M^{3+} are divalent and trivalent cations, respectively; the value of x is equal to the molar ratio of $M^{3+}/(M^{2+}+M^{3+})$, where the interlayer anion has valence n. The identities of M^{2+}, M^{3+}, x and A^{n-} may vary over a wide range, thus giving rise to a large class of isostructural materials with varied physiochemical properties.[55, 56]

The intercalation chemistry of LDH hosts is very extensive. A huge variety of anions can be incorporated into the interlayer region of these hosts.[53, 56] The schematic diagram of the intercalation reaction is shown in Figure 1.5
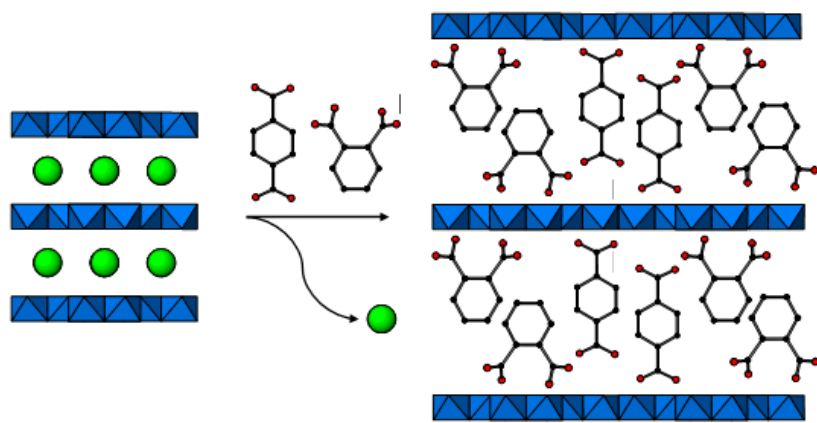
Figure 1. 5. General structure of layered double hydroxide and schematic showing the intercalation of 1,2-benzenedicarboxylate and 1,4- benzenedicarboxylate. Graphic taken from Inorganic biomaterials chemistry at the UCL School of Pharmacy (http://www.garethrwilliams.org.uk/research.htm)

1.3.3 Hydroxylapatite, $Ca_5(PO_4)_3(OH)$

Apatite is the most abundant naturally occurring phosphate mineral on Earth. Consequently, it is the major source of phosphorous, both as an ore and as the base of the global phosphorous cycle. The structure and chemistry of apatite allow for numerous substitutions, including metal cations (K, Na, Mn, Ni, Pb, Cu, REEs) that replace Ca in the structure, and anionic complexes (AsO_4^{3-}, SO_4^{2-}, CO_3^{2-}, SiO_4^{4-}) that substitute for PO_4^{3-}.[57-63] These substitutions are usually in trace concentrations, but large concentrations ard even complete solid solutions exist for certain substituents. Moreover, apatite is commonly found in low temperature sedimentary environments and commonly precipitate form hydrothermal solution.[57, 64] Because of its high affinity for many trace metals, the presence of apatite in environments can strongly influence the fate of trace elements.

Substitutions can occur in HAP for the calcium ions, the phosphate groups, or the hydroxyl groups in the channel. It is assumed that oxyanions substitute into phosphate or channel hydroxyl sites, and cations replace Ca sites. One of the main complications in determining the location of cationic substitutions based only on experimental data is that the calcium ions in HAP occur in two distinct sites, Ca1 and Ca2.
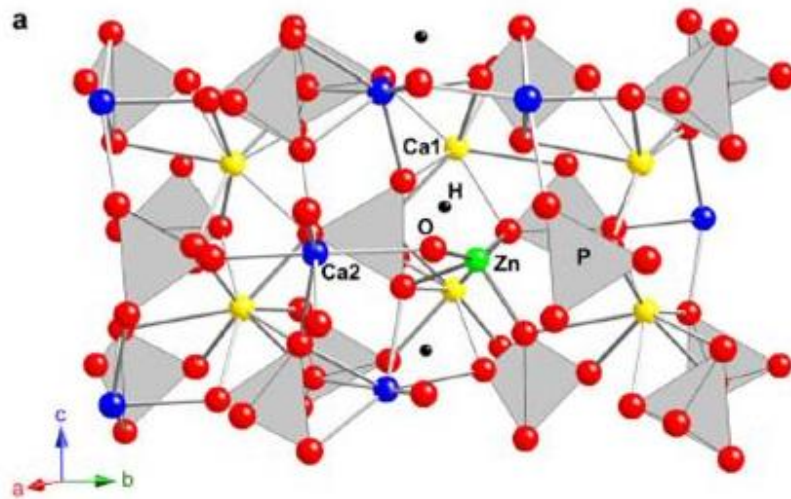
Figure 1. 6. The structure of hydroxylapatite. Graphic taken from the website (http://electronicstructure.wikidot.com/cation-substitutions-in-hydroxyapatite)

1.4 X-ray absorption spectroscopy

1.4.1 EXAFS Overview

X-ray absorption spectroscopy (XAS) is a spectroscopic technique that used provides information on the local structure of an element in a sample. XAS has been widely applied in different scientific fields, including molecular and condensed matter physics, material science, chemistry, biology, mineralogy, and soil science since its modern development in the early 1970s.[65] The experiment is usually performed at synchrotron radiation sources, which provide intense and tunable X-ray beams. XAS spectra can be collected in the gas-phase, solution, or solids. Moreover, little or no sample pretreatment is typically required, making it ideally suited for complex systems. The structural information obtained from XAS is useful for identifying the chemical speciation of an element, including its oxidation state, coordination geometry, and neighboring ligands.

X-ray absorption spectroscopy is the measurement of absorption changes associated with transitions from core electronic states of the element to the excited electronic states and the continuum; the former is known as X-ray near-edge structure (XANES), and the latter as extended X-ray absorption fine structure (EXAFS), which studies the fine structure in the absorption at energies greater than the threshold for electron release. These two methods give complementary structural information, the XANES spectra are more sensitive to the oxidation states and symmetry of the element, and the EXAFS can be useful to determine numbers, types, and distances of near-neighbor atoms.[66] [67]

1.4.2 X-ray absorption coefficient (µ)

The absorption of X-rays by a material can be given by the percentage decrease in the incident X-ray intensity (I_0) or by the energy-dependent absorption length of the material through the exponential factor, µx:

$$I = I_0 e^{-\mu x}$$

The absorption coefficient (µ) varies according to individual elements. Elements such as Pb have greater X-ray absorption coefficients than lighter elements, such as O.

The X-ray absorption coefficient (µ) is a function of the incident X-ray energy:

$$\mu x = \ln(\frac{I_0}{I_t})$$

The probability for absorption increases sharply when the incident X-ray energy equals the energy required to excite an electron to an unoccupied electron orbital. These steps in the absorption coefficient are termed absorption edges.

1.4.3 Absorption edge

The absorption edges are the specific energies where the absorption coefficient suddenly increases. Each element has a specific set of absorption edges at the binding energies of its electrons. Therefore, XAS is an element specific technique. Figure 1.7 is an example of the absorption edges of Pb. The edges are named according to the principal quantum number of the electron that is excited. The energy of a specific edge increases as the atomic number of the element increases. Electrons in the K-shell show greater binding energy than those in L and M shells because the K-shell is closer to the atom's nucleus.
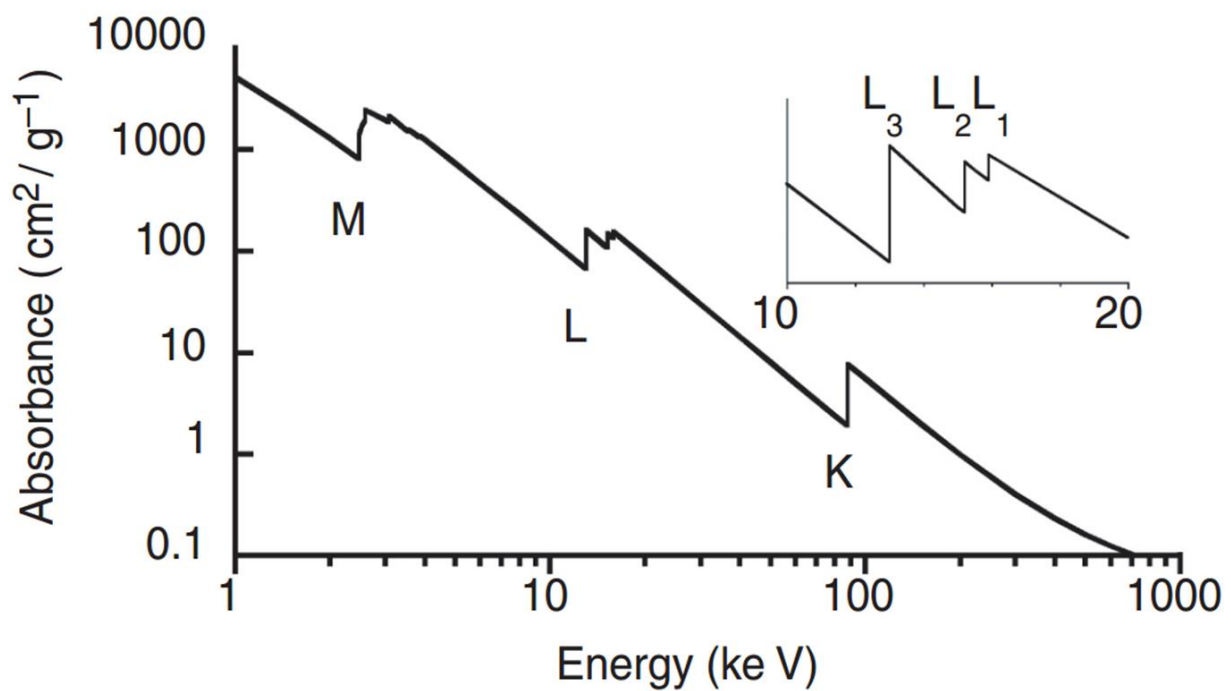
Figure 1. 7. X-ray absorption edges of Pb. Three major transition are seen (K, L, and M edges)[68] Graphic taken form reference 70 .

1.4.4 X-ray absorption near-edge structure (XANES)

XANES is the part of the absorption spectrum near an absorption edge, ranging from approximately -50 to +200 eV relative to the edge energy (Figure 1.8). XANES provides detailed information about the average oxidation state and coordination geometry of the atoms of the given element. The shape of the absorption edge is related to the density of states available for the excitation of the photoelectron. Therefore, the coordination geometry and the oxidation state of the atom affect the XANES part of the spectrum (Figure 1.9).

In this study, W L_1- and L_3-edge XANES were used to provide information on the local symmetry and coordination of the tungstate sorbed on various surfaces. All XANES spectra of the model compounds are given in the Appendix. The local symmetry of W is determined by the area of pre-edge peak of the W L_1-edge XANES, which is due to a $2S \rightarrow 5d$ transition.[69] This transition is dipole-forbidden for regular octahedral symmetry. However, it is partially allowed for a distorted octahedral structure, which gives rise to the absence of an inversion symmetry because the p orbitals are mixed with 5d orbitals. Therefore, tungsten tetrahedra exhibit a large pre-edge area in W L_1-edge XANES. For the L_3-edge, the white line feature in transition metals is attributed to electronic transitions from the $2p_{3/2}$ orbital to vacant s and d orbitals. Teo and Lee have reported that mainly the p-d transition contributes to the white line intensity.[70] Therefore, the L_3-edge X-ray absorption white line reflects the electronic states of the vacant d orbitals of the atom. In the case of W L_3-edge X-ray absorption, the prominent peak in the white line is caused by the $2p \rightarrow 5d$ transition. The splitting of the white lines depends on the symmetry of the W unit because the splitting corresponds to ligand field splitting of the d orbitals.[71-74] Therefore, W L_3-edge XANES provides direct structural information for W units via splitting of the white line. In this study, the combination of the area of the pre-edge peak of W L_1-edge

XANES spectra and the energy separation between the peaks in the W L_3-edge white line were used to obtain more reliable information on the structure of the W species.
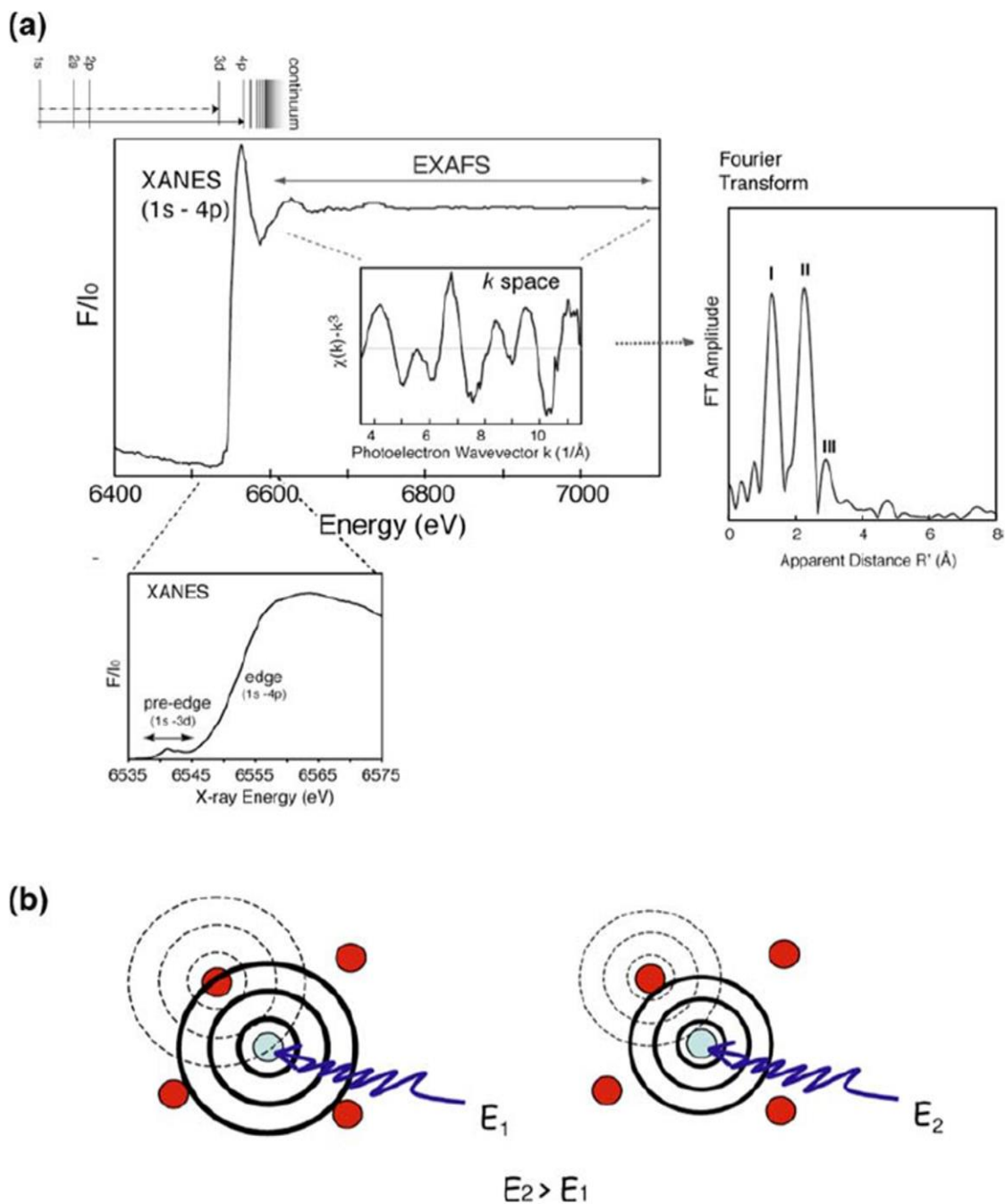
Figure 1. 8. a, Mn K-edge XANES and EXAFS spectra. The energy levels are indicated at the top of the panel. The expanded views show the Mn K-edge XANES and the k-space EXAFS spectrum. The Fourier transform of the k-space EXAFS data is shown on the right. B. Schematic views of the outgoing and backscattered photoelectron waves at bottom illustrate the concept of interference in EXAFS. (Left: constructive interference; right: destructive interference) Graphic taken from reference 11.
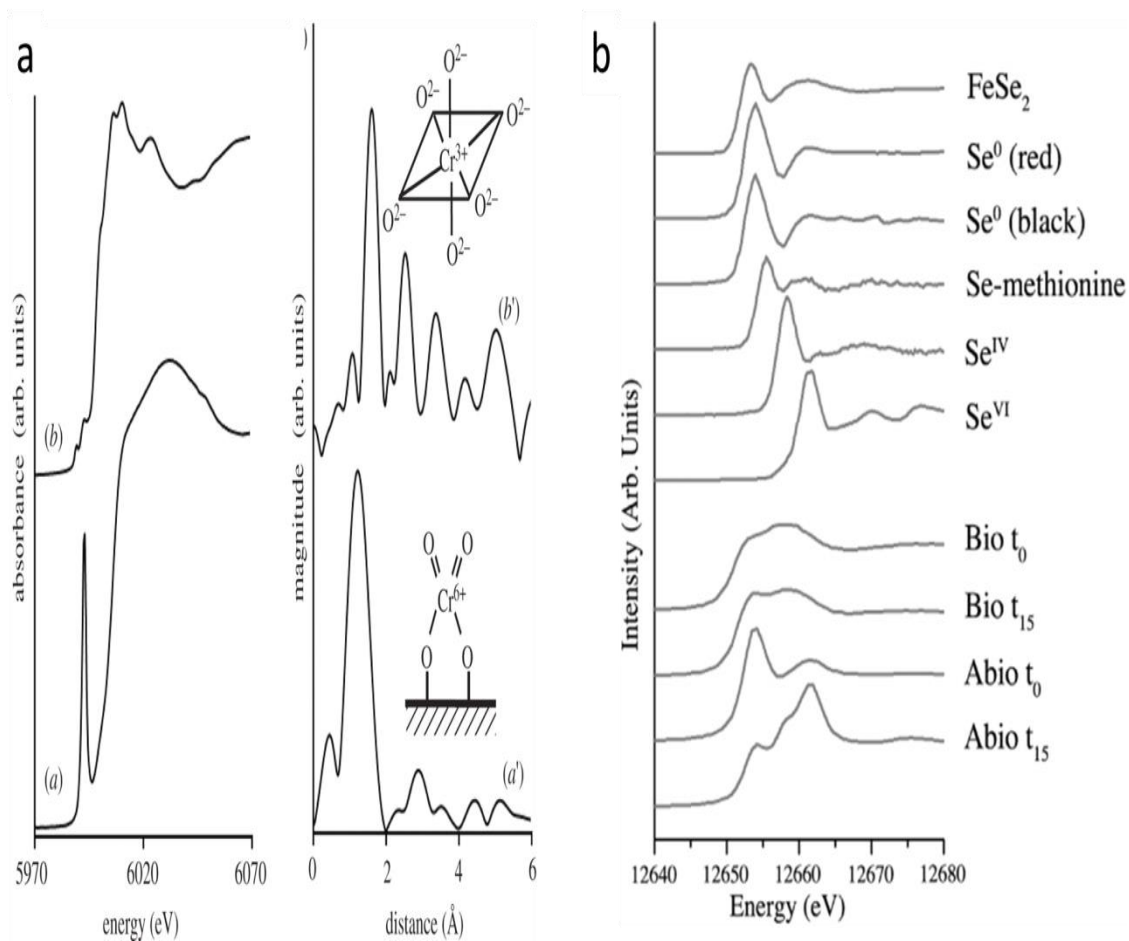
Figure 1. 9. Examples of XANES spectra. a, Cr K-edge XANES spectra for different coordination environments.[75] Tetrahedrally coordinated Cr(VI) shows a strong pre-edge feature, while small steps appear in the pre-edge region for Cr(III) octahedra. b, Se K-edge XANES spectra for different oxidation states.[76] The different oxidation states of sulfur show different absorption energies. Graphics taken from references 12(a) and 13(b).

1.4.5 Extended X-ray absorption fine structure (EXAFS)

EXAFS is the oscillatory part of the absorption coefficient above the absorption edge extending to approximately 1000 eV or higher (Figure 1.8). The EXAFS region is used to determine local molecular bonding environments of the specific absorber element. The EXAFS spectrum contains information on the types and numbers of atoms in coordination with absorber atoms, their interatomic distance, and the degree of local bonding disorder.

At energies somewhat greater than the lowest unoccupied molecular orbital (LUMO) level, the absorption of an X-ray provides sufficient energy to cause the absorbing atom to release the electron. Any excess energy is carried off as translational kinetic energy, which is alternatively reflected in the wavelength associated with the electron treated as a wave phenomenon. The kinetic energy of the photoelectron is equal to the difference between the incident X-ray energy (E) and the binding energy of the photoelectron (E_0):

$$KE = E - E_0$$

The wave nature of the departing electron results in interference owing to scattering by nearby atoms. Thus, the EXAFS oscillations result from the interference between the outgoing photoelectron wave and components of backscattered waves from neighboring atoms in the. The relative phase is determined by the photoelectron wavelength and the interatomic distances between the absorber and scattering atoms (Figure 1.8 b). Each atom at the same radial distance from the absorber contributes to the same component of the EXAFS signal (Figure 1.10). This group of atoms at a particular radial distance is called a shell. The number of atoms in the shell is the coordination number (CN).

The EXAFS equation can be expressed as follows[77, 78]:

$$\chi_i(k) \equiv \frac{\left(N_i S_0^2\right) F_{\text{eff}_i}(k)}{kR_i^2} \sin\left[2kR_i + \varphi_i(k)\right] e^{-2\sigma_i^2 k^2} e^{\frac{-2R_i}{\lambda(k)}}$$

The terms $F_{\text{eff}i}(k)$, $\psi i(k)$, and $\lambda(k)$ are the effective scattering amplitude of the photoelectron, the phase shift of the photoelectron, and the mean free path of the photoelectron, respectively. All of those terms can be calculated using the ab initio computer program FEFF.[79] The R_i distance is one-half the path length of the photoelectron. The value of R_{oi} is one-half the path length used in the theoretical calculation which can be modified by ΔR_i.
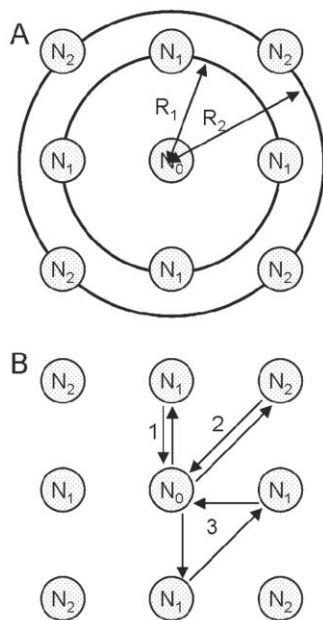
Figure 1. 10. Schematic of the absorber atom (N_0) surrounded by two shells of atoms, N_1 at distance R_1 and N_2 at distance R_2. Single (1) and multiple (2, 3) backscattering paths are depicted in b. Graphic taken from reference 2.

1.4.6 Tungstate coordination geometries and relevant model compounds for X-ray absorption spectroscopy

Reference compounds were chosen to represent a range of W(VI) coordination environments, including isolated tetrahedra and octahedral, and various polymeric forms (Figure 1.11). The compounds $Na_2WO_4 \cdot 2H_2O$ and $CaWO_4$ contain exclusively isolated tungstate tetrahedra, whereas Ba_2NiWO_6 contains exclusively isolated tungstate octahedra (O_h symmetry). Polymeric tungstate reference compounds include phosphotungstic acid ($H_3PW_{12}O_{40}$), sodium metatungstate ($Na_6W_{12}O_{40} \cdot xH_2O$), sodium ditungstate ($Na_2W_2O_7$), and tetrabutyl-ammonium hexatungstate (TBA-W_6O_{19}). TBA-W_6O_{19} contains isolated W_6O_{19} units in which six distorted tungstate octahedra share edges. Tungsten occurs as distorted octahedra in WO_3, sharing all corners in a perovskite-like structure. $Na_2W_2O_7$ contains both tetrahedral and octahedral tungsten in a 1:1 ratio. Phosphotungstic acid has a Keggin-type structure with tungstate octahedra around a tetrahedral phosphate center.
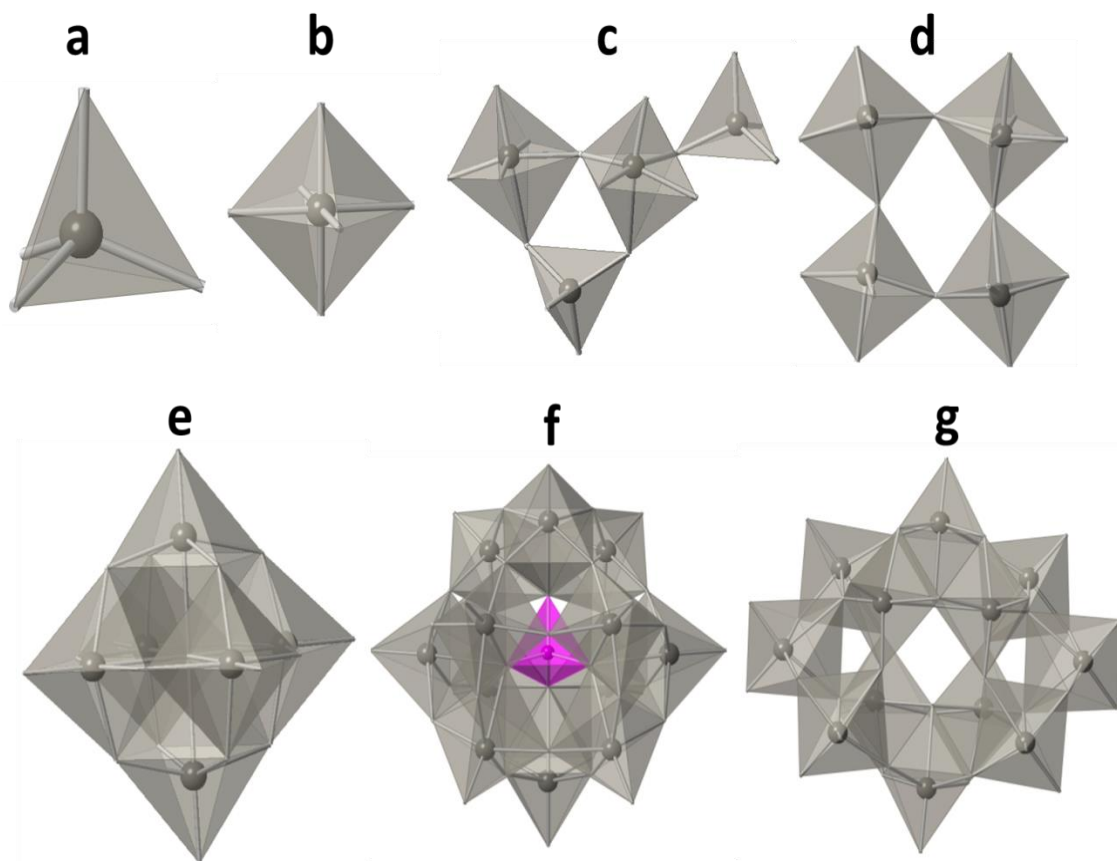
Figure 1. 11.. Structural representations of selected tungstate model compounds with different coordination environments. a) $Na_2WO_4 \cdot 2H_2O$ (tetrahedral), b) Ba_2NiWO_6 (isolated and perfect octahedral), c) $Na_2W_2O_7$ (tetrahedral and octahedral), d) WO_3 (distorted octahedral, only corner sharing), e) $TBA-W_6O_{19}$ (distorted octahedral, only edge sharing), f) phosphotungstic acid (distorted octahedral, Keggin type), g) sodium metatungstate (distorted octahedral).

1.5 Outline of the thesis

Chapter 2 addresses tungstate sorption on the aluminum oxyhydrixde mineral boehmite. We first consider tungstate speciation in aqueous solution using reported stability constants of known tungstate complexes. Batch uptake experiments were carried out to investigate tungstate sorption behavior on boehmite over a range of environmentally relevant conditions. XAS analysis shows that polymerization of tungstate appears to be favored during sorption onto boehmite. At pH 8, where monotungstate is the dominant solution species, polymerization on the surface is accompanied by a change in coordination from tetrahedral (in solution) to octahedral in the surface complex. This study suggests that sorption onto boehmite is an effective means for environmental remediation of dissolved tungstate.

In chapter 3, we determined the effect of Co(II) on tungstate sorption on the boehmite surface. This behavior was investigated over a range of Co(II) and tungstate concentrations at constant pH 7.5. In this study, we focused on high cobalt coverage, which results in formation of CoAl LDH on the boehmite surface. Sorption studies showed that enhanced tungstate uptake is strongly related to the CoAl LDH formation on the boehmite surface. XAS was utilized to investigate tungstate and cobalt in the surface complexes. This study showed that the mobility of tungstate may be effectively limited by the presence of Co(II) on the boehmite surface at neutral and basic conditions.

Chapter 4 demonstrates the possible application of CoAl LDH for tungstate removal from aqueous media at pH8, where tungstate is typically soluble and mobile. Batch reaction experiments with CoAl LDH were conducted as a function of tungstate concentration. Anion exchange resulting in layer expansion was studied using X-ray diffraction. The large sorption

capacity of CoAl LDH for tungstate is expected to effectively limit tungstate in aqueous systems via the anion exchange mechanism. Tungstate speciation was characterized using XAS. This study revealed CoAl LDH is an effective sorbent for tungstate removal from aqueous media. However, further studies of competitive reactions with other anions are needed to examine the prospective application of LDH for tungstate removal from aqueous systems.

The mechanism of tungstate incorporation into hydroxyapatite (HAP) was investigated in Chapter 5. HAP is well known for its structural flexibility, resulting in the incorporation of various anions in the structure. The incorporation of tungstate into HAP may be an alternative way for the long-term immobilization in natural environments. The structure and mode of tungstate incorporation into HAP are important for determining the solubility and long-term stability of tungstate-coprecipitated phases and therefore the potential remobilization of the contaminant. The local structure of tungstate in HAP was investigated using XAS, and the results suggest tungstate replaced phosphate by forming defect sites. In parallel experiments, tungstate sorption reactions were perfromed as a function of tungstate concentration and pH. Although we provide some constraints on the structure of surface complexes, further studies are needed to distinguish the sorption mechanism and the surface complex of tungstate on the HAP structure.

References

1. Strigul, N., Does speciation matter for tungsten ecotoxicology? *Ecotox Environ Safe* **2010,** *73*, (6), 1099-1113.
2. Koutsospyros, A.; Braida, W.; Christodoulatos, C.; Dermatas, D.; Strigul, N., A review of tungsten: From environmental obscurity to scrutiny. *J Hazard Mater* **2006,** *136*, (1), 1-19.
3. Strigul, N.; Koutsospyros, A.; Arienti, P.; Christodoulatos, C.; Dermatas, D.; Braida, W., Effects of tungsten on environmental systems. *Chemosphere* **2005,** *61*, (2), 248-258.
4. Osseoasare, K., Solution Chemistry of Tungsten Leaching Systems. *Metall Trans B* **1982,** *13*, (4), 555-564.
5. Smith, B. J.; Patrick, V. A., Quantitative determination of sodium metatungstate speciation by W-183 NMR spectroscopy. *Aust J Chem* **2000,** *53*, (11-12), 965-970.
6. Rollinson, C. L., *The chemistry of chromium, molybdenum and tungsten*. Pergamon Press: 1975; Vol. 21.
7. NIOSH, Criteria for a Recoommended Standard: Occupational Exposure to Tungsten and Cemented Tungsten, Carbide. **1997,** *Publication No. 77-127*.
8. ACGIH, Tungsten and Compounds: TLV Chemical, Substances. *Documentation* **2001,** *7th edition*.
9. Dermatas, D.; Braida, W.; Christodoulatos, C.; Strigul, N.; Panikov, N.; Los, M.; Larson, S., Solubility, sorption, and soil respiration effects of tungsten and tungsten alloys. *Environ Forensics* **2004,** *5*, (1), 5-13.
10. Bednar, A. J.; Boyd, R. E.; Jones, W. T.; McGrath, C. J.; Johnson, D. R.; Chappell, M. A.; Ringelberg, D. B., Investigations of tungsten mobility in soil using column tests. *Chemosphere* **2009,** *75*, (8), 1049-1056.
11. Bednar, A.; Kirgan, R.; Johnson, D.; Russell, A.; Hayes, C.; McGrath, C., Polytungstate analysis by SEC-ICP-MS and direct-infusion ESI-MS. *Land Contamination & Reclamation* **2009,** *17*, (1), 129-137.
12. Butler, A.; Medina, V.; Larson, S.; Nestler, C., Uptake of lead and tungsten in Cyperus esculentus in a small-arms range simulation. *Land Contamination & Reclamation* **2009,** *17*, (1), 153-159.
13. Clausen, J. L.; Korte, N., Environmental fate of tungsten from military use. *Sci Total Environ* **2009,** *407*, (8), 2887-2893.
14. Johnson, D.; Inouye, L.; Bednar, A.; Clarke, J.; Winfield, L.; Boyd, R.; Ang, C.; Goss, J., Tungsten bioavailability and toxicity in sunflowers (Helianthus annuus L.). *Land Contamination & Reclamation* **2009,** *17*, (1), 141-151.
15. Tajima, Y., Lacunary-substituted undecatungstosilicates sensitize methicillin-resistant Staphylococcus aureus to beta-lactams. *Biol Pharm Bull* **2001,** *24*, (9), 1079-1084.
16. TAJIMA, Y., Tungstophosphate induced thromboembolic complications in vivo. *Biomedical research* **2003,** *24*, (1), 39-49.
17. Domingo, J. L., Vanadium and tungsten derivatives as antidiabetic agents - A review of their toxic effects. *Biol Trace Elem Res* **2002,** *88*, (2), 97-112.
18. Seiler, R. L.; Stollenwerk, K. G.; Garbarino, J. R., Factors controlling tungsten concentrations in ground water, Carson Desert, Nevada. *Appl Geochem* **2005,** *20*, (2), 423-441.

19. Sheppard, P. R.; Ridenour, G.; Speakman, R. J.; Witten, M. L., Elevated tungsten and cobalt in airborne particulates in Fallon, Nevada: Possible implications for the childhood leukemia cluster. *Appl Geochem* **2006,** *21*, (1), 152-165.

20. Sheppard, P. R.; Speakman, R. J.; Ridenour, G.; Witten, M. L., Temporal variability of tungsten and cobalt in Fallon, Nevada. *Environ Health Persp* **2007,** *115*, (5), 715-719.

21. Sheppard, Temporal Variability of Tungsten and Cobalt in Fallon, Nevada (vol 115, pg 715, 2007). *Environ Health Persp* **2012,** *120*, (2), A57-A57.

22. Pardus, M. J.; Sueker, J. K.; Gass, T. E., Occurrence and geochemistry of tungsten in the Carson River Basin, Nevada, U.S. *Abstr Pap Am Chem S* **2005,** *230*, U1730-U1731.

23. Fierro, J. L. G., *Metal Oxides: chemistry and applications*. CRC press: 2005.

24. Weckhuysen, B. M.; Wachs, I. E.; Schoonheydt, R. A., Surface chemistry and spectroscopy of chromium in inorganic oxides. *Chem Rev* **1996,** *96*, (8), 3327-3349.

25. Walanda, D. K.; Burns, R. C.; Lawrance, G. A.; von Nagy-Felsobuki, E. I., Electrospray mass spectrometry of aqueous solutions of isopolyoxotungstates. *J Clust Sci* **2000,** *11*, (1), 5-28.

26. Cruywagen, J. J.; Vandermerwe, I. F. J., Tungsten(Vi) Equilibria - a Potentiometric and Calorimetric Investigation. *J Chem Soc Dalton* **1987**, (7), 1701-1705.

27. Aveston, J., Hydrolysis of Tungsten(6) - Ultracentrifugation Acidity Mearurements + Raman Spectra of Polytungstates. *Inorg Chem* **1964,** *3*, (7), 981-&.

28. Hastings, J. J.; Howarth, O. W., A W-183, H-1 and O-17 Nuclear-Magnetic-Resonance Study of Aqueous Isopolytungstates. *J Chem Soc Dalton* **1992**, (2), 209-215.

29. Himeno, S.; Takamoto, M.; Ueda, T., Formation of alpha- and beta-Keggin-type [PW12O40](3-) complexes in aqueous media. *B Chem Soc Jpn* **2005,** *78*, (8), 1463-1468.

30. Chen, Y. G.; Gong, J.; Qu, L. Y., Tungsten-183 nuclear magnetic resonance spectroscopy in the study of polyoxometalates. *Coordin Chem Rev* **2004,** *248*, (1-2), 245-260.

31. Furrer, G.; Phillips, B. L.; Ulrich, K. U.; Pothig, R.; Casey, W. H., The origin of aluminum flocs in polluted streams. *Science* **2002,** *297*, (5590), 2245-2247.

32. Casey, W. H., Large aqueous aluminum hydroxide molecules. *Chem Rev* **2006,** *106*, (1), 1-16.

33. Bednar, A. J.; Jones, W. T.; Boyd, R. E.; Ringelberg, D. B.; Larson, S. L., Geochemical parameters influencing tungsten mobility in soils. *J Environ Qual* **2008,** *37*, (1), 229-233.

34. Keith, L. S.; Moffett, D. B.; Rosemond, Z. A.; Wohlers, D. W., ATSDR evaluation of health effects of tungsten and relevance to public health. *Toxicol Ind Health* **2007,** *23*, (5-6), 347-387.

35. Lagarde, F.; Leroy, M., Metabolism and toxicity of tungsten in humans and animals. *Met Ions Biol Syst* **2002,** *39*, 741-759.

36. Tajima, Y.; Amagai, H.; Okamura, N., Phosphotungstate Shows a Heparin-Like Anticoagulant Effect but Inhibits Heparin. *Thromb Res* **1989,** *55*, (3), 329-339.

37. Tajima, Y.; Nagasawa, Z.; Tadano, J., A Factor Found in Aged Tungstate Solution Enhanced the Antibacterial Effect of Beta-Lactams on Methicillin-Resistant Staphylococcus-Aureus. *Microbiol Immunol* **1993,** *37*, (9), 695-703.

38. Tajima, Y.; Nagasawa, Z.; Tanabe, I.; Kusaba, K.; Tadano, J., Possible Mechanism of Action of Beta-Lactam-Enhancing Factor on Methicillin-Resistant Staphylococcus-Aureus. *Microbiol Immunol* **1994,** *38*, (8), 639-648.

39. Tajima, Y.; Nagasawa, Z.; Tanabe, I.; Kusaba, K.; Tadano, J., Anionic properties of beta-lactam-enhancing factor on methicillin-resistant Staphylococcus aureus. *Res Microbiol* **1996,** *147*, (4), 279-286.

40. Strigul, N.; Galdun, C.; Vaccari, L.; Ryan, T.; Braida, W.; Christodoulatos, C., Influence of speciation on tungsten toxicity. *Desalination* **2009,** *248*, (1-3), 869-879.

41. Strigul, N.; Koutsospyros, A.; Christodoulatos, C., Tungsten speciation and toxicity: Acute toxicity of mono- and poly-tungstates to fish. *Ecotox Environ Safe* **2010,** *73*, (2), 164-171.

42. Song, I. K.; Shnitser, R. B.; Cowan, J. J.; Hill, C. L.; Barteau, M. A., Nanoscale characterization of redox and acid properties of keggin-type heteropolyacids by scanning tunneling microscopy and tunneling spectroscopy: Effect of heteroatorn substitution. *Inorg Chem* **2002,** *41*, (5), 1292-1298.

43. Cavani, F., Heteropolycompound-based catalysts: A blend of acid and oxidizing properties. *Catal Today* **1998,** *41*, (1-3), 73-86.

44. Okuhara, T.; Mizuno, N.; Misono, M., Catalysis by heteropoly compounds - recent developments. *Appl Catal a-Gen* **2001,** *222*, (1-2), 63-77.

45. Gustafsson, J. P., Modelling molybdate and tungstate adsorption to ferrihydrite. *Chem Geol* **2003,** *200*, (1-2), 105-115.

46. Xu, N.; Christodoulatos, C.; Braida, W., Modeling the competitive effect of phosphate, sulfate, silicate, and tungstate anions on the adsorption of molybdate onto goethite. *Chemosphere* **2006,** *64*, (8), 1325-1333.

47. Gecol, H.; Ergican, E.; Miakatsindila, P., Biosorbent for tungsten species removal from water: Effects of co-occurring inorganic species. *J Colloid Interf Sci* **2005,** *292*, (2), 344-353.

48. Nordin, J. P.; Sullivan, D. J.; Phillips, B. L.; Casey, W. H., Mechanisms for fluoride-promoted dissolution of bayerite [beta-Al(OH)(3)(s)] and boehmite [gamma-AlOOH]: F-19-NMR spectroscopy and aqueous surface chemistry. *Geochim Cosmochim Ac* **1999,** *63*, (21), 3513-3524.

49. Strathmann, T. J.; Myneni, S. C. B., Effect of soil fulvic acid on nickel(II) sorption and bonding at the aqueous-boehmite (gamma-AIOOH) interface. *Environ Sci Technol* **2005,** *39*, (11), 4027-4034.

50. Li, W.; Feng, J.; Kwon, K. D.; Kubicki, J. D.; Phillips, B. L., Surface Speciation of Phosphate on Boehmite (gamma-AlOOH) Determined from NMR Spectroscopy. *Langmuir* **2010,** *26*, (7), 4753-4761.

51. Sugiyama, S.; Kanda, Y.; Ishizuka, H.; Sotowa, K. I., Removal and regeneration of aqueous divalent cations by boehmite. *J Colloid Interf Sci* **2008,** *320*, (2), 535-539.

52. Granados-Correa, F.; Jimenez-Becerril, J., Chromium (VI) adsorption on boehmite. *J Hazard Mater* **2009,** *162*, (2-3), 1178-1184.

53. Goh, K. H.; Lim, T. T.; Dong, Z., Application of layered double hydroxides for removal of oxyanions: A review. *Water Res* **2008,** *42*, (6-7), 1343-1368.

54. Lopezsalinas, E.; Ono, Y., Intercalation Chemistry of a Mg-Al Layered Double Hydroxide Ion-Exchanged with Complex Mcl4(2-) (M=Ni, Co) Ions Form Organic Media. *Microporous Mater* **1993,** *1*, (1), 33-42.

55. Evans, D. G.; Xue, D. A., Preparation of layered double hydroxides and their applications as additives in polymers, as precursors to magnetic materials and in biology and medicine. *Chem Commun* **2006**, (5), 485-496.

56. Khan, A. I.; O'Hare, D., Intercalation chemistry of layered double hydroxides: recent developments and applications. *J Mater Chem* **2002,** *12*, (11), 3191-3198.

57. Hughes, J. M.; Rakovan, J., The crystal structure of apatite, Ca-5(PO4)(3)(F,OH,Cl). *Rev Mineral Geochem* **2002,** *48*, 1-12.

58. Pan, Y.; Fleet, M. E., Compositions of the apatite-group minerals: substitution mechanisms and controlling factors. *Reviews in Mineralogy and Geochemistry* **2002,** *48*, (1), 13-49.

59. Sutter, B.; Ming, D. W.; Clearfield, A.; Hossner, L. R., Mineralogical and chemical characterization of iron-, manganese-, and copper-containing synthetic hydroxyapatites. *Soil Sci Soc Am J* **2003,** *67*, (6), 1935-1942.

60. Tang, Y. Z.; Reeder, R. J.; Lee, Y. J., Zinc incorporation into hydroxylapatite. *Geochim Cosmochim Ac* **2009,** *73*, (13), A1313-A1313.

61. Peng, G. Y.; Luhr, J. F.; McGee, J. J., Factors controlling sulfur concentrations in volcanic apatite. *Am Mineral* **1997,** *82*, (11-12), 1210-1224.

62. Comodi, P.; Liu, Y.; Stoppa, F.; Woolley, A., A multi-method analysis of Si-, S-and REE-rich apatite from a new find of kalsilite-bearing leucitite (Abruzzi, Italy). *Mineralogical Magazine* **1999,** *63*, (5), 661-661.

63. Mason, H. E.; Kozlowski, A.; Phillips, B. L., Solid-state NMR study of the role of H and Na in AB-type carbonate hydroxylapatite. *Chemistry of Materials* **2007,** *20*, (1), 294-302.

64. Rakovan, J.; Reeder, R. J., Differential Incorporation of Trace-Elements and Dissymmetrization in Apatite - the Role of Surface-Structure during Growth. *Am Mineral* **1994,** *79*, (9-10), 892-903.

65. Sayers, D. E.; Stern, E. A.; Lytle, F. W., New Technique for Investigating Noncrystalline Structures - Fourier Analysis of Extended X-Ray - Absorption Fine Structure. *Phys Rev Lett* **1971,** *27*, (18), 1204-&.

66. Kelly, S.; Hesterberg, D.; Ravel, B., Analysis of soils and minerals using X-ray absorption spectroscopy. *Methods of soil analysis. Part* **2008,** *5*, 387-463.

67. Koningsberger, D.; Prins, R., X-ray absorption: principles, applications, techniques of EXAFS, SEXAFS, and XANES. **1988**.

68. Penner-Hahn, J. E., X-ray Absorption Spectroscopy. *eLS* **2004**.

69. Yamazoe, S.; Hitomi, Y.; Shishido, T.; Tanaka, T., XAFS study of tungsten L-1- and L-3-edges: Structural analysis of WO3 species loaded on TiO2 as a catalyst for photo-oxidation of NH3. *J Phys Chem C* **2008,** *112*, (17), 6869-6879.

70. Teo, B.-K.; Lee, P., Ab initio calculations of amplitude and phase functions for extended X-ray absorption fine structure spectroscopy. *Journal of the American Chemical Society* **1979,** *101*, (11), 2815-2832.

71. George, G. N.; Cleland, W. E.; Enemark, J. H.; Smith, B. E.; Kipke, C. A.; Roberts, S. A.; Cramer, S. P., L-Edge Spectroscopy of Molybdenum Compounds and Enzymes. *Journal of the American Chemical Society* **1990,** *112*, (7), 2541-2548.

72. Bare, S. R.; Mitchell, G. E.; Maj, J. J.; Vrieland, G. E.; Gland, J. L., Local Site Symmetry of Dispersed Molybdenum Oxide Catalysts - Xanes at the Mo L2,3-Edges. *J Phys Chem-Us* **1993,** *97*, (22), 6048-6053.

73. Evans, J.; Mosselmans, J. F. W., L-Edge Studies on Molybdenum. *J Phys Chem-Us* **1991,** *95*, (24), 9673-9676.

74. Aritani, H.; Tanaka, T.; Funabiki, T.; Yoshida, S.; Kudo, M.; Hasegawa, S., Structure of Mo-Mg binary oxides in oxidized reduced states studied by X-ray absorption

spectroscopy at the Mo K edge and Mg K edge. *J Phys Chem-Us* **1996,** *100*, (13), 5440-5446.

75.   Che, M.; Mori, K.; Yamashita, H., Elaboration, characterization and properties of silica-based single-site heterogeneous photocatalysts. *P Roy Soc a-Math Phy* **2012,** *468*, (2143), 2113-2128.

76.   Fellowes, J. W.; Pattrick, R. A. D.; Lloyd, J. R.; Charnock, J. M.; Coker, V. S.; Mosselmans, J. F. W.; Weng, T. C.; Pearce, C. I., Ex situ formation of metal selenide quantum dots using bacterially derived selenide precursors. *Nanotechnology* **2013,** *24*, (14).

77.   Stern, E., Structure determination by X-ray absorption. *Contemporary Physics* **1978,** *19*, (4), 289-310.

78.   Stern, E.; Heald, S., Basic principles and applications of EXAFS. *Handbook of synchrotron radiation* **1983,** *1*.

79.   Rehr, J. J.; Albers, R. C., Theoretical approaches to x-ray absorption fine structure. *Rev Mod Phys* **2000,** *72*, (3), 621-654.

Chapter 2. Tungstate Sorption Mechanisms on Boehmite: Systematic Uptake Studies and X-ray Absorption Spectroscopy Analysis

Abstract

Mechanisms of tungstate sorption on the mineral boehmite (γ-AlOOH) were studied using a combination of batch uptake experiments and X-ray absorption spectroscopy. Batch uptake experiments over the range of pH 4-8 and [W] = 50-2000 µM show typical sorption trends of oxyanions, and isotherm experiments reveal continued uptake with increasing tungstate concentration without any clear maximum. Desorption experiments showed that sorption is irreversible at pH 4, and only partly reversible at pH 8. Tungsten L_1- and L_3-edge XANES spectra of wet pastes recovered from uptake experiments at pH 4 and 8 indicate all sorbed tungstates are octahedrally coordinated, even though the dominant solution species at pH 8 is monotungstate. Tungsten L_3-edge EXAFS analysis shows that sorbed tungstate occurs as polymeric form(s), as indicated by the presence of corner- and edge-sharing of distorted tungstate octahedra. The occurrence of polymeric tungstate at the boehmite surface at pH 8 indicates that sorption is accompanied by polymerization and a change from tetrahedral coordination (in solution) to distorted octahedral coordination (on the surface). The strong tendency for tungstate polymerization on boehmite can explain the continued uptake without reaching an apparent maximum in sorption, as well as the limited desorption behavior. Our results provide the basis for a predictive model of the uptake of tungstate by boehmite, which can be important for understanding tungstate mobility, toxicity, and bioavailability.

Keywords: tungstate, tungstate speciation, boehmite (γ-AlOOH), sorption mechanism, polymerization, X-ray absorption spectroscopy

2.1. Introduction

Until recently, little consideration has been given to the environmental impact of tungsten. This industrially important metal has been widely thought to be nontoxic in its pure or alloyed forms.[1, 2] However, recent studies have shown that oxidized forms of tungsten are soluble under appropriate conditions of pH and redox potential.[3] Oxidation of metallic forms of tungsten result in dissolution and formation of soluble anions that are mobile in aquatic and soil systems. Tungsten in the VI oxidation state, tungstate, forms many different oxyanions, including monooxyanion and polyoxyanion forms.[4-6] The study of tungstate behavior in the environment is complex due to the occurrence of multiple species associated with polymerization and their interactions with environmental materials. The oxidation, dissolution, and mobilization of tungsten may lead to adverse environmental effects, including soil acidification as well as toxic effects on plants, soil microorganisms and invertebrates.[7-9] Recent studies have shown that the toxicity of tungstate is related to its speciation. Strigul et al. studied toxicities of tungstate species in fish, and reported that polymeric tungstates were more toxic than monotungstate.[10] Investigation of tungstate behavior in aqueous systems, including its toxicity, has become increasingly important as its use in industry and releases to the environment have escalated.

Tungsten is in the same chemical group with Cr and Mo. The oxyanions of these elements form dimeric or polymeric species in solution under appropriate conditions.[11] Two important oxidation states of Cr in solution are Cr(VI) with mostly tetrahedral coordination and Cr(III) with octahedral coordination in aqueous solution.[12] Chromium(VI) forms monomeric and polymeric species such as chromate (CrO_4^{2-}), dichromate ($Cr_2O_7^{2-}$), and less commonly trichromate ($Cr_3O_{10}^{2-}$) and tetrachromate ($Cr_4O_{13}^{2-}$), depending on pH and concentration in the solution. The dominant oxyanion species of tungstate and molybdate at basic pH are monomeric

forms with tetrahedral coordination, such as WO_4^{2-} and MoO_4^{2-}. As pH is decreased, tungstate and molybdate form polymeric species with mainly octahedral coordination. The polymerization is dependent on pH and tungsten or molybdenum concentration. Furthermore, the kinetics of formation of some polymeric species is sluggish, so that equilibrium speciation is not necessarily obtained over the time scale of lab experiments.[4] The tendency for polymerization in the VIB group increases with increasing atomic number.[11] Tungstate has generally seen less study than molybdate and chromate regarding environmental behavior.[13] Tungstate speciation has been studied by several researchers with [187]W nuclear magnetic resonance (NMR) spectroscopy, electrospray ionization mass spectroscopy (ESI-MS), and Raman spectroscopy.[4-6, 14] General trends of tungsten polymerization are known under acidic conditions, but the mechanisms and kinetics are still not completely understood. [4, 6, 14, 15]

Sorption processes on mineral surfaces play an important role in regulating the distribution and mobility of trace metals in natural aquatic and soil systems. Tungstate has been shown to strongly adsorb on iron oxyhydroxide mineral surfaces at low pH conditions.[16, 17] Gustafsson used the Diffuse Layer Model and the CD-MUSIC model to describe tungstate (and molybdate) sorption on ferrihydrite, accounting for monomeric and polymeric tungstates to fit the experimental data for both models.[17] The competitive sorption of tungstate and other oxyanions on goethite was studied by Xu et al.[16] Tungstate sorption was found to be strongly competitive with molybdate and phosphate at the surface, whereas silicate and sulfate sorption was affected minimally by tungstate. Tungstate speciation in natural soils was studied by Bednard et al. and Clausen et al. with various analytical techniques.[2, 3] These studies found tungstate forming polymeric species with phosphate and silicate, and suggested the general transformation pathway of tungstates in nature. However, little is known of the influence that

tungstate speciation plays in sorption behavior over a broader pH range and on other mineral sorbents. This fundamental information is important inasmuch as it may control tungstate mobility, toxicity, and bioavailability in natural systems. However, because of the complexity of tungstate speciation, the sorption mechanisms of tungstate remain poorly understood.

In the present study, the aluminum oxyhydroxide mineral boehmite, AlO(OH), was chosen as a model sorbent, representing solids containing octahedrally coordinated aluminum. Boehmite occurs naturally as a common weathering product and is an effective sorbent owing to its high surface area and basic point of zero charge (~8.7). Its sorption properties have been studied for various metal cations and anions such as Pb, Ni, phosphate, and chromate.[18-21]

In this study, we first consider tungstate speciation in aqueous solution using reported stability constants of known tungstates, combined with characterization by X-ray absorption spectroscopy (XAS) and electrospray ionization mass spectroscopy (ESI-MS). Batch uptake experiments were carried out to investigate tungstate sorption behavior on boehmite over a range of environmentally relevant conditions. Tungsten L_1- and L_3-edge XANES was used to distinguish coordination environment around W atoms. The local structure and coordination of tungsten at the surface were determined using tungsten L_3-edge EXAFS, which allowed us to further characterize the binding mechanism as well as the dependence of tungstate sorption on environmental parameters such as pH, metal concentration and ionic strength. This work will provide a foundation for subsequent studies of tungstate sorption on other solids as well as other oxyanion species, such as molybdates and vanadates, which show similar behavior in solution. The findings also have possible implications for tungsten toxicity in natural environments.

2.2. Materials and Experiments

2.2.1 Sorbent

Boehmite from CONDEA Chemie GmbH was used in this study. Powder XRD was used to confirm the structure, and no other phases were detected. The specific surface area (SSA) of the boehmite was found to be 136 m^2/g by five-point N_2 Bruner-Emmett-Teller (BET) analysis, and a point of zero charge was determined as 8.7 in a previous study.[19, 22] Boehmite suspensions were equilibrated at designated pH conditions for at least one day prior to further experiments.

2.2 Batch uptake experiments

All sorption experiments were performed under atmospheric conditions. Tungstate stock solutions were prepared using $Na_2WO_4 \cdot 2H_2O$ (Alfa Aesar) and deionized water. Tungstate was added to suspensions from 0.01 M or 0.1 M stock solutions. The stock solutions were pre-titrated to target pH values prior to addition to the suspensions. Both titrated and fresh stock solutions were compared in sorption studies and XAS studies, but no difference was observed from titrating stock solutions.

Batch uptake experiments were conducted for a range of tungsten concentrations, from 50 to 2000 µM, at pH 4, 6.5, and 8. Based on tungstate speciation calculations, pH 4 and 8 represent solution conditions for which polytungstates and monotungstate, respectively, represent the major components in the solution. The pH 6.5 condition represents a mixture of monomeric and polymeric species. The boehmite suspensions were equilibrated overnight before being titrated to the desired pH using HCl or NaOH. After an additional 24 h equilibration time, a pre-determined amount of the 0.1 M or 0.01 M Na_2WO_4 solution was added to 1 g/L boehmite suspensions to achieve the target W concentration. Small amounts of 0.1 M HCl or NaOH were used to adjust the pH after adding the Na_2WO_4 solution to the suspension. After 24 hours of

equilibration on a shaker table, the suspensions were centrifuged for 10 min at 10,000 rpm, and 10 mL aliquots of supernatant were collected from each sample. Tungsten concentration in the aliquots was measured with direct coupled plasma atomic emission spectroscopy (DCP-AES) to calculate the amount of tungsten sorbed on the boehmite surface. Selected samples were filtered using a vacuum pump, and the wet pastes were prepared for XAS analysis.

2.2.3 Desorption experiments

Desorption experiments were conducted following the sorption reactions (as described above) for selected samples. Two concentrations (200 and 1000 µM) of Na_2WO_4 solution were reacted with boehmite suspension for 24 h, and the suspension was centrifuged for 10 min at 10,000 rpm. The solution was discarded, and the moist particles were re-suspended in tungstate-free solution with the same pH condition and background electrolyte concentration. Aliquots (5 mL) were taken at designated time periods, and W concentration in the solution was measured by DCP-AES to allow calculation of sorbed W.

2.2.4 ESI-Mass spectroscopy

All ESI-MS data were measured with a Thermo TSQ Quantum Access Triple Quadrupole Mass Spectrometer at the Proteomics Center at Stony Brook Universtiy. The mass spectrometer was connected to an electrospray ionization unit. The samples were infused with 50 % acid nitrile and DI water at 5 µL/min in negative ion mode. The flow rate of the sheath gas was maintaied at 15 L/min for all samples, and the capillary temperature optimized at 270 ℃. The spray needle voltage was 2.0 to 3.0 kV. For the data acquisition, the quadrupole mass filter was scanned from m/z 200 to 3000 for 1 s. A 2 mM Na_2WO_4 solution was titrated to pH 4 or 8 before ESI-MS measurement. Solutions were aged 5 h after adjusting to the designated pH; this spanned the typical period required for preparing the stock solution and initiating a sorption experiment.

2.2.5 X-ray absorption spectroscopy

2.2.5.1 Tungsten L$_1$- and L$_3$-edge EXAFS and XANES

Tungsten L$_1$- and L$_3$-edge XANES and L$_3$-edge EXAFS were collected at beamlines 20BM and 12BM at the Advanced Photon Source (APS, Argonne National Laboratory) and at X11A, X18B, and X19A at the National Synchrotron Light Source (NSLS, Brookhaven National Laboratory). Spectra were collected at the W L$_1$ and L$_3$ edges using Si(111) monochrometer crystals with detuning of 10–30%. Energy calibration was performed with a Ga filter (K-edge, 10.367 keV) or a W metal foil for the W L$_3$-edge (10.207 keV), and a Pt metal foil (L$_3$-edge, 11.564 keV) or a W metal foil for the W L$_1$-edge (12.2 keV). The monochrometer was calibrated by assigning the indicated energy to the first peak of the derivative of the edge spectrum of the element used for calibration.

EXAFS and XANES spectra for model compounds were collected in transmission mode. Model compounds were mixed with boron nitride to achieve the proper edge step, and then loaded into Lucite sample holders and sealed using two layers of Kapton tape. All spectra for sorption samples and solutions were taken in fluorscence mode using a partially implanted planar silicon (PIPS) detector at the NSLS and a 13-element Ge detector at the APS. Wet pastes obtained from vacuum filtration of reacted suspensions were sealed in Lucite sample holders with Kapton tape, and stored in sealed poly bags with wet tissues to prevent drying. Samples were placed at a 45° angle to the incident beam for fluorescence measurements. Multiple spectra were routinely collected and averaged to achieve acceptable signal/noise.

2.2.5.2 Tungsten L$_3$-edge EXAFS fitting

Data analysis was conducted using iFeffit[23] and WinXAS[24, 25]. Shell by shell fitting was performed in real space. In fitting the model compounds, coordination numbers were fixed

because the structures are well known. All scattering paths were calculated by FEFF7 according to the published structures.[23, 26] Fitting of model compounds was begun using only single scattering paths. In some instances, like paths close to each other were combined to minimize the number of paths necessary to get an acceptable fit. The significance of multiple scattering (MS) from linear chains, e.g., O-W-O, has been previously noted by Kuzmin et al.[27] This study reported that the contribution from multiple scattering (MS) paths is important for properly explaining the observed EXAFS spectra. Their study showed that the contribution of a MS path with 4 legs from near-linear O-W-O chains is most significant for EXAFS fitting. In the present study, fitting results were compared with and without this MS contribution.

The primary challenges in fitting W L_3-edge EXAFS spectra for soprtion samples arise from the existence of multiple, overlapping paths for polymeric species and the likely existence of multiple species, particularly at higher tungsten concentrations. A distinction between tetrahedral and octahedral coordination can be made on the basis of average, first-shell W-O distances. The average W-O distance in tetrahedral tungstates is ~1.8 $\overset{\circ}{A}$, while polytungstates have longer average W-O distances (~1.95 $\overset{\circ}{A}$), reflecting octahedral coordination. However, the octahedral coordination in polytungstates is invariably distorted, resulting in a range of individual W-O distances (1.76-2.4 $\overset{\circ}{A}$). The octahedra may be connected by corner- and/or edge-sharing. Because of the distortion observed in W octahedra, fitting typically requires using two or more W-O paths, whereas tetrahedral W is best fit with a single W-O path. Although the common polymeric tungstate species differ in the details of their configuration, they share several common characteristics that distinguish them from monomeric, tetrahedral species. W-W distances differ between octahedra linked by corner- vs. edge-sharing, although the range of characteristic distances for each linkage can overlap slightly. Nevertheless, peaks in the range

3.3-3.8 Å that are fit well by W-W paths provide strong evidence of polymeric tungstates, even if the exact species cannot be identified. Further complications in fitting result if multiple polymeric species exist. The peaks around thses distances in sorption samples were fit with W-W paths.

The general fitting procedure followed three steps. First, the main peak corresponding to first-shell W-O backscattering was fit using one or more paths. The best fits for sorption samples were typically achieved using two or three W-O paths for the first main peak in FT magnititude. Second, a near-linear O-W-O MS path was introduced. Multiple scattering (MS) is found to have an effect mainly at low k in the chi functions, and was found to be necessary to achieve an acceptable fit of the splitting in the first oscillation near 3.5-5 Å $^{-1}$. Finally, the peaks in the range 3.0–3.8 Å were fit with W-W and/or W-Al paths. Reference compounds were fit to validate the strategy described, however, their coordination numbers were constrained to be consistent with known structure data. In addition, to reduce the number of paths using in fitting, like paths with similar distances were combined.

The EXAFS data for the lowest concentration sorption samples were fit first with single scattering paths for octahedral coordination. We constrained total coordination number of first shell with 6 if the fitting results were not reasonable with floating coordination numbers. We assumed that a W-Al path contributes to the EXAFS signal in even higher tungstate concentration sorption samples, so the parameters of a W-Al path, obtained from the results of the 5 µM sorption sample, were fixed in the fitting processes. The fitting results of higher concentration samples were compared with and without a W-Al path adopted from the result of the lowest concentration sample. We also adopted two W-W paths, corner- and edge-sharing, to fit the second shell for the higher concentration smples.

2.2.5.3 Reference Samples for X-ray Absorption Spectroscopy

XAS data were collected for several tungstate-containing model compounds for comparison with the sorption and solution samples and also to validate the fitting strategy. Compounds were chosen to represent a range of W(VI) coordination environments, including isolated tetrahedra and octahedra and various polymeric forms. The compounds $Na_2WO_4 \cdot 2H_2O$ and $CaWO_4$ contain exclusively isolated tungstate tetrahedra, whereas Ba_2NiWO_6 contains exclusively isolated tungstate octahedra (O_h symmetry). Polymeric tungstate reference compounds include phosphotungstic acid ($H_3PW_{12}O_{40}$), sodium metatungstate ($Na_6W_{12}O_{40} \cdot xH_2O$), sodium ditungstate ($Na_2W_2O_7$), and tetrabutyl-ammonium hexatungstate (TBA-W_6O_{19}). TBA-W_6O_{19} contains isolated W_6O_{19} units in which six distorted tungstate octahedra share edges. Tungsten occurs as distorted octahedra in WO_3, sharing all corners in a perovskite-like structure. $Na_2W_2O_7$ contains both tetrahedral and octahedral tungsten in a 1:1 ratio. Phosphotungstic acid has a Keggin type structure with tungstate octahedral around a phosphate center. The reagents were used as purchased. Ba_2NiWO_6 was synthesized by the method described by Yamazoe, using $BaCO_3$ (Alfa Aesar), $NiCO_3$ (Alfa Aesar), WO_3 (Sigma Aldrich) reagents.[28] TBA-W_6O_{19} was prepared according to the procedure described by Sanche et al., using Na_2WO_4, acetic anhydride (Sigma Aldrich) and dimethyformamide (Sigma Aldrich).[29] $Na_2W_2O_7$ was synthesized by the method described in previous studies.[30] $H_3PW_{12}O_{40}$ (Sigma Aldrich) and $Na_6W_{12}O_{40} \cdot xH_2O$ (Acros Organics) were used as provided. Powder XRD confirmed the structures of all model compounds, and no impurity phases were detected.

2.3. Results

2.3.1. Tungstate aqueous speciation

Calculation of tungstate speciation in ambient temperature aqueous solutions is complicated by the existence of multiple polymeric species and a wide variation in the kinetics involved in their formation.[4, 6, 15, 31] For example, previous studies have shown that paratungstate A ($W_7O_{24}^{6-}$) forms rapidly from acidification of sodium tungstate solution, followed by a slow isomerization reaction forming paratungstate B ($H_2W_{12}O_{42}^{10-}$), for which equilibrium may require months.[4] Several metatungstate species may form, with variable kinetics, upon further acidification. In the present study, only polymeric tungstate species that have been directly observed in solution using ^{183}W NMR were included in our aqueous speciation calculations.[4] Furthermore, we limited the calculation to species that were expected to form in significant proportion over the duration of the laboratory experiments, eliminating those species for which formation kinetics were known to be excessively long. Therefore, these calculations do not necessarily represent final equilibrium states. Stability constants are given in Table 2.1. Calculations were performed using the program PhreeqC over a range of total W concentrations at ionic strength 0.01 M.[32]

The calculated speciation with 1 mM tungstate in solution is shown in Figure 2.1. Monotungstate is the dominant species at pH > 6.5, consistent with previous studies[1, 4, 14], whereas formation of several polytungstates is favored at lower pH conditions. These calculations confirm that polytungstate species are favored as monotungstate (WO_4^{2-}) is acidified.[4]

Table 2. 1. Stability constants of polytungstate species used for simulation of aqueous speciation (at 298K) [4]

Species	Solution Species Reaction	Stability Constant (log K)	Reference
Paratungstate A	$7\ WO_4^{2-} + 8\ H^+\ <=>\ W_7O_{24}^{6-} + 4\ H_2O$	68.17	
Paratungstate B	$12\ WO_4^{2-} + 14\ H^+\ <=>\ H_2W_{12}O_{41}^{10-} + 6\ H_2O$	118.00	4
a-Metatungstate	$12\ WO_4^{2-} + 18\ H^+\ <=>\ H_2W_{12}O_{40}^{6-} + 8\ H_2O$	144.72	

Figure 2. 1. Calculated aqueous tungstate speciation at $[WO_4^{2-}]_{tot}$ = 1 mM. Tungstate stability constants are reported in Table 2.1. Monotungstate is the dominant species above pH 6.5. Several polytungstates such as $H_2W_{12}O_{40}^{6-}$, $H_2W_{12}O_{42}^{10-}$, and $W_7O_{24}^{6-}$ exist at low pH values.

2.3.2 Electro-spray Ionization Mass spectroscopy

Results for ESI-MS experiments from 2 mM Na_2WO_4 solutions at pH 4 and 8 are shown in Figure 2.2. Both pH 4 and 8 solutions showed the expected natural abundance isotope ratio near 248 m/z with side peaks (tungsten isotopes of 180, 182, 183, 184 and 186 AMU yield tungstate ion at 245, 247, 248, 249, and 251 m/z respectively).[14] Consistent with the speciation calculation, monotungstate is dominant in the pH 8 solution. At pH 4, the 248 m/z peak is present, along with multiple peaks at higher m/z values, consistent with the presence of polymeric tungstates such as $W_3O_{10}^{2-}$, $H_2W_{12}O_{40}^{6-}$, $NaW_2O_7^-$, $NaW_4O_{13}^-$, $HW_2O_7^-$, $W_4O_{13}^{2-}$, and $W_6O_{19}^{2-}$. This result is similar to the findings of Walanda et al.[14], who suggested that polymerization occurs via formation of intermediate species of the general forms $W_mO_{3m+1}^{2-}$, $HW_mO_{3m+1}^-$, $NaW_mO_{3m+1}^-$, which are observed in our study. Other studies have reported a number of intermediate species; however, they are thought to be metastable, short-lived speces.[4, 14, 33] Our solution samples, which were aged 5 h before ESI-MS measurements were made, will not have reached final equilibrium with respect to polymerization. Therefore, the multiple m/z signals are likely to include such intermediate species. Exact concentrations of individual tungstate species cannot be determined reliably because suitable references containing the different species are not available. Furthermore, it is possible that some signals result from fragmentation of larger polytungstates by collision-induced dissociation.[34] While the ESI-MS results cannot provide a quantitative speciation of the tungstate solution at low pH, they confirm the dominance of polymeric species and the likely occurrence of multiple polymeric tungstates for the conditions of the sorption experiments performed here.
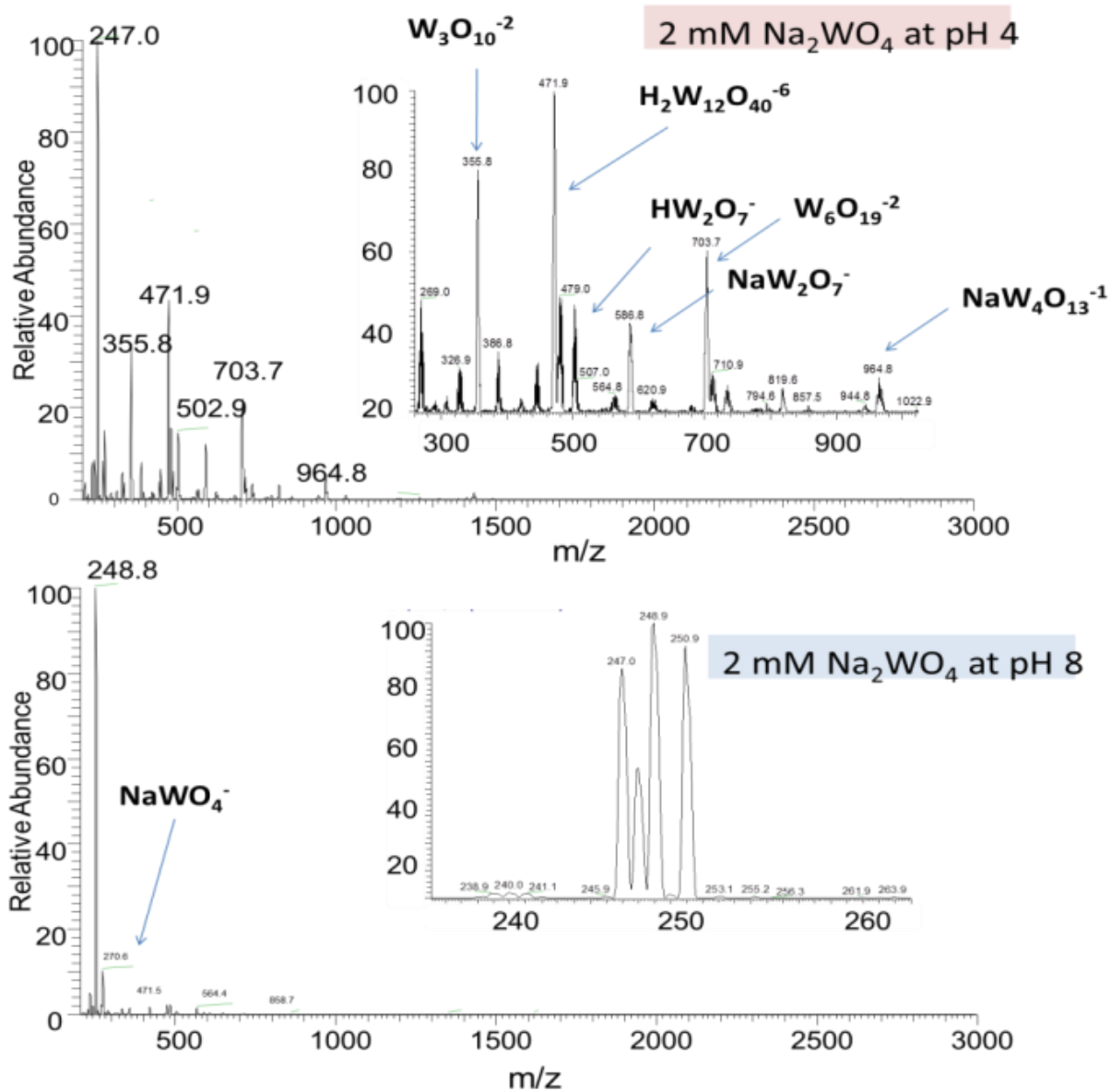
Figure 2. 2. ESI-MS results from 2 mM tungstate solutions at pH 4 and pH 8. Both pH 4 and 8 solutions show a strong peak near 249 m/z, corresponding to monotungstate. Multiple peaks at high m/z in the pH 4 solution correspond to polytungstate species.

2.3.3 Batch uptake trends

The effect of pH on tungstate sorption by boehmite was investigated at an initial tungstate concentration of 50 µM at two ionic strength conditions using NaCl as a background electrolyte (Fig. 3). Adsorption edges show the general behavior expected for anions, with maximum sorption in the pH range 4-5, and decreasing sorption with increasing pH, approaching minimum values near and above the PZC of boehmite, 8.7. A smaller decrease in sorption is observed at pH values below the maximum. The efficiency of W sorption is slightly affected by ionic strength. Slightly greater tungstate sorption is observed at 0.1 M NaCl for pH > 5, while the boehmite suspension at 0.01 M NaCl shows slightly greater sorption at pH < 5. The lower tungstate sorption with 0.1 M NaCl at pH < 5 could be explained by competing reactions of tungstate and Cl$^-$ on the positively charged boehmite surface. Also, polymeric tungstate with large negative charge, e.g., $H_2W_{12}O_{42}^{10-}$, could form electrostatic bonds with Na$^+$ thereby reducing polytungstate sorption on boehmite at higher NaCl concentrations. The greater tungstate sorption at 0.1 M NaCl above pH 5 is similar to observations by Wei et al., who studied phosphate sorption on boehmite from the same source (CONDEA Chemie GmbH).[35] These authors attributed greater phosphate uptake at higher NaCl concentration to Na$^+$ coadsorption on the surface.
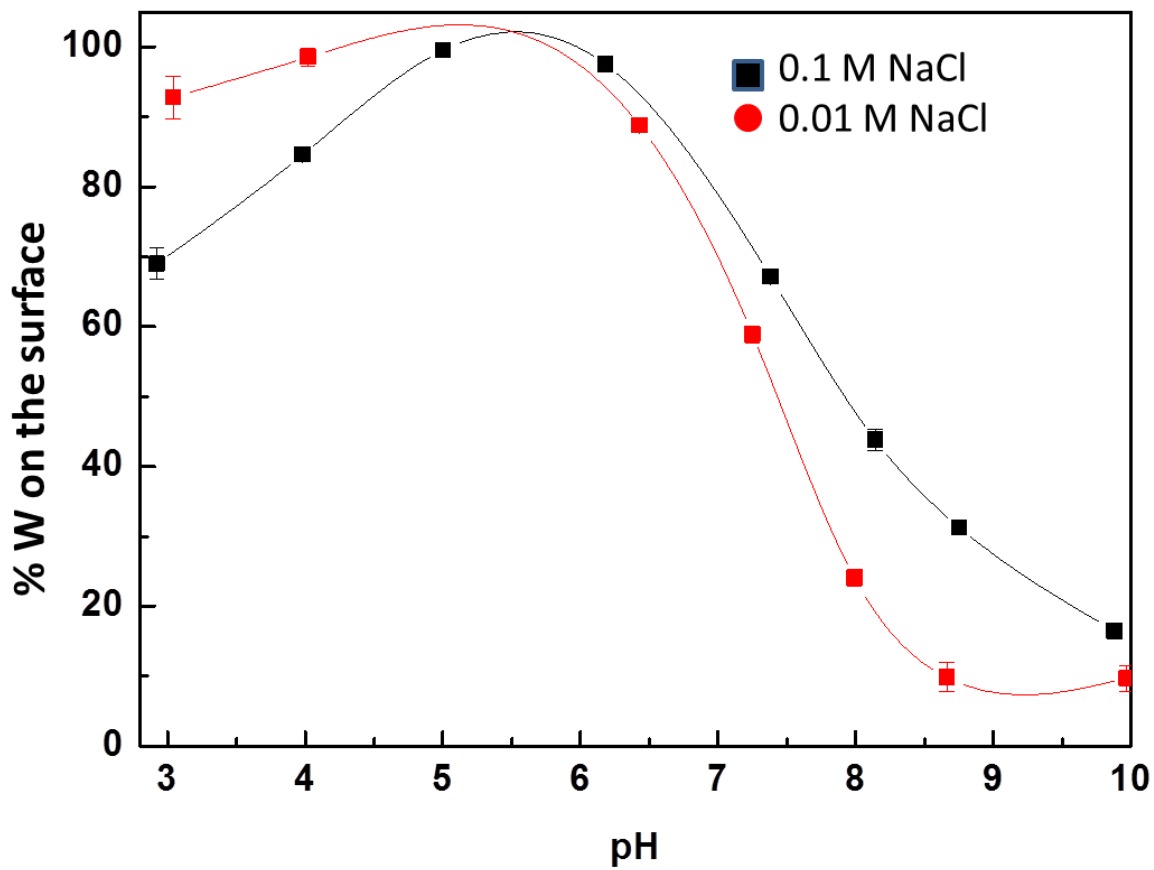
Figure 2. 3. Effect of pH on tungstate sorption on boehmite at different ionic strength conditions.

Uptake experiments were performed to construct isotherms in the range 50 to 2000 µM total tungstate at pH 4, 6 and 8. These pH conditions were chosen to represent solutions in which polytungstate species (pH 4) or a monotungstate (pH 8) dominates, or in which a mixture is present (pH 6), as indicated by the speciation calculations described above. We performed initial kinetic experiments of tungstate sorption (initial $[WO_4^{2-}] = 200$ µM , and 0.19 mmole/g sorbed on boehmite at pH 4), which confirmed that sorption is fast, with ~80% of the equilibrium amount of tungstate sorbed within the initial few hours, and >90% sorbed within 24 h. On this basis, all subsequent sorption experiments were conducted over 24 h duration. In all pH conditions, the amount of W sorbed on the surface increased as W concentration in the solution increased, without reaching a maximum in the concentration range studied. As we expected from the pH edge experiments, W showed greatest sorption at pH 4. The tungstate surface coverage increased from 0.04 mmole/g to 0.72 mmole/g at pH 4, and increased from 0.01 to 0.21 mmole/g at pH 8.
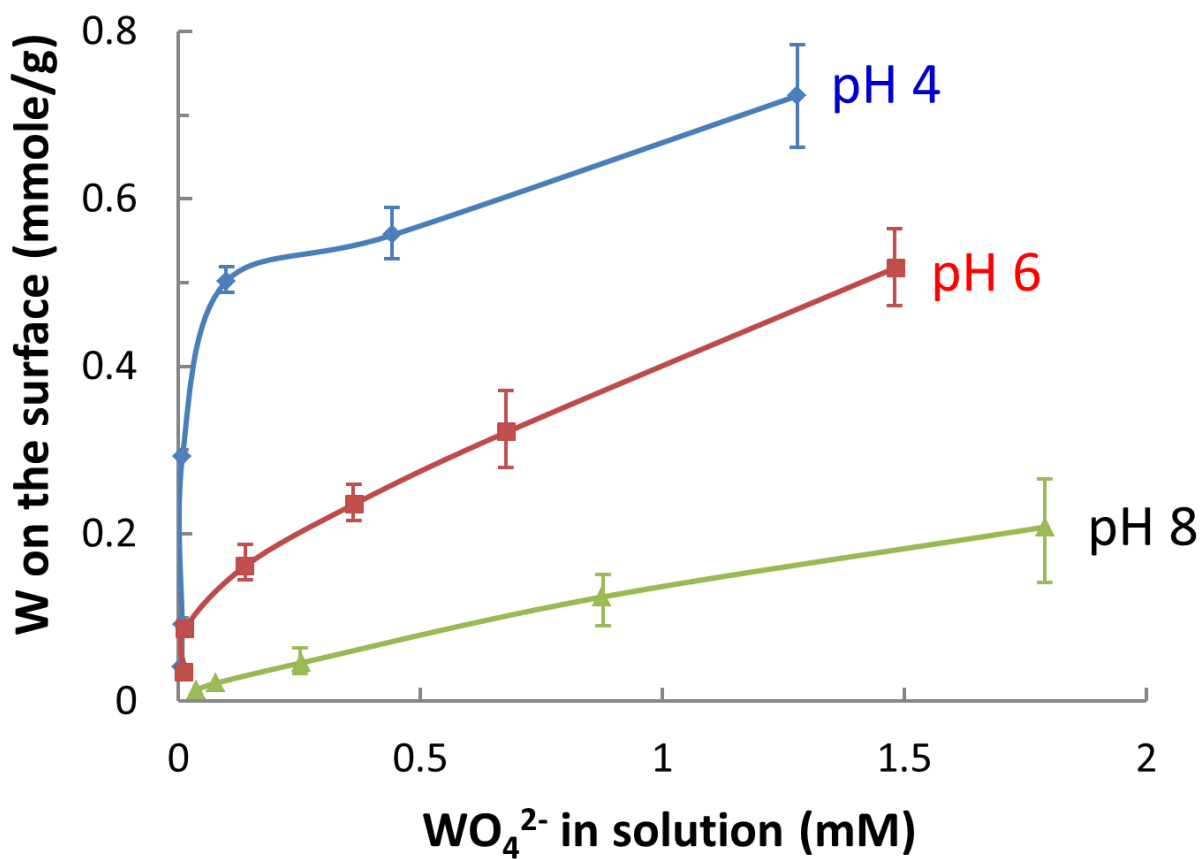
Figure 2. 4. Tungstate isotherm experiments on boehmite were conducted as a function of pH and tungsten concentration at room temperature. Continued tungstate uptake was observed in the isotherm experiments.

2.3.4 Desorption Experiments

Desorption experiments were performed at 200 μM and 1000 μM initial W concentration at pH 4 and pH to establish sorption reversibility. Tungstate sorbed for 24 h on boehmite at pH 4 showed largely irreversible behavior in desorption experiments, with more than 95% of the tungstate remaining on the surface for both initial concentrations studied. Sorption was found to be partly reversible at pH 8, as shown in Figure 2.5. Approximately 25-30 % of the tungstate on the surface was released into the solution at pH 8, with slightly greater release at 200 μM than at 1000 μM. These desorption results imply different sorption mechanisms on the boehmite surface at pH 4 and pH 8. X-ray absorption spectroscopy was used to provide further insight to dominant sorption mechanisms.
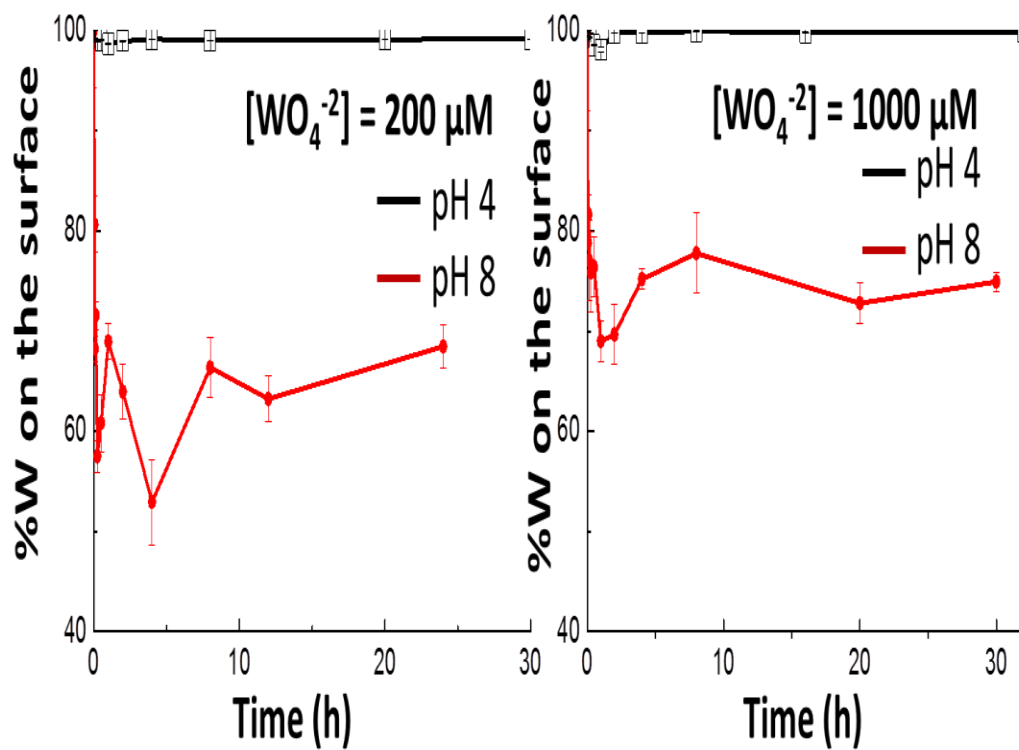
Figure 2. 5. Tungsten desorption from boehmite at pH 4 (square) and 8 (circle). Sorption is more reversible at pH 8 than at pH 4, suggesting different sorption mechanisms.

2.3.5 Tungsten L_1- and L_3-edge XANES

Both the L_1- and L_3-edge XANES spectra of tungsten have proven useful for characterizing tungstate coordination environments.[28] A pre-edge feature is observed in the L_1-edge, associated with electron transitions from 2s to unoccupied valence orbitals. This transition is dipole forbidden in symmetric octahedral environments, but allowed for tetrahedral and distorted octahedral environments. Previous studies have shown that the intensity and shape of the pre-edge feature relate to coordination and degree of (octahedral) distortion.[36] Tungsten L_1-edge XANES spectra of selected reference and sorption samples and detailed explanations are provided in supporting information. Tungsten L_3-edge XANES has been studied less than the L_1-edge. Recently, Yamazoe et al. demonstrated that second derivatives of the L_3-edge show differences corresponding to coordination environment, analogous to the ligand field splitting of 5d orbitals observed for different coordination environments of Mo(VI).[28] Here, we combine the complementary L_1- and L_3-edge XANES data to discriminate between tetrahedral and octahedral coordination of W, including identification of distortion for octahedral environments, which is a characteristic feature of polymeric tungstates. Tungsten L_1-edge XANES spectra are shown in Figure 2.7, while tungsten L_3-edge XANES will be more discussed in section 3.6 below.

2.3.6 W L_3-edge XANES Analysis

Yamazoe et al. demonstrated that differences in the second derivatives of W L_3-edge XANES spectra could be used to distinguish between tetrahedral and octahedral W(VI) coordination, as well as the presence of distortion of octahedra.[28] Reference samples containing only W(VI) tetrahedra show a single minimum with a weak shoulder on the low-energy side, as observed for $Na_2WO_4 \cdot 2H_2O$ and $CaWO_4$ (Fig. 6). Model compounds containing only W(VI) octahedra show splitting to create two minima. Yamazoe showed that the shape of the minima

and the degree of splitting between them are dependent on the coordination type and the degree of distortion of the octahedra.[28] Figure 2.6 shows second derivatives of W L_3-edge XANES spectra of the lowest W concentration sorption samples (5 μM) at pH 4 and 8, compared with tetrahedral and octahedral model compounds. Findings for higher concentration samples are summarized in Table 2.2. Second derivative spectra of both sorption samples display two well separated minima, consistent with distorted octahedral coordination of W(VI). Notably, these second derivative spectra are nearly identical for samples at both pH conditions. In Figure 2.6, sorption samples are clearly distinguished from $Na_2W_2O_7$, which contains both tetrahedral and octahedral W(VI). Although, it is not possible to rule out a minor contribution from tetrahedrally coordinated W(VI), the dominant component in the sorption samples is clearly octahedral, which is distorted.
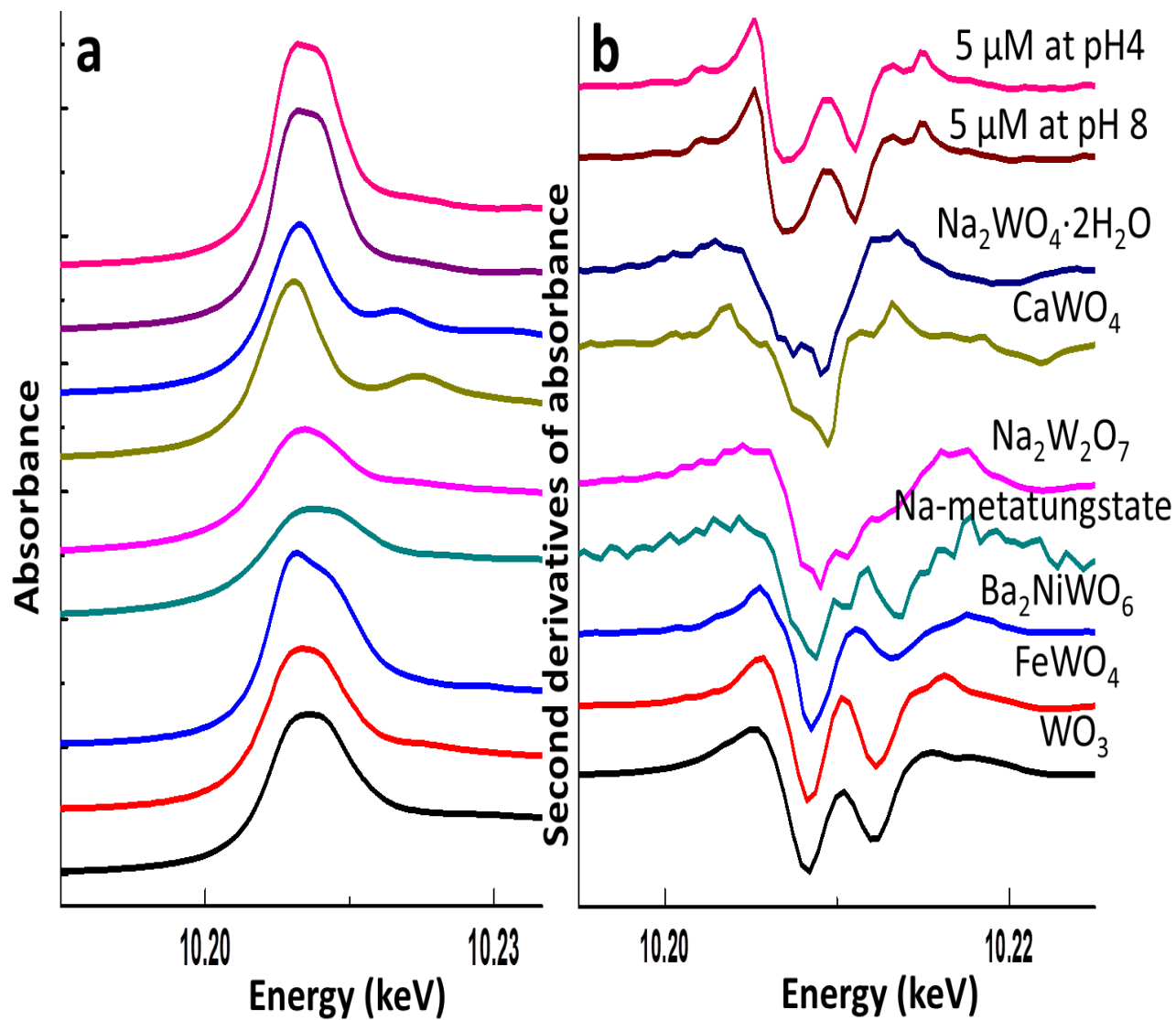
Figure 2. 6. XANES (a) and Second derivative spectra (b) of W L_3-edge XANES for selected model compounds showing differences that distinguish tetrahedral and octahedral coordination of W(VI).

2.3.7 W L$_1$-edge XANES analysis

W L$_1$-edge XANES has been widely utilized to distinguish W coordination geometry. [28, 37, 38] The shape, position, and area of this pre-edge peak in W L$_1$-edge XANES spectra have been used to distinguish between octahedral and tetrahedral coordination, as well as the degree of distortion in octahedral geometry.[28] Figure 2.7 shows W L$_1$-edge XANES spectra selected model compounds representing a range of coordination geometries. A prominent high intensity peak in the pre-edge region is indicative of tetrahedrally coordinated tungsten, as shown by Na$_2$WO$_4$·H$_2$O and CaWO$_4$. Reference compounds with octahedral coordination, such as Ba$_2$NiWO$_6$, TBA-W$_6$O$_{19}$, phosphotungstic acid, and WO$_3$, display pre-edge peaks that are lower in intensity and of different shape than tetrahedral compounds. The intensity of the pre-edge feature for the octahedrally coordinated compounds is sensitive to the degree of distortion. Phosphotungstic acid, and WO$_3$ have distorted octahedra, so their pre-edge features have greater intensity than that for Ba$_2$NiWO$_6$, which has O$_h$ symmetry for the tungsten octahedron. The compound Na$_2$W$_2$O$_7$ contains both tetrahedral and octahedral W in the ratio 1:1. Its XANES spectrum clearly shows a pre-edge peak with intensity intermediate between perfect octahedral and tetrahedral compounds.

Figure 2.7 also shows XANES spectra of 1 mM sodium tungstate solutions at pH 4 and pH 8. The intensity of the pre-edge feature from the pH 4 solution is lower than for the solution at pH 8 and similar in intensity to the feature from phosphotungstic acid, indicating distorted octahedral coordination. The higher intensity of the pre-edge feature for the pH 8 solution spectrum is similar to that for Na$_2$WO$_4$·H$_2$O and consistent with tetrahedral coordination. These solution spectra are consistent with the aqueous speciation calculations showing monotungstate dominating at pH 8 and polytungstate dominating at pH 4.

XANES data for tungstate-sorbed boehmite samples are compared to reference compounds and tungstate solutions at different pH values in Figure 2.7. The intensities of the pre-edge feature for the sorption samples are similar to those for phosphotungstic acid, indicating either distorted octahedral coordination, or possibly a mixture of tetrahedral and octahedral coordination.
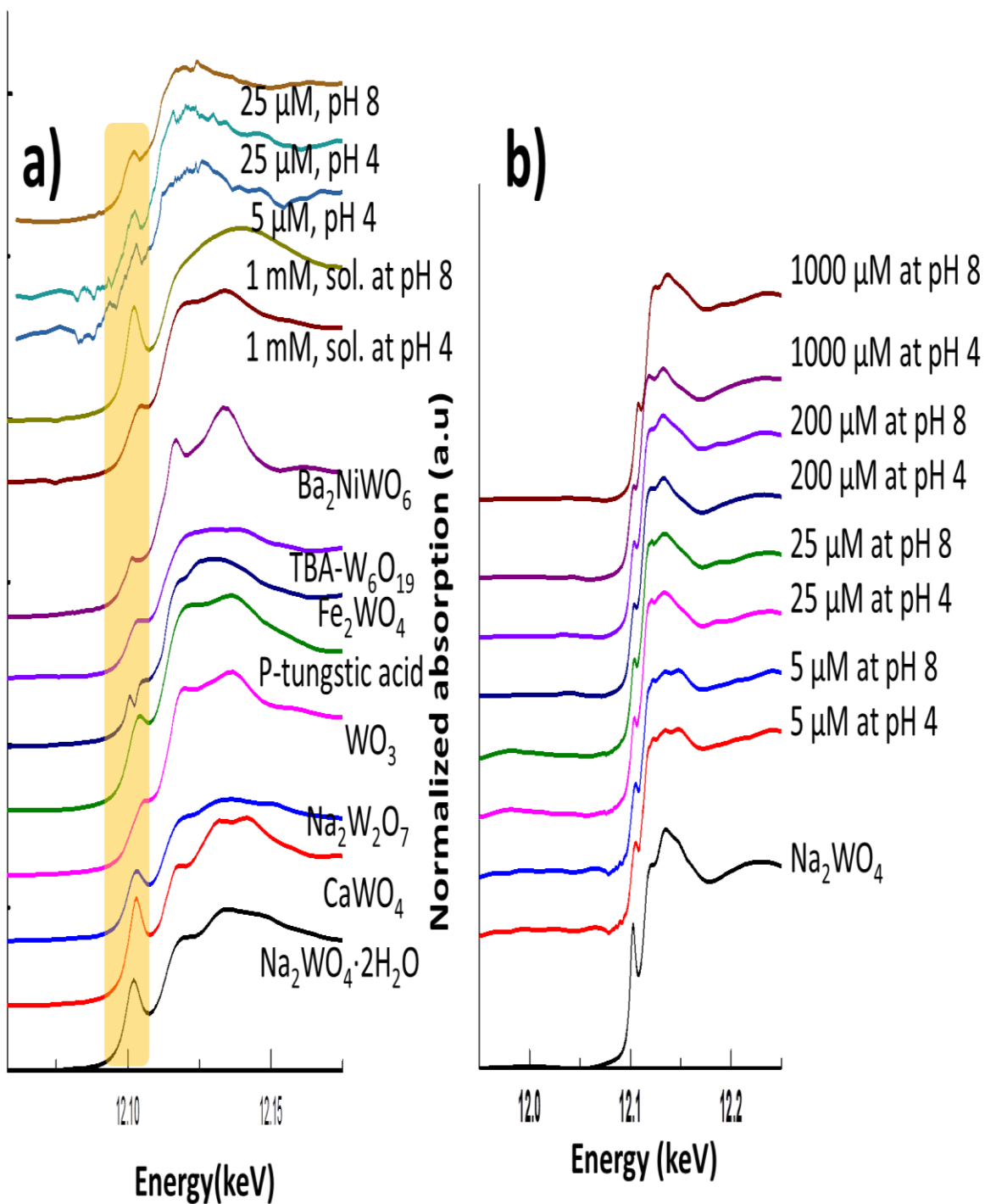
Figure 2. 7. a) Normalized W L_1-edge XANES spectra for selected reference compounds, 1 mM tungstate solutions at pH 4 and pH 8, and sorption samples at W concentrations of 5 and 25 μM. b) W L_1-edge XANES results of sorption samples comparing to Na_2WO_4, tetrahedral coordination.

2.3.8 Combining of L_1-edge and L_3-edge XANES

By combining the pre-edge peak area from L_1-edge XANES with the energy separation between minima in the L_3-edge second derivatives, clear differences are evident among W(VI) coordination environments (Figure 2.8). $Na_2WO_4 \cdot 2H_2O$ and $CaWO_4$, both with tetrahedrally coordinated W, lie at one end of a trend, distinguished by a large pre-edge area in W L_1-edge XANES and a small energy separation in W L_3-edge second derivatives. On the other end of this trend lies Ba_2NiWO_6, with perfect octahedral coordination, having a relatively small pre-edge area and a large energy seperation in the second derivative. Reference compounds with more distorted octahedra, such as WO_3, phosphotungstic acid, and sodium metatungstate, lie at intermediate positions along the trend, reflecting intermediate values of pre-edge peak area and energy separation. All of the sorption samples are tightly clustered at an intermediate position along the trend (within the yellow circle, Figure 2.8). Their proximity near $Na_2W_2O_7$, which contains both tetrahedral and octahedral W(VI) might suggest that the sorption samples also contain mixtures of W(VI) tetrahedra and octrahedra. However, the second derivative spectra for the L_3-edge (Figure 2.6) clearly indicate that all sorption samples are octahedrally coordinated, as described in the previous section.
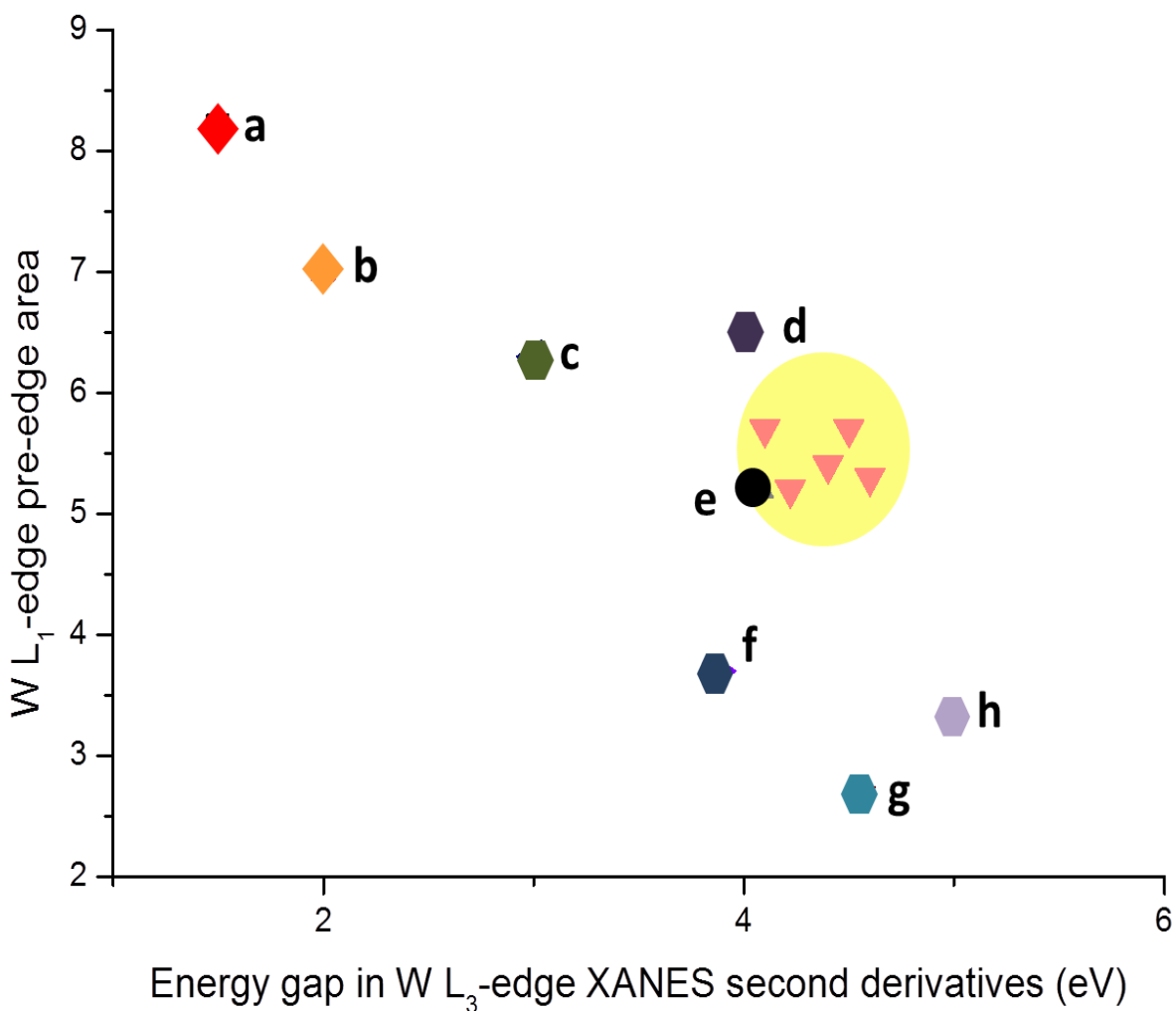
Figure 2. 8. The relationship between the splitting of the minima in the L_3-edge XANES second derviatives and the pre-edge peak area of L_1-edge XANES. a) $Na_2WO_4 \cdot 2H_2O$, b) $CaWO_4$, c) Phosphotungstic acid, d) WO_3, e) $Na_2W_2O_7$, f) Sodium metatungstate, g) Ba_2NiWO_6, h) TBA-W_6O_{19}. All sorption samples are tightly clustered (yellow circle).

Table 2. 2. The summary of enregy gap in W L_3-edge XANES second derivatives and the pre-edge area in W L_1-edge XANES for all sorptio samples.

Name	Energy gap (eV)[a]	Pre-edge area (eV)[b]
5 µM at pH 4	4.22	5.2
5 µM at pH 8	4.22	5.3
200 µM at pH 4	4.1	5.7
200 µM at pH 8	4.5	5.7
1000 µM at pH 4	4.6	5.4
1000 µM at pH 8	4.4	5.3

a : energy gap of W L_3-edge XANES second derivatives

b : Pre-edge area of W L_1-edge XANES

2.3.9 W L$_3$-edge EXAFS

2.3.9.1 Model compounds and tungstate reference solutions

W L$_3$-edge EXAFS provides further insight to local structure of sorbed W(VI). EXAFS chi functions and corresponding Fourier transforms are shown in Figure 2.9 for selected model compounds and aqueous tungstate solutions at pH 4 and 8. Fitting results are summarzied in Table 2.3.

The 1 mM pH 4 and 8 solutions show distinct differences in their chi curves and FT magnititudes (Figure 2.9). The chi function for the pH 8 solution shows a single beat and the FT magnitude shows a corresponding single peak, similar in character to the Na$_2$WO$_4$.2H$_2$O reference sample, which contains only tungstate tetrahedra. The pH 8 solution data were best fit with a single shell of W-O atoms at 1.78 Å, which is characteristic of tetrahedral W(VI) coordination, and consistent with the dominance of monomeric tetrahedral species expected at pH 8. In contrast, the pH 4 solution shows several oscillations with different phases in the chi curve, with evident splitting in the first two oscillations, similar to the splitting observed for the polymeric reference samples. The FT magnitude for the pH 4 solution shows a split first peak with weaker peaks at higher R. The split first peak compares with the polymeric reference compounds but with a different asymmetry in intensities. The distinguishing feature of polytungstates is connected W(VI) octahedra, which should be evident in FT data as peaks at greater distances, like those seen in model compounds (in Figure 2.9). The peaks in the range 3.3-3.8 Å are consistent with edge- and corner-sharing of tungstate octahedra, and confirmed by fitting reference compounds. At pH 4, polymerization is favored, with H$_2$W$_{12}$O$_{40}$$^{6-}$ being the dominant species based on the calculations in section 3.1 and confirmed by the ESI-MS results showing the likely presence of multiple polytungstate speciecs. The structure of H$_2$W$_{12}$O$_{40}$$^{6-}$

contains two distinct W-W distances, ~3.3 Å for edge-sharing and ~3.8 Å for corner-sharing. These distances are consistent with our EXAFS result for the solution at pH 4. However, we cannot uniquely identify the metatungstate species or rule out the presence of other polymeric tungstate species, inasmuch as they share the distinctive edge- and corner-sharing of W(VI) octahedra and would not be distinguishable by EXAFS. Nevertheless, the EXAFS results confirm the dominance of polymeric tungstate species in the pH 4 solution, whereas the pH 8 solution contains monomeric tetrahedral tungstate.

$Na_2WO_4 \cdot 2H_2O$ is representative of a monotungstate, with W(VI) in tetrahedral coordination with four oxygen atoms at 1.79 Å. Na-metatungstate ($Na_6(H_2W_{12}O_{40}) \cdot xH_2O$) contains distorted W(VI) octahedra with two tungsten atoms at 3.3 Å (edge-sharing) and two tungsten atoms at 3.7 Å (corner-sharing). WO_3 was fit with six oxygen atoms in three shells (2 each at 1.77, 1.93, and 2.14 Å). W-W distances occur at ~3.7 Å in the exclusively corner-sharing structure. TBA-W_6O_{19} contains distorted W(VI) octahedra; the first shell was fit with one oxygen atom at 1.71 Å, four oxygen atoms at 1.93 Å, and one oxygen atom at 2.32 Å. The W(VI) octahedra in TBA-W_6O_{19} are edge-sharing, with W-W distances at ~3.3 Å. The different shapes of the first peak in the Fourier transform magnitudes were attributed to the distortion of W-O. More distorted model compounds such as Na-metatungstate and TBA-W_6O_{19} show split features in the first shell (Figure 2.9).
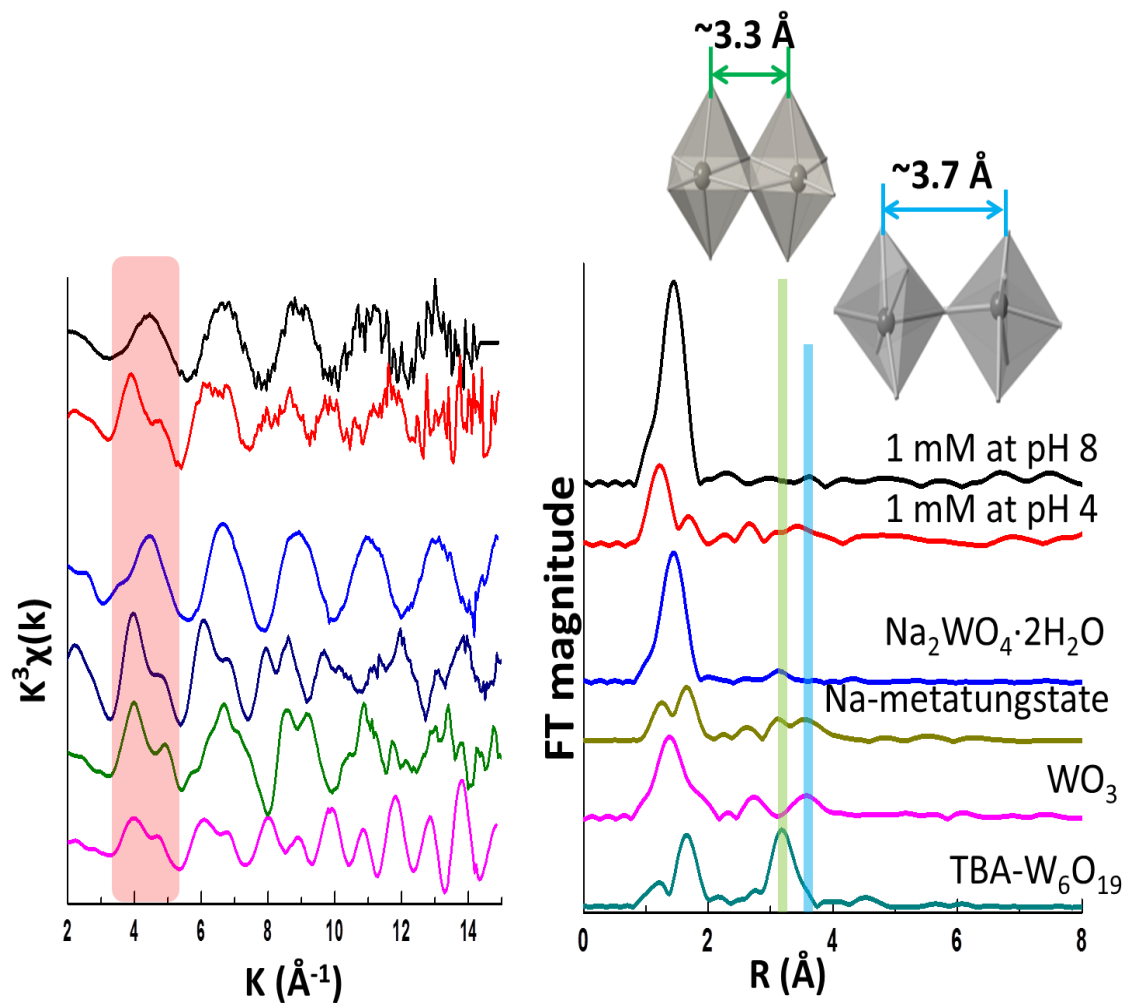
Figure 2. 9. W L_3-edge EXAFS chi functions (left) and corresponding Fourier transform magnitudes (right, not corrected for phase shifts) for 1 mM tungstate solutions (pH 4 and 8) and selected model compounds. The peaks near 3.3 – 3.7 Å in the FT magnitude correspond to W-W backscattering from edge- and corner sharing tungsten units. 1 mM Na_2WO_4 solution at pH 8 showed strong peak near 1.78 Å while several other peak appeared at further distance in 1 mM at pH 4.

Table 2. 3. Summary of W L$_3$-edge EXAFS fitting results of model compounds

Sample	Path	CN[a]	R(Å)[b]	σ^2(Å^2)[c]	ΔE0 (eV)
Na$_2$WO$_4$·2H$_2$O	W-O1	4*	1.78	0.004	10.7
	W-O2	4*	3.71	0.013	
TBA-W$_6$O$_{19}$	W-O1	1.0*	1.71	0.002	10.5
	W-O2	4.0*	1.92	0.003	
	W-O3	1*	2.32	0.004	
	W-W1	4.0*	3.30	0.004	
WO$_3$	W-O1	2*	1.78	0.001	11.3
	W-O2	2*	1.93	0.007	
	W-O3	2*	2.14	0.004	
	W-W	2*	3.78	0.002	
	W-W	4*	3.9	0.006	
Na$_6$(H$_2$W$_{12}$O$_{40}$)·xH$_2$O	W-O	3*	1.76	0.009	5.6
	W-O	2*	1.93	0.002	
	W-O	1*	2.17	0.008	
	W-W	2*	3.24	0.012	
	W-W	2*	3.68	0.006	

*: fixed in the fitting,

a : coordination number (±20%), b: distance in Å (±0.02 Å),

c : Debye-Waller factor,

2.3.9.2 Tungstate sorption samples

The W L$_3$-edge EXAFS of tungstate-sorbed boehmite samples at different tungstate concentrations and pH conditions are compared in Figure 2.10. Based on the experimental isotherms, we chose sorption samples for EXAFS study at three total W concentrations: 5, 200, and 1000 µM. At pH 4, these concentrations result in coverages of 0.022, 0.197, and 0.557 mmol/g, corresponding to less than theoretical monolayer coverage, near monolayer coverage, and greater than monolayer coverage, respectively. The surface coverages at pH 8, 0.007, 0.014, and 0.125 mmol/g, are all less than the theoretical monolayer coverage. The most striking observation is that the chi functions are broadly similar for all samples, with the only obvious exception being the 1000 µM sample at pH 4 (Figure 2.10). All chi functions show a split first oscillation and a sharp second oscillation apparently from interference with a second or additional beat. The 1000 µM sample at pH 4 shows an asymmetry in the split first oscillation in the chi function compared to other samples, as well as a different or additional phase obvious at higher k.

The corresponding FT magnitudes show generally similar first peaks, corresponding to first-shell W-O coordination, but important differences are evident in weaker peaks at higher R values. For the lowest concentration samples, 5 µM tungstate, no discernible differences are evident between pH 4 and 8 conditions. Similarly, the FT magnitudes for the 200 µM samples at pH 4 and 8 are similar to one another, but differ from the 5 µM sample by the presence of a pair of weak but distinct peaks at 2.5-3.0 Å (Figure 2.10, not corrected for phase shifts), consistent with backscattering from W or Al. The FT magnitude for the 1000 µM sample at pH 8 is indistinguishable from the 200 µM sample, whereas the 1000 µM sample at pH 4 shows more

features in the range 3.0-3.5 Å (Figure 2.10, not corrected for phase shifts). Fitting described in

the following section provides further information about local structure.
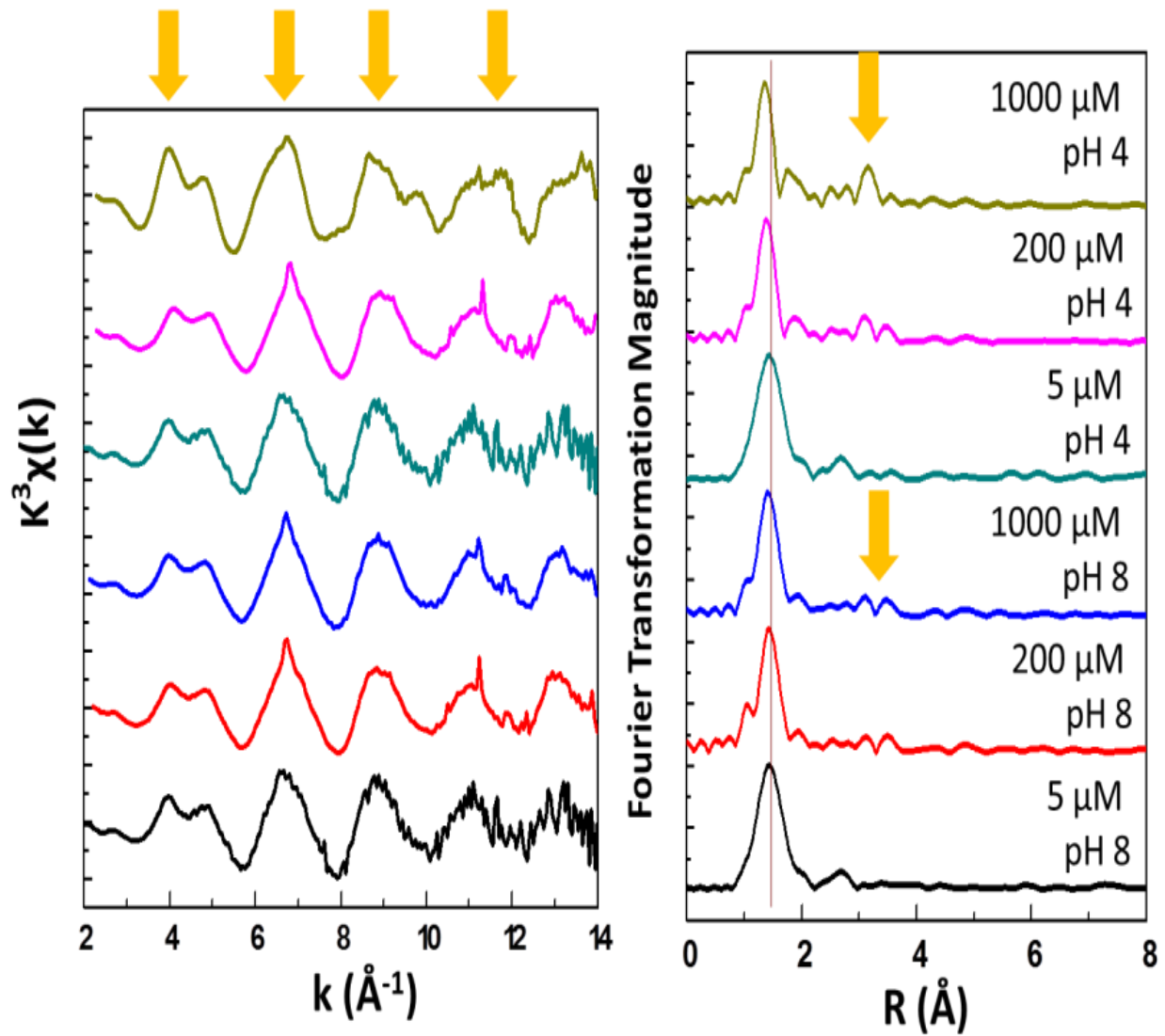
Figure 2. 10. W L$_3$-edge EXAFS data for tungstate sorbed on boehmite. Arrows indicate the differences between sorption samples in EXAFS spectra.

2.3.10 W L$_3$-edge EXAFS fitting

Shell by shell fitting in real space was performed as described in section 2.5.2. Fitting results for representative samples are shown in Figure 2.10, and all fit results are summarized in Table 2.4. Both 5 µM tungstate sorption samples (pH 4 and 8) were fit best with two W-O paths (1.75 and 2.14 Å) for the first peak with a combined coordination number (CN) of 6.3 (± 1.2). This gave a clearly better fit than a single path. The split first shell, with an average W-O distance of 1.95 Å, is consistent with octahedral coordination in which the W atom is off-centered, confirming that the dominant W(VI) component sorbed on boehmite is octahedrally coordinated. This finding agrees with W L$_1$- and L$_3$-edge XANES results, showing distorted octahedral coordination at both pH 4 and 8. Based on fits of polymeric tungstate model compounds, and consistent with the findings of Kuzmin,[27] it was necessary to introduce a multiple scattering (MS) contribution to satisfactorily fit the splitting in the first oscillation in the chi functions at 3–3.5 Å^{-1}. A four-leg, near linear O-W-O path, based on the configuration in sodium metatungstate, was found to be suitable. The weak peak at 2.7 Å in the FT (not corrected for phase shift) was alternately fit with a W-Al path and a W-W path. The fit with 2.2 Al at 3.1 Å was favored, inasmuch as fits with a W-W path gave a distance (2.8 Å) considered to be unrealistically short. Furthermore, the intensity of this peak decreases as tungstate concentration increases in the solution.

Fitting of the 200 and 1000 µM pH 8 samples gave similar fit results. The first peak was again best fit with two W-O paths at 1.75 and 2.15 Å. A MS path was again found to be necessary. The peaks near 3.3–3.8 Å were best fit with two W-W path at 3.23 and 3.73 Å, with combined CN of 2.2 ± 0.4. Fits were also attempted with W-Al paths, however, these fits were

either not satisfactory or resulted in W-Al distances that were not reasonable. The peaks near 3.3-3.8 Å appear with increasing tungstate concentration, while the peak at 3.1 Å in the 5 µM pH 8 sample diminishes as tungstate concentration increases, indicating that increasing W-W coordination (near 3.3-3.8 Å) is linked to tungstate concentration.

The 200 µM sorption sample was best fit with three W-O paths at 1.73, 1.90 and 2.19 Å, and a W-W path at 3.25 Å. In fitting the 200 µM sorption sample, a second W-W path was introduced to fit the right shoulder near 3.3 Å in the FT (not corrected for phase shift) which is similar to the feature in the sorption samples at pH 8. The 1000 µM sorption sample was best fit with three W-O paths at 1.74, 1.98, and 2.21 Å, and a W-W path at 3.25 Å. The coordination number for the first shell of the 200 µM and 1000 µM at pH 4 samples was set to a value of 6 based on analysis of the W L_1- and L_3-edge XANES results. We constrained the CN of each W-O path to 2 based on the W-O paths in model compounds. Fits using two and three W-O paths constrained to total CN of 6 were compared for fitting the first peak in the FT. Not surprisingly, the use of three W-O paths gave a better fit to the first oscillation in the chi function and the first peak in the FT, but neither case fit the observed splitting of this oscillation ideally. Fit results were compared with and without a W-Al path, with slightly better results obtained by including W-Al, and especially the small feature near 2.5 Å in the FT (not corrected for phase shift) occurring at the same position of the W-Al path in the 5 µM sorption samples. The second shell in the 1000 µM at pH 4 sample was best fit with a W-W path near 3.25 Å, consistent with edge-sharing W-W. This peak also appears with increasing tungstate cocentration in the solution. We also attempted fits using additional W-W paths to explore possible destructive interference resulting from multiple closely spaced W-W backscattering paths. However, this resulted in unrealistic parameters with no clear improvement in fit results.
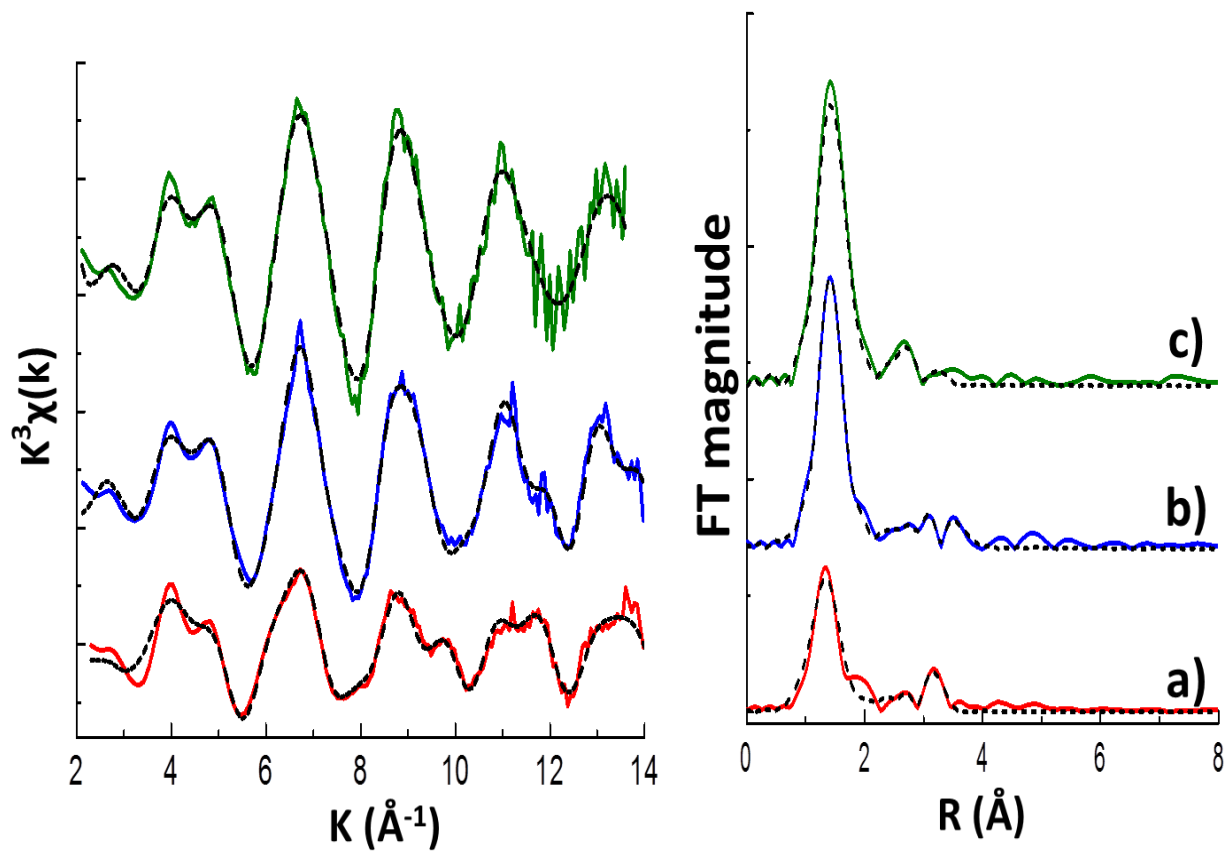
Figure 2. 11. EXAFS chi functions (left) and FT magnitudes (right) and corresponding fits for selected sorption samples. a) 1000 µM at pH 4, b) 1000 µM at pH 8, c) 5 µM at pH 4 Colored lines are EXAFS data for sorption samples and dotted lines are fitting results.

Table 2. 4. Summary of EXAFS fitting results for tungstate-sorbed boehmite samples

Sample	Path	CN[a]	R (Å)[b]	σ^2 (Å^2)[c]	$\Delta E0$ (eV)
5 µM	W-O1	3.1	1.75	0.002	
	W-O2	3.2	2.14	0.009	3.4
pH 4 and 8	W-Al	2.2	3.14	0.01	
	W-O1	3.0	1.75	0.003	
1000 µM	W-O2	4.0	2.14	0.009	
	W-Al	2*	3.14	0.012	-0.4
pH 8	W-W1	0.6	3.23	0.004	
	W-W2	1.6	3.73	0.007	
	W-O1	2*	1.73	0.003	
	W-O2	2*	1.90	0.019	
200 µM	W-O3	2*	2.19	0.007	
	W-Al	2*	3.19	0.012	-4.1
pH 4	W-W	2.4	3.25	0.008	
	W-W	1.3	3.69	0.008	
	W-O1	2*	1.74	0.003	
1000 µM	W-O2	2*	1.98	0.019	
	W-O3	2*	2.21	0.006	-1.2
pH 4	W-Al	2*	3.15	0.015	
	W-W	3.4	3.25	0.008	

*: fixed in the fitting,

a : coordination number (±20%), b: distance in Å (±0.02 Å),

c : Debye-Waller factor

2.4. Discussion

Tungstate shows a strong affinity for sorbing onto boehmite at low and neutral pH conditions, with decreasing uptake at higher pH. Observed uptake above the PZC value of boehmite (pH 8.7) indicates that tungstate sorption is not due entirely to electrostatic attraction. This result is consistent with previous studies investigating the reaction of tungstates with other mineral-water interfaces.[16, 17, 39] The absence of a maximum in uptake of tungstate with increasing concentration in the solution suggests that tungstate sorption on the surface is not limited by the surface site availability. The desorption experiments show that tungstate uptake is essentially irreversible at pH 4 and only partly reversible at pH 8. Sorption irreversibility is commonly attributed to formation of a surface precipitate or to coprecipitation, where release of the adsorbate to solution is restricted either because of its greater stability on (or in) the solid or due to a kinetic hindrance.[40, 41] These desorption results imply some differences in sorption complex on the boehmite surface at pH 4 and pH 8.

The most striking finding in our study, however, is the almost exclusive occurrence of polymeric tungstates at the boehmite surface from sorption experiments at both pH 4 and 8. While not surprising for pH 4 sorption samples, this finding was unexpected at pH 8, where monotungstate dominates in solution. Furthermore, the tungsten XANES and EXAFS signatures of the sorbed polymeric tungstates are almost indistinguishable between these two pH conditions, showing clear variation only with increasing total tungsten concentration. The L_1- and L_3-edge XANES results confirm distorted octahedral coordination of W(VI) for all sorption samples. The L_3-edge EXAFS is consistent with such coordination, and also confirms W-W distances that correspond directly to corner- and edge-sharing of W(VI) octahedra. These XANES and EXAFS signatures are distinguishing characteristics of polymeric tungstate species. However, because

many different polytungstates share these features in some combination, we are unable to identify individual species. It is also possible, perhaps even likely, that multiple tungstate species occur on the boehmite surface. Possible evidence supporting that may be found in the change of EXAFS results with increasing concentration. ESI results show several types of polytungstates in pH 4 solution, and previous studies reported various intermediate polytungstate species.[4-6, 14] Those polymeric tungstates are possible candidates for surface complexes. Yet, the XANES and EXAFS of the sorption samples do not match exactly any particular model compounds we examined. While ESI-MS result of pH 4 stock solution shows monotungstate as only a minor component, monotungstate is the dominant species in stock solution at pH 8. Our XANES and EXAFS results confirm the polytungstates as the major surface complexes. However, it is not possible to entirely rule out the occurrence of a minor component of tetrahedral tungstate co-existing with polymeric forms on the surface.

The occurrence of one or more polymeric tungstate species in sorption samples at pH 4, where polymerization dominates in solution, is not surprising. However, our results at pH 8 lead us to conclude that one or more polymeric tungstate species forms during uptake at the boehmite surface, inasmuch as the dominant solution species is a monomer. Furthermore, this is accompanied by a change from tetrahedral coordination of W(VI) in solution to octahedral coordination in the polymeric surface complex. The precise details of how the polymerization and change in coordination occur remain unclear, as does the actual form of the surface species. Yet, interaction of tungstate with the boehmite surface seemingly must favor a coordination change and polymerization. Previous studies of tungstate sorption on iron and manganese oxide have suggested the existence of monomeric tungstate with octahedral coordination on the surface at pH 8.[39] However, the tungstate concentrations used in that study (0.15-100 µM) were

restricted to the lower end of the range in our study (5-1000 µM), so that only our lowest concentration sample can be compared with their results. Yet, our results are consistent with octahedral coordination and the absence of clear W-W backscattering could provide plausible evidence for a monomeric tungstate on the surface at this low W concentration (5 µM). However, we cannot entirely rule out the possibility that polymeric tungstate exists on the surface, especially at pH 4 where the polymeric species $H_2W_{12}O_{40}^{6-}$ is dominant in solution. We also note that Clausen et al. reported polytungstates species present in firing range soils at pH 6, with EXAFS data suggesting an α-Keggin type cluster.[42] We are not aware of any other reports of polymeric tungstate sorption complexes at basic pH conditions.

The inability to identify the particular type of the sorbed polymeric tungstate(s) because of the similarities they share in coordination and configuration raises interesting questions. First, do multiple species occur at surface, i.e., more than one type of polymeric unit? This possibility might be anticipated at low pH because of the presence of multiple polytungstate species in solution, some of which may be metastable species associated with slow polymerization kinetics. The subtle changes observed in EXAFS with increasing W concentration at pH 4 may reflect the appearance of additional surface species at the higher end of the concentration range. Differences in the EXAFS are also observed with increasing concentration at pH 8, although the highest concentration samples differ from those at pH 4 (Figure 2.10).

A related question is whether the differences in sorption reversibility between pH 4 and 8 can be explained by different surface complexes. Sorption at pH 4 is largely irreversible, whereas at pH 8 some reversibility (25-30 %) is observed. EXAFS results for the 1000 µM sorption samples reveal differences between pH 4 and 8, suggesting that structural differences in the surface complexes could be responsible the desorption behavior. However, no obvious

differences in the EXAFS are observed between the pH 4 and 8 sorption samples at the lower concentration 200 µM); yet the same difference in sorption reversibility is found at both concentrations. This suggests that pH may play the more important role in controlling the observed sorption reversibility. Polymerization behavior in solution may provide a useful analogy. At low pH polymerization of W(VI) is clearly favored, whereas at near neutral and higher pH, monomeric tungstate is favored. Hence, we might speculate that the surface complexes are more stable at pH 4 than at pH 8. This would be consistent with irreversible sorption at the lower pH but some limited degree of reversibility at the higher pH. The effect of pH on surface charge may also play a role in sorption reversibility. The more positively charged surface at pH 4 would create more favorable circumstances for sorbed polytungstates, which have large negative charges. Neither explanation precludes differences in the surface complexes themselves. Nor does it rule out the possible existence of multiple tungstate species on the surface could be an alternative explanation for different reversibility, although exact tungstate species are not distinguishable by EXAFS as note earlier.

It is also interesting to consider if formation of polymeric tungstates at the surface is analogous (in some ways) to surface precipitation. In both cases, W(VI) forms extended structures at the surface. We consider that no distinction between them would be difficult using EXAFS.

In view of the similarities noted between tungstate and molybdate systems, it is interesting to compare their sorption behavior. Molybdate shows a distribution of species in solution broadly similar to tungstate, favoring monomeric species at neutral and high pH and formation of polymeric species at low pH.[11] Arai investigated molybdate species sorbed on the goethite surface using Mo K-edge EXAFS.[43] This study reported the existence of monomeric

tetrahedral molybdate at the surface at near neutral pH and a mixture of monomeric tetrahedral and polymeric octahedral molybdate at acidic pH. Increasing Mo loading favored the formation of the polymeric form. Wasylenki et al. used Mo K-edge EXAFS to investigate molybdate species sorbed on birnessite (MnO_2).[44] In sorption experiments performed at pH 8.0-8.5, where monomeric tetrahedral molybdate is the dominant solution species, they found the sorbed species to be a polymeric molybdate with distorted octahedral coordination. This finding differs from the results of Arai at near neutral pH, where monomeric tetrahedral molybdate was reported. This difference may reflect the differing properties of the sorbent phases and/or their surface charge. However, both studies identified the tendency for molybdate to polymerize when sorbed at metal (hydr)oxide surface, although at different pH conditions. In our study, we find that tungstate exhibits a strong tendency to sorb as a polymeric species to the surface of boehmite over the entire range of experimental conditions studied. At pH 8, sorption is accompanied by a change in W(VI) coordination from tetrahedral (in solution) to distorted octahedral (on the surface). The tendency that we observe for polymerization of tungstate over the entire pH range 4-8 may reflect the different sorbent (boehmite) and/or a greater inherent tendency for tungstate to polymerize compared to molybdate. Further studies of tungstate sorption on different mineral surfaces are needed to evaluate the importance of surface-driven tungstate polymerization.

The coordination change and the polymerization of tungstate sobred on boehmite at pH 8 were observed by XANES and EXAFS in our study. However, the mechanisms still remain unclear. Our hypothesis is that formation of an inner-sphere surface complex could induce the observed symmetry change from tetrahedral WO_4^{2-} to octahedral coordination, with the addition of water molecules. Like other tetrahedral oxyanions (e.g., PO_4^{3-}), we presume that tetrahedral tungstate would initially form a bidentate binuclear surface complex on the boehmite surface at

pH 8.[39] Our EXAFS fitting results for 5 μM sorption sample at pH 8 support formation of an inner-sphere complex, showing a W-Al path at 3.14 Å . The W-O bonds for the oxygens bridging with Al atoms at the surface would lengthen, thereby lowering their bond strengths and also allowing introduction of water molecules that ultimately result in the symmetry change to octahedral coordination. (Figure 2.12)

Previous studies of tungstate species sorbed on aluminum oxide surfaces observed the coordination change of tungsten sorbed on the Al_2O_3 surface with two water molecules coordinated to tungsten.[37, 38] This hypothesis indicates the sorption modes of tungstate on mineral surfaces play important roles in the coordination change. Similar results were observed in previous studies of molybdate species on various oxide catalyst surfaces, such as δ-MnO_2, TiO_2, ferrihydrite, Al_2O_3, goethite, and hematite.[45-50] In these studies, molybdates forming inner-sphere complexes on δ-MnO_2, TiO_2, and hematite were found to have octahedral symmetry, while tetrahedral molybdates found on ferrihydrite and Al_2O_3 surfaces were interpreted to form outer-sphere complexes.[51] Furthermore, the different symmetries of Mo on Fe (oxyhydr)oxides implies that specific properties of the surface influence the symmetry change. Yet, the coordination change was clearly induced by the inner-sphere surface complexation of Mo in these studies. Further studies of tungstate sorption on various mineral surfaces are needed to reveal the relationship between the properties of the mineral surfaces and the symmetry change of adsorbed tungstate species.
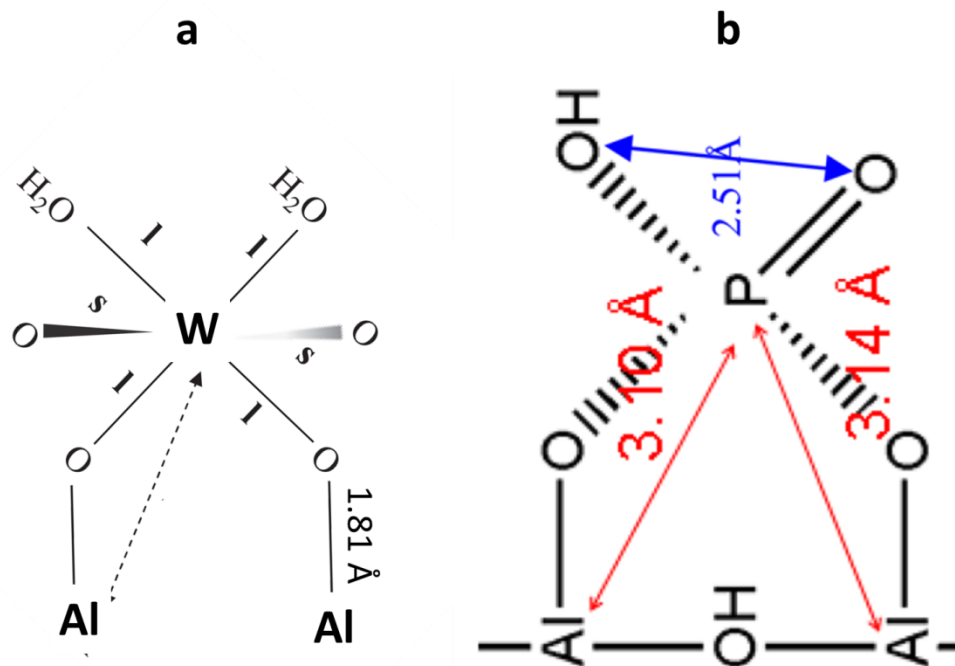
Figure 2. 12. Geometric models for (a) tungstate and (b) phosphate surface complexes on boehmite at pH 8.[39] (l: long, s: short) Bidentate binuclear model for tungstate was constructed using EXAFS fitting results. Graphic in (b) taken from reference 1.

We can envision two possible surface polymerization mechanisms: the polymerization of neighboring tungstate species sorbed on the surface and the additive polymerization with the tetrahedral residue in a terminal position. Schematic models for these mechanisms are shown in Figure 2.13. The former would be dependent on a sufficiently high surface coverage of tungstate to allow linkages that result in edge- or corner-sharing of tungstate octahedra. Furthermore, this mechanism may not be consistent with the continued tungstate uptake that we observed in the isotherm results, sincethis model reqires that polymerization occurs only between tungstate sorbed on the surface.

The second possible model is an example of open-chain polymerization, and is similar to the tungstate polymerization mechanism suggested by Walanda et. al in solution based on ESI-MS results.[14] Monotungstate surface complexes, which would be octahedral as described above, could act as preferred sites for attachment of tetrahedral tungstate species in solution. Hence, the tetrahedral tungstate at the end is open to form tungstate chains with additional monomers. Additional monomers share two oxygen atoms with tungstate seeds (tetrahedral), resulting in the coordination change of W to octahedral. Once the seeds have been formed by the surface sorption, polymerization is driven by the addition of monomers. This model allows continued attachment from solution, and is therefore consistent with the isotherm results. With the present information, we cannot determine which of these two possible mechanisms of tungstate polymerization are most likely in our experiments. Further studies using complementary approaches are needed to understand these mechanisms better.

a

b
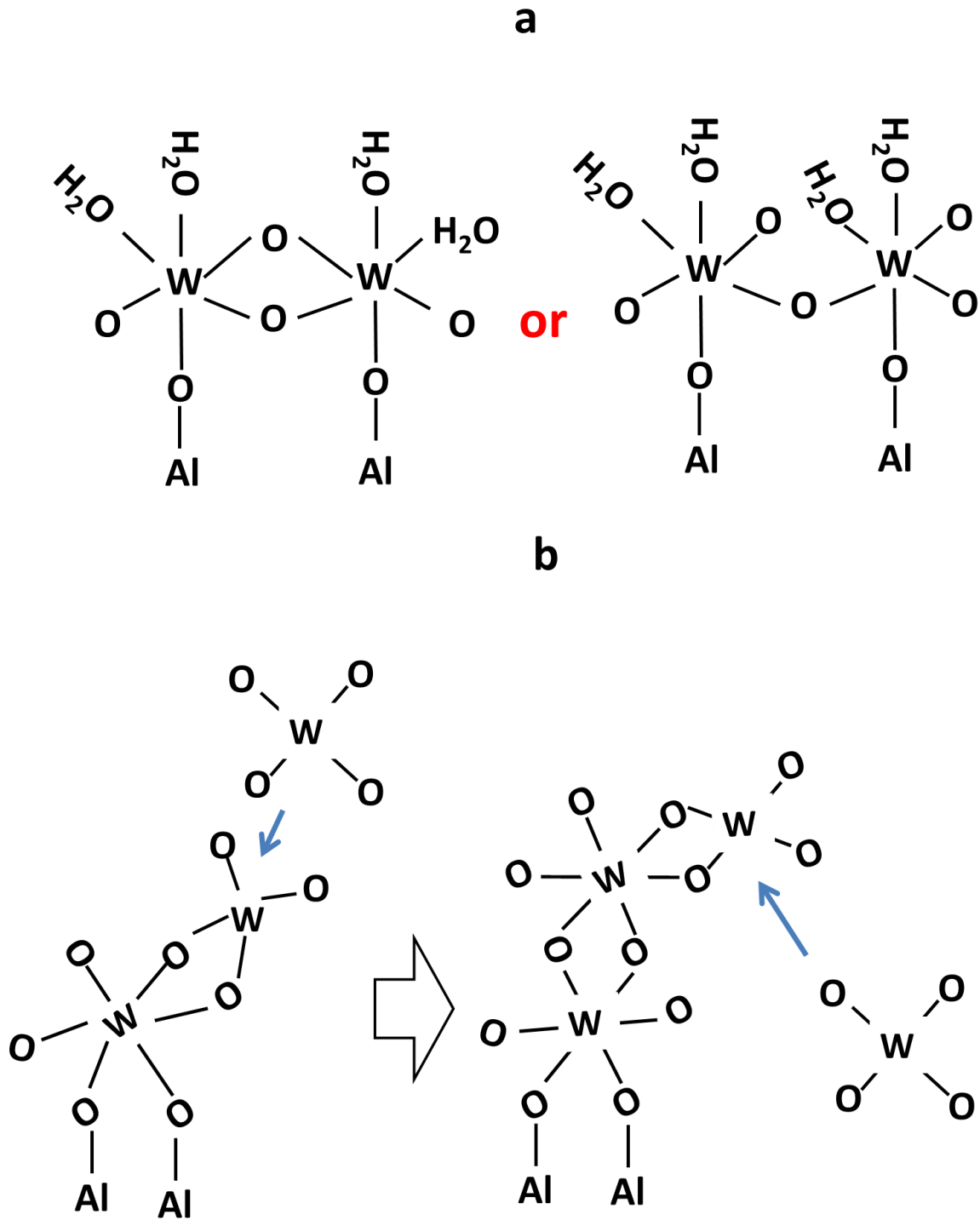
Figure 2. 13. Models of the surface polymerization of tungstate on the boehmite surface. The polymerization of neighboring tungstate surface complexes is shown in a. The open chain polymerization mechanism is depicted in b.

Strigul reported that speciation of tungstate is likely to be important for controlling its mobility, toxicity, and bioavailability in aquatic systems.[1] Our present findings demonstrate that tungstate forms stable polymeric surface complexes when sorbed on boehmite over a range of pH conditions. Hence the mobility of dissolved tungstate may be effectively limited by sorption on the boehmite surface. However, we still lack an understanding of the toxicity and bioavailability of polytungstates bound on the surface of fine mineral particles. Evaluation of the toxicity of polytungstates sorbed on other mineral surfaces will also be important for a complete understanding of the detailed environmental behavior of tungstate.

2.5. Conclusions

In this study, we examined the systematics and microscopic mechanisms of tungstate sorption onto boehmite over a range of pH values and tungstate concentrations. Batch uptake results reveal sorption behavior that is expected for anions, with tungstate binding strongly and irreversibly at low pH and less strongly with increasing pH. XAS analysis confirms the presence of polytungstate on the surface over the pH range 4-8, although the exact tungstate species cannot be determined. Polymerization of tungstate appears to be favored during sorption onto boehmite. At pH 8, where monotungstate is the dominant solution species, polymerization is accompanied by a change in coordination from tetrahedral (in solution) to octahedral in the surface complex. The results suggest that sorption onto boehmtie is an effective means for environmental remediation of dissolved tungstate. The role of the mineral surface in favoring polymerization of tungstate remains unclear, and further studies should be undertaken using different sorbent phases. The results of this study may also be significant for understanding tungstate mobility and bioavailability, which are strongly influenced by its sorption behavior,

and should be accounted for in models concerned with the solubility, mobility, and accumulation of tungsten species in natural environments.

Acknowledgements

Reference

1. Strigul, N., Does speciation matter for tungsten ecotoxicology? *Ecotox Environ Safe* **2010,** *73*, (6), 1099-1113.
2. Clausen, J. L.; Korte, N., Environmental fate of tungsten from military use. *Sci Total Environ* **2009,** *407*, (8), 2887-2893.
3. Bednar, A. J.; Jones, W. T.; Boyd, R. E.; Ringelberg, D. B.; Larson, S. L., Geochemical parameters influencing tungsten mobility in soils. *J Environ Qual* **2008,** *37*, (1), 229-233.
4. Smith, B. J.; Patrick, V. A., Quantitative determination of sodium metatungstate speciation by W-183 NMR spectroscopy. *Aust J Chem* **2000,** *53*, (11-12), 965-970.
5. Hastings, J. J.; Howarth, O. W., A W-183, H-1 and O-17 Nuclear-Magnetic-Resonance Study of Aqueous Isopolytungstates. *J Chem Soc Dalton* **1992**, (2), 209-215.
6. Cruywagen, J. J.; Vandermerwe, I. F. J., Tungsten(Vi) Equilibria - a Potentiometric and Calorimetric Investigation. *J Chem Soc Dalton* **1987**, (7), 1701-1705.
7. Dermatas, D.; Braida, W.; Christodoulatos, C.; Strigul, N.; Panikov, N.; Los, M.; Larson, S., Solubility, sorption, and soil respiration effects of tungsten and tungsten alloys. *Environ Forensics* **2004,** *5*, (1), 5-13.
8. Strigul, N.; Koutsospyros, A.; Arienti, P.; Christodoulatos, C.; Dermatas, D.; Braida, W., Effects of tungsten on environmental systems. *Chemosphere* **2005,** *61*, (2), 248-258.
9. Ringelberg, D. B.; Reynolds, C. M.; Winfield, L. E.; Inouye, L. S.; Johnson, D. R.; Bednar, A. J., Tungsten Effects on Microbial Community Structure and Activity in a Soil. *J Environ Qual* **2009,** *38*, (1), 103-110.
10. Strigul, N.; Koutsospyros, A.; Christodoulatos, C., Tungsten speciation and toxicity: Acute toxicity of mono- and poly-tungstates to fish. *Ecotox Environ Safe* **2010,** *73*, (2), 164-171.
11. Fierro, J., *Metal Oxides: chemistry and applications*. CRC press: 2006; Vol. 108.
12. Weckhuysen, B. M.; Wachs, I. E.; Schoonheydt, R. A., Surface chemistry and spectroscopy of chromium in inorganic oxides. *Chem Rev* **1996,** *96*, (8), 3327-3349.
13. Bailar, J. C.; Trotman-Dickenson, A. F., *Comprehensive inorganic chemistry*. Pergamon Press: 1973.
14. Walanda, D. K.; Burns, R. C.; Lawrance, G. A.; von Nagy-Felsobuki, E. I., Electrospray mass spectrometry of aqueous solutions of isopolyoxotungstates. *J Clust Sci* **2000,** *11*, (1), 5-28.
15. Aveston, J., Hydrolysis of Tungsten(6) - Ultracentrifugation Acidity Mearurements + Raman Spectra of Polytungstates. *Inorg Chem* **1964,** *3*, (7), 981-&.
16. Xu, N.; Christodoulatos, C.; Braida, W., Modeling the competitive effect of phosphate, sulfate, silicate, and tungstate anions on the adsorption of molybdate onto goethite. *Chemosphere* **2006,** *64*, (8), 1325-1333.
17. Gustafsson, J. P., Modelling molybdate and tungstate adsorption to ferrihydrite. *Chem Geol* **2003,** *200*, (1-2), 105-115.
18. Sugiyama, S.; Kanda, Y.; Ishizuka, H.; Sotowa, K. I., Removal and regeneration of aqueous divalent cations by boehmite. *J Colloid Interf Sci* **2008,** *320*, (2), 535-539.
19. Li, W.; Feng, J.; Kwon, K. D.; Kubicki, J. D.; Phillips, B. L., Surface Speciation of Phosphate on Boehmite (gamma-AlOOH) Determined from NMR Spectroscopy. *Langmuir* **2010,** *26*, (7), 4753-4761.

20. Strathmann, T. J.; Myneni, S. C. B., Effect of soil fulvic acid on nickel(II) sorption and bonding at the aqueous-boehmite (gamma-AIOOH) interface. *Environ Sci Technol* **2005,** *39*, (11), 4027-4034.

21. Granados-Correa, F.; Jimenez-Becerril, J., Chromium (VI) adsorption on boehmite. *J Hazard Mater* **2009,** *162*, (2-3), 1178-1184.

22. Nordin, J.; Persson, P.; Laiti, E.; Sjoberg, S., Adsorption of o-phthalate at the water-boehmite (gamma-AlOOH) interface: Evidence for two coordination modes. *Langmuir* **1997,** *13*, (15), 4085-4093.

23. Zabinsky, S. I.; Rehr, J. J.; Ankudinov, A.; Albers, R. C.; Eller, M. J., Multiple-Scattering Calculations of X-Ray-Absorption Spectra. *Phys Rev B* **1995,** *52*, (4), 2995-3009.

24. Ressler, T., WinXAS: A new software package not only for the analysis of energy-dispersive XAS data. *J Phys Iv* **1997,** *7*, (C2), 269-270.

25. Newville, M., IFEFFIT: interactive XAFS analysis and FEFF fitting. *J Synchrotron Radiat* **2001,** *8*, 322-324.

26. Ankoudinov, A. L. Relativistic Spin-dependent X-ray Absorption Theory. University of Washington, 1996.

27. Kuzmin, A.; Purans, J.; Benfatto, M.; Natoli, C. R., X-Ray-Absorption Study of Rhenium L3 and L1 Edges in Reo3 - Multiple-Scattering Approach. *Phys Rev B* **1993,** *47*, (5), 2480-2486.

28. Yamazoe, S.; Hitomi, Y.; Shishido, T.; Tanaka, T., XAFS study of tungsten L-1- and L-3-edges: Structural analysis of WO3 species loaded on TiO2 as a catalyst for photo-oxidation of NH3. *J Phys Chem C* **2008,** *112*, (17), 6869-6879.

29. Sanchez, C.; Livage, J.; Launay, J. P.; Fournier, M., Electron Delocalization in Mixed-Valence Tungsten Polyanions. *J Am Chem Soc* **1983,** *105*, (23), 6817-6823.

30. Liu, S. J.; Chen, Q. Y.; Zhang, P. M., Thermodynamic properties of Na2W2O7(s) and Na2W4O13(S) in the temperature range 298.15-1000 K. *Thermochim Acta* **2001,** *371*, (1-2), 7-11.

31. Rozantsev, G. M.; Sazonova, O. I., Thermodynamic parameters of interconversions of isopolyanions in solutions of tungsten(VI). *Russ J Coord Chem+* **2005,** *31*, (8), 552-558.

32. Parkhurst, D. L., User's guide to PHREEQC: A computer program for speciation, reaction-path, advective-transport, and inverse geochemical calculations. **1995**.

33. Vanput, J. W., Crystallization and Processing of Ammonium Paratungstate (Apt). *Int J Refract Met H* **1995,** *13*, (1-3), 61-76.

34. Ohlin, C. A., Reaction Dynamics and Solution Chemistry of Polyoxometalates by Electrospray Ionization Mass Spectrometry. *Chem-Asian J* **2012,** *7*, (2), 262-270.

35. Li, W.; Feng, X. H.; Yan, Y. P.; Sparks, D. L.; Phillips, B. L., Solid-State NMR Spectroscopic Study of Phosphate Sorption Mechanisms on Aluminum (Hydr)oxides. *Environ Sci Technol* **2013,** *47*, (15), 8308-8315.

36. Kuzmin, A.; Purans, J., Local atomic and electronic structure of tungsten ions in AWO(4) crystals of scheelite and wolframite types. *Radiat Meas* **2001,** *33*, (5), 583-586.

37. Hilbrig, F.; Gobel, H. E.; Knozinger, H.; Schmelz, H.; Lengeler, B., X-Ray Absorption-Spectroscopy Study of the Titania-Supported and Alumina-Supported Tungsten-Oxide System. *J Phys Chem-Us* **1991,** *95*, (18), 6973-6978.

38. Horsley, J. A.; Wachs, I. E.; Brown, J. M.; Via, G. H.; Hardcastle, F. D., Structure of Surface Tungsten-Oxide Species in the Wo3/Al2o3 Supported Oxide System from X-Ray

Absorption near-Edge Spectroscopy and Raman-Spectroscopy. *J Phys Chem-Us* **1987,** *91*, (15), 4014-4020.

39.   Kashiwabara, T.; Takahashi, Y.; Marcus, M. A.; Uruga, T.; Tanida, H.; Terada, Y.; Usui, A., Tungsten species in natural ferromanganese oxides related to its different behavior from molybdenum in oxic ocean. *Geochim Cosmochim Ac* **2013,** *106*, 364-378.

40.   Tang, Y. Z.; Reeder, R. J., Enhanced Uranium Sorption on Aluminum Oxide Pretreated with Arsenate. Part I: Batch Uptake Behavior. *Environ Sci Technol* **2009,** *43*, (12), 4446-4451.

41.   Tang, Y. Z.; McDonald, J.; Reeder, R. J., Enhanced Uranium Sorption on Aluminum Oxide Pretreated with Arsenate. Part II: Spectroscopic Studies. *Environ Sci Technol* **2009,** *43*, (12), 4452-4458.

42.   Clausen, J. L.; Bostick, B. C.; Bednar, A.; Sun, J.; Landis, J. D. *Tungsten Speciation in Firing Range Soils*; DTIC Document: 2011.

43.   Arai, Y., X-ray Absorption Spectroscopic Investigation of Molybdenum Multinuclear Sorption Mechanism at the Goethite-Water Interface. *Environ Sci Technol* **2010,** *44*, (22), 8491-8496.

44.   Wasylenki, L. E.; Weeks, C. L.; Bargar, J. R.; Spiro, T. G.; Hein, J. R.; Anbar, A. D., The molecular mechanism of Mo isotope fractionation during adsorption to birnessite. *Geochim Cosmochim Ac* **2011,** *75*, (17), 5019-5031.

45.   Mensch, C. T. J.; Vanveen, J. A. R.; Vanwingerden, B.; Vandijk, M. P., Extended X-Ray Absorption Fine-Structure Study of Mo/Al2o3 Samples Prepared by Equilibrium Adsorption of Ammonium Heptamolybdate. *J Phys Chem-Us* **1988,** *92*, (17), 4961-4964.

46.   Bare, S. R.; Mitchell, G. E.; Maj, J. J.; Vrieland, G. E.; Gland, J. L., Local Site Symmetry of Dispersed Molybdenum Oxide Catalysts - Xanes at the Mo L2,3-Edges. *J Phys Chem-Us* **1993,** *97*, (22), 6048-6053.

47.   Aritani, H.; Tanaka, T.; Funabiki, T.; Yoshida, S.; Eda, K.; Sotani, N.; Kudo, M.; Hasegawa, S., Study of the local structure of molybdenum-magnesium binary oxides by means of Mo L(3)-edge XANES and UV-vis spectroscopy. *J Phys Chem-Us* **1996,** *100*, (50), 19495-19501.

48.   Takenaka, S.; Tanaka, T.; Funabiki, T.; Yoshida, S., Structures of molybdenum species in silica-supported molybdenum oxide and alkali-ion-modified silica-supported molybdenum oxide. *J Phys Chem B* **1998,** *102*, (16), 2960-2969.

49.   Radhakrishnan, R.; Reed, C.; Oyama, S. T.; Seman, M.; Kondo, J. N.; Domen, K.; Ohminami, Y.; Asakura, K., Variability in the structure of supported MoO3 catalysts: Studies using Raman and X-ray absorption spectroscopy with ab initio calculations. *J Phys Chem B* **2001,** *105*, (36), 8519-8530.

50.   Lede, E. J.; Requejo, F. G.; Pawelec, B.; Fierro, J. L. G., XANES Mo L-edges and XPS study of mo loaded in HY zeolite. *J Phys Chem B* **2002,** *106*, (32), 7824-7831.

51.   Kashiwabara, T.; Takahashi, Y.; Tanimizu, M.; Usui, A., Molecular-scale mechanisms of distribution and isotopic fractionation of molybdenum between seawater and ferromanganese oxides. *Geochim Cosmochim Ac* **2011,** *75*, (19), 5762-5784.

Chpter 3. Co-sorption of tungstate and cobalt on boehmite: Mechanisms of uptake enhancement

Abstract

Co(II) effects on tungstate sorption on the boehmite (γ-AlOOH) surface were studied using systematic batch uptake experiments and X-ray absorption spectroscopy. Tungstate uptake over the range of $[WO_4^{2-}]$ = 50-1000 µM increased with increasing tungstate concentrations in the solution, and the isotherm experiments revealed that tungstate uptake is strongly linked to the amount of Co(II) on the surface. Desorption experiments showed that tungstate sorption is less reversible with the Co(II) existence. The CoAl LDH formation on the surface was confirmed using XRD and XAS. Tungsten L_3-edge XANES revealed that all sorption samples are octahedral W(VI). The change of energy gaps in L_3-edge XANES and the desorption results support the tungstate intercalation mechanism for enhanced tungstate uptake at higher tungstate concentrations. The results of W L_3-edge XAS suggest that the surface sorption reaction mainly occurs on the surface at low tungstate concentration, while CoAl LDH plays an important role in tungstate sorption at higher tungstate concentration. Our results provide the importance of the LDH formation of cation, which influences tungstate sorption and the mobility.

3.1. Introduction

Recently, tungsten has received attention because of increasing awareness of its presence in soil and aquatic systems. Although it had long been considered as environmentally benign, recent findings suggest that oxidized species are both mobile and potentially toxic.[1] Tungsten metal and alloy, which are regarded as nontoxic materials, undergo oxidative dissolution under suitable conditions, forming tungstate, W(VI). The formation of tungstate may lead to adverse environmental effects, including soil acidification and toxicity effects in plants, soil microorganisms and invertebrates.[2-4] Recent studies have suggested that the toxicity of tungstates

is strongly linked to their speciation.[1] Under acidic soil and aquatic conditions, orthotungstate, WO_4^{2-}, the dominant species at near-neutral and basic pH, polymerizes to form a range of polymeric species. The polymerization reactions are complex, and strongly related to W concentration, solution pH, and reaction time.[1, 5] Recent studies have suggested that polytungstates may be more toxic than orthotungstate[1], underscoring the importance of determining environmental factors that limit the mobility and reactivity of tungstates in natural and engineered systems.

The fate of contaminants in aquatic and soil systems is commonly controlled by sorption reactions at mineral surfaces. Tungstate has been shown to adsorb on mineral surfaces depending on pH and other factors.[6-8] Tungstate uptake onto ferrihydrite has been studied experimentally and modeled using a diffuse layer model and the CD-MUSIC model, accounting for sorption of monomeric and polymeric tungstate.[7] Tungstate shows sorption behavior on mineral surfaces that is typical for anions, consistent with their dominant speciation in solution over a wide pH range.[6, 7] Maximum sorption occurs at acidic pH, and uptake decreases with increasing pH, so that sorption becomes significantly less effective at near neutral pH and higher. In a separate study we examined the character of surface complexes resulting from tungstate uptake onto boehmite at pH 4 and 8.(Chapter 2) A striking finding was the dominance of polymeric surface complexes—thought to be more toxic—at both pH conditions, even though the solution species at pH 8 is orthotungstate. The decreased effectiveness of sorption in limiting the mobility of dissolved tungstate at near neutral and basic pH makes it important to identify other factors that might enhance uptake on common mineral surfaces in order to develop effective methods for tungstate remediation in the environment.

Other studies have demonstrated that the presence of anions and cations together in aqueous solution may have a profound effect on their mutual sorption behaviors[9-15] Often, these mutual effects result not only in the formation of more stable surface complexes, but also enhanced uptake on the surface.[11, 13, 16] Previous studies demonstrated the co-precipitation reaction with cations and anion on mineral surfaces.[9-12] Other studies reported only the enhanced uptake by the change of point of zero charge and surface area.[14, 15, 17, 18] The cation effects on the anion speciation were reported in Cd(II) and phosphate co-sorption study on hematite by Elzinga et. al.[19] Tungstate sorption on γ-alumina has been observed to increase with the addition of cations.[20, 21] In these studies, tungstates were more effectively sorbed on the surface at and above neutral pH in the presence of Co(II) or Ni(II). The authors suggested that the increased tungstate uptake was a result of ternary complex on the surface with the cation at the surface, although no direct evidence was provided to support this. Furthermore, Co(II) (or Ni(II)) sorption mechanisms on aluminum (oxyhydr)oxide surfaces have been well known for the formation of polymeric Co(II) (or Ni(II)) species, Co(or Ni)Al Layered double hydroxide.

It is well known that several divalent cations, including Ni(II), Mn(II), Co(II), and Zn(II), may form layered double hydroxides (LDHs) on sorbents containing A(III) and Si(IV).[22] Co(II) sorption has been extensively investigated on a wide variety of mineral surfaces.[23-29] In previous studies sorption studies on alumina, Co(II) sorption mechanisms were found to depend on surface loading.[30] At low surface coverage (below 0.25 µmole/m^2), Co(II) forms mononuclear, inner-sphere complexes, while Co(II) reacts to form a Co-Al LDH as the surface loading increased (above 0.5 µmole/m^2).[30] Distinctive features in in EXAFS spectra have been used to confirm the formation of LDH on the surface, although some of these features are similar to Co(OH)$_2$ precipitates.[31] This Co(II)-Al LDH phase, based on the hydrotalcite structure, has been

identified in previous spectroscopic studies.[24, 25, 31-33] The formation of a Co(II)-containing as hydrotalcite-like structure, with a high capacity for anion sorption, could be an important mechanism for enhanced tungstate uptake on aluminum-containing solids.

Aluminum-containing minerals are abundant in soils and other environmental systems. In the present study we focus on the common mineral boehmite (γ-AlOOH), which has a simple, well–characterized structure.[34] Furthermore, Co(II) sorption mechanisms on aluminum oxide have been well studied.[25, 32] Boehmite also commonly has as high surface area (136 m^2/g in this study), which can facilitate sorption experiments. It is representative of aluminum minerals with octahedral coordination. Aluminum oxide minerals are also well suited for X-ray absorption spectroscopy (XAS), due to the low absorption edge energy of aluminum.

The goal of this study was to determine the effect of Co(II) on tungstate sorption on the boehmite surface at near-neutral pH, where enhancement of tungstate sorption is observed. The effect of Co(II) on tungstate uptake was investigated over a range of Co(II) and tungstate concentration at constant pH, 7.5. In this study, we focused on high cobalt surface coverage, which results in formation of CoAl LDH on the boehmite surface. Sorption studies showed enhanced tungstate uptake is strongly related to the CoAl formation on the boehmite surface. XAS was utilized to investigate tungstate and cobalt surface complexes on the surface. The findings allow us to propose strategies for enhancing tungstate remediation in contaminated systems.

3.2. Materials and Experiments

3.2.1. Chemicals

Boehmite from CONDEA Chemi GmbH was used in this study without further treatment. Powder XRD confirmed the structure without second phases. The surface area as measured by

BET analysis is 136 m^2/g, and point of zero charge (PZC) has been reported at 8.7.[34] Boehmite was equilibrated at pH 7.5 at least one day prior to further experiments. 0.01 M NaCl was added as a background electrolyte.

CoAl layered double hydroxide (LDH) was synthesized with the method previously described,[35] with the ratio 2(Co) : 1(Al). $CoCl_2$ (Acros) solution was added drop-wise into $AlCl_3 \cdot 6H_2O$ (Fisher scientific) solution at pH 8, controlled using an auto titrator with 0.1 M NaOH solution. Pinkish-colored, milky suspension formed upon addition of $CoCl_2$ solution. After reaction, the suspension was filtered and dried in an oven at 60 ℃. A powder XRD pattern was collected for the dry solid without any further processing.

3.2.2. Sorption isotherm / Desorption

All sorption and desorption experiments were conducted under atmospheric condition, using boehmite suspensions with 1 g/L particle loading and 0.01 M NaCl background electrolyte. Preliminary experiments were conducted that compared the sequence of addition of Co(II) and tungstate; in one set, Co and tungstate were added simultaneously to the equilibrated suspension and in a second set, Co was equilibrated in the suspension followed by addition of tungstate. Comparison showed no difference in the results of sorption behavior or XAS results. On this basis, for all subsequent sorption experiments desired amounts of Co(II) were added first from a 0.01 M $CoCl_2$ solution and allowed to equilibrate for 24 hr. Total Co concentrations of 100, 500, and 2000 μM were obtained. After equilibration, tungstate was added to obtain total W concentrations over the range 50-1000 boehmite suspensions with 1 g/L particle loading and 0.01 M NaCl, and again allowed to equilibrate for 24 h. For all sorption experiments, pH was maintained at a value of 7.5 using an auto-titrator with 0.1 M NaOH or HCl.

After equilibration, a small aliquot from each suspension was filtered with 0.45 μm pore syringe filter, and then tungstate concentration was analyzed in the solution using DCP-AES

(direct-coupled plasma atomic emission spectroscopy). Samples were filtered to retain solids, which were then used to collect W L_3-edge and Co K-edge EXAFS spectra as described below. Control experiments were performed using similar procedure except for the absence of boehmite sorbent (Co(II) = 100, 500, and 2000 µM; and tungstate = 50–2000 µM) to test for precipitation, but no precipitate was observed.

In separate experiments tungstate sorption on CoAl LDH was performed at W selected concentrations (25, 100, and 1000 µM) at pH 7.5 for 24 h with 0.01 M NaCl as a background electrolyte. The W-reacted CoAl LDH samples were vacuum-filtered, rinsed, and air-dried. XRD and W L_3-edge XAS were then collected as described below.

Desorption experiments were conducted for selected samples following sorption reactions as described above. First, 2000 µM Co(II) solution was reacted with boehmite suspension for 24 h, and the suspension centrifuged for 10 min at 10,000 rpm. The solution was discarded, and the moist particles were resuspended in Co(II)-free solution with the same pH and background electrolyte condition. Aliquots were taken at designated time periods, and Co concentration in the solution was measured by DCP-AES to allow calculation of sorbed Co. Second, 200 µM $Na_2WO_4 \cdot 2H_2O$ was reacted on the Co(II) treated boehmite surface for 24 h. The same procedures for Co(II) desorption experiments were performed to calculate W and Co concentrations on the surface.

3.2.3. Powder XRD

Powder XRD was used to confirm the identity of boehmite and CoAl LDH phases. Selected sorption samples after sorption experiments were filtered and dried at room temperature, and then analyzed by powder XRD. A Scintag Pad-X diffractometer, using Cu Kα radiation, was used with a scan rate was 0.2 °/minute from 5-45 2Θ. The XRD patterns of boehmite with the Co(II) sorption was compared with a pure boehmite pattern and the Co(II)

95

pre-treated boehmite. The peak positions and broadening for CoAl LDH were tracked for different tungstate concentrations.

3.2.4. X-ray absorption spectroscopy

Tungsten L_3-edge EXAFS and XANES were collected at beamline 12BM at the Advance Photon Source (Argonne National Laboratory). Cobalt K-edge EXAFS was collected at beamline X11B at the National Synchrotron Light Source (Brookhaven National Laboratory). Spectra were collected at the W L_3-edge (10.207 keV) and Co K-edge (7.709 keV) using a Si(111) monochrometer crystal with detuning of 10-30% for harmonic rejection. Energy calibration was performed with W metal foil (L_3-edge, 10.207 keV) or a Ga filter (K-edge, 10.367 keV), and Co metal foil (K-edge, 7.709 keV). The monochrometer was calibrated by assigning the indicated energies to the first peak of the derivative of the edge spectrum. All samples for the XAS data collection were loaded into Lucite holders and sealed with Kapton tape. Reference materials ($Na_2WO_4 \cdot 2H_2O$, WO_3, $Na_2W_2O_7$, $(TBA)_2W_6O_{16}$, $Co(OH)_2$) were mixed with boron nitride to obtain the proper edge step. The XAS data for the reference materials were collected in transition mode with gas-filled ionization chambers at room temperature. Fluorescence mode was used to collect XAS spectra for sorption samples and CoAl LDH with a Lytle detector or a Canberra 13-element solid-state Ge detector positioned at 90° to the incident beam. All samples were scanned multiple times to obtain adequate signal to noise ratio.

3.2.5. EXAFS analysis

Data processing was performed using the program WinXAS.[36, 37] Shell by shell fitting was conducted in R-space using standard procedures. All theoretical scattering paths were calculated using FEFF7 based on published structures of relevant model compounds.[38] Fitting of model compounds was begun using only single scattering paths, and scattering paths of like backscatters close to each other were combined to minimize the number of paths necessary to get

an acceptable fit. A single threshold energy value (ΔE_0) was allowed to vary during fitting. The amplitude reduction factor was fixed at $S_0{}^2 = 0.9$.

In W L_3-edge EXAFS fitting, a significant contribution of multiple scattering (MS) from near-linear chains, O-W-O, has been reported in previous studies.[39] (Our paper) Therefore, a MS path with 4 legs from near-linear O-W-O units was applied in all fitting.

In the fitting of W L_3-edge EXAFS spectra for sorption samples, no constraints were applied to fit first-neighbor oxygen shells. Debye-Waller factors were fixed at 0.008 (W-W and W-Co paths) and 0.01 Å^2 (a W-Al path) for second and higher shells, based on fits to model compounds. These values are in the range expected for higher shells (0.005-0.015 Å^2). The first main peak was found to be best fit using two W-O paths. A near-linear O-W-O MS path was introduced to account for the distinctive splitting in the first oscillation near 3.5-5 Å^{-1} in the chi function. We found that the MS contribution was mainly evident at low k in the chi function. In fitting the low-W (25 µM) sorption samples, a W-Al path was necessary to fit the peak near 2.7 Å in the Fourier transform (not corrected for phase shift), which is shorter than typical W-W and W-Co distances. For the higher concentration samples, two W-O paths were used to fit the first peak, and fitting results were compared using W-W, W-Co and their combination for the higher shells, 3.0-3.5 Å (not corrected for phase shift). Estimated errors are ±20% for the first oxygen shell and ±50% for the higher shells. Estimated Debye-Waller factors are ±0.001 Å^2 and ±0.005 Å^2 for first and higher shells respectively.

3.3. Results

3.3.1. Sorption Isotherm

Figure 3.1 shows tungstate sorption isotherm on Co(II)-sorbed boehmite. In preliminary sorption experiments, tungstate sorption was significantly affected by Co(II) at neutral and basic conditions, but slightly at acidic pH. Therefore, pH 7.5 was chosen for this study to minimize

Co(OH)$_2$ precipitate and to obtain greater Co(II) effects on tungstate sorption on the boehmite surface. The blank tests were conducted with 2000 µM Co(II) and tungsate concentrations in the solution without boehmite. In these tests, we did not observe any precipitation at pH 7.5. Overall, tungstate uptake increases as tungstate concentrations increase in the solution. The more interesting observation is the link between initial Co(II) concentration and the tungstate uptake on the boehmite surface. Figure 3.1 clearly shows more tungstate sorbed on the surface over the entire W concentration range as Co(II) concentration increases. This enhancement of tungstate uptake onto boehmite is significant, amounting to a three-fold increase over the Co concentration range studied. Sorbed tungstate over the range of initial tungstate concentrations (50-1000 µM) are 0.011-0.073 mmole/g, 0.021-0.126 mmole/g, and 0.029-0.216 mmole/g with no Co(II), 500 µM, and 2000 µM Co(II), respectively. At these conditions, the amount of Co(II) sorbed on the boehmite surface is 0.052 mmole/g for 500 µM and 0.150 mmole/g for 2000 µM, respectively. These results indicate that tungstate uptake is strongly related to the presence of Co(II) on the surface.
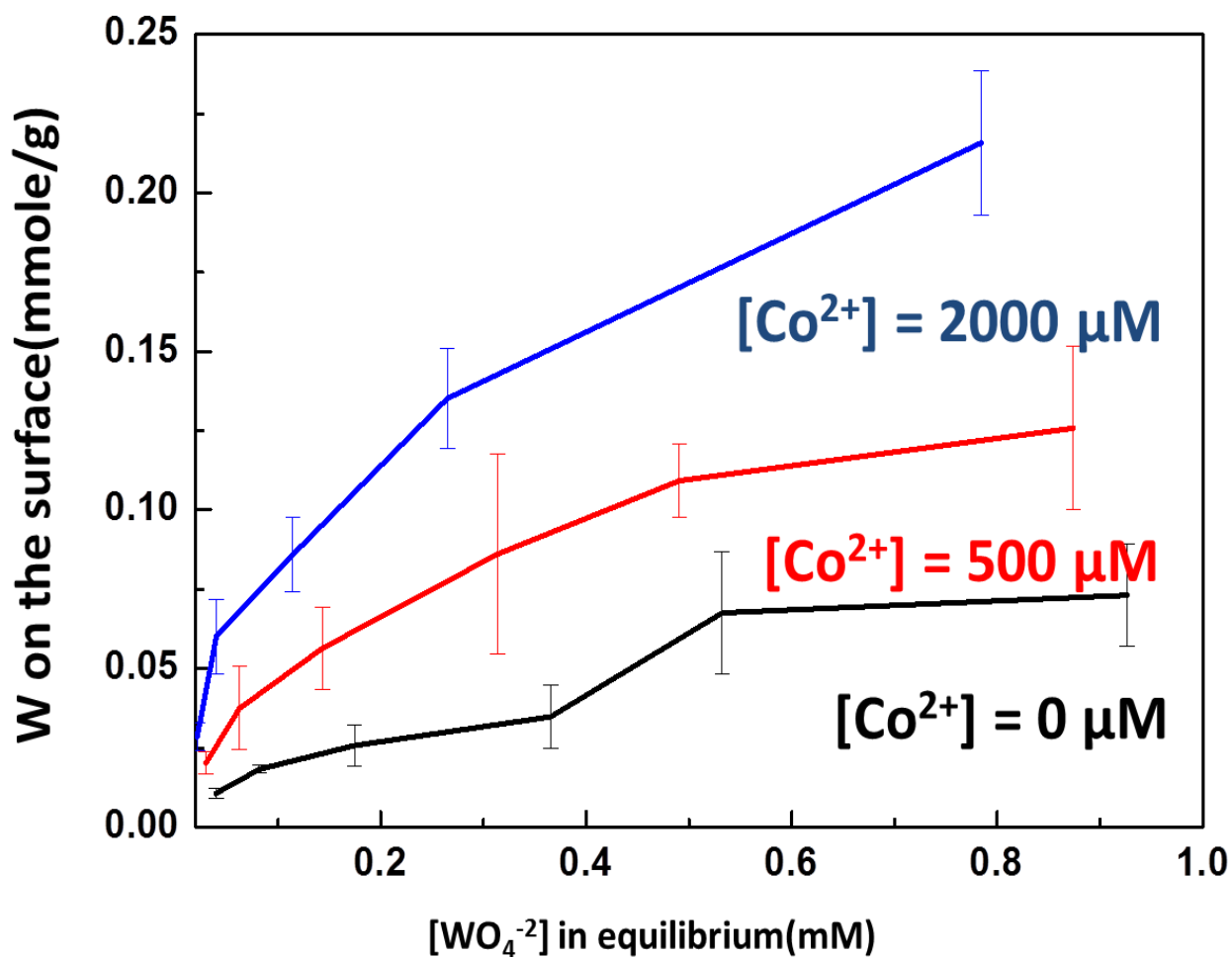
Figure 3. 1. Tungstate sorption isotherm on the boehmite surface over the range $[WO_4^{2-}]$ = 50-1000 µM conducted at two different Co(II) concentrations and in the absence of Co at pH 7.5. Enhanced tungstate uptake is observed with increasing Co(II) on the boehmite surface.

a) [Co(II)] = 2000 μM

b) [WO$_4^{2-}$] = 200 μM
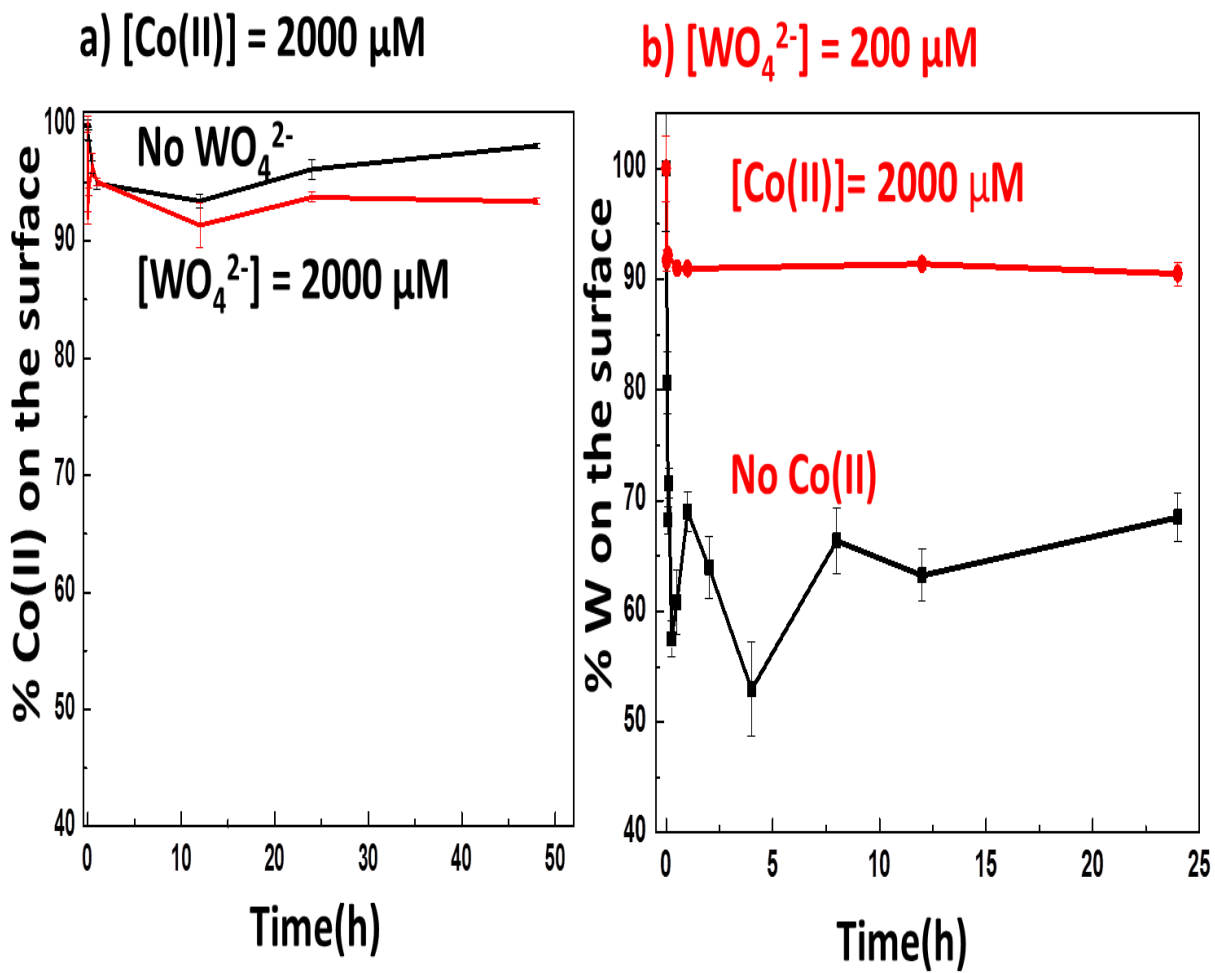
Figure 3. 2. Desorption results for (a) Co(II) and (b) tungstate on the boehmite surface at pH 7.5. Tungstate sorption (b) is more irreversible with Co(II) present on the surface. Black lines; single sorbate, Co(II) or tungstate. Red lines; Co(II) and tungstate co-sorption.

3.3.2. Desorption

Co(II) desorption behavior was compared with and without tungstate present. Co(II) sorption on boehmite is found to be mostly irreversible regardless of tungstate concentration, with ~95% of Co(II) retained on the surface (Figure 3.2-a). Desorption behavior of tungstate shows an interesting contrast. Tungstate sorbed on the Co(II) treated boehmite surface is mostly irreversible (>90%), while tungstate on Co-free boehmite surface shows significantly greater reversibility, with ~30 % released from the surface. This result shows that Co(II) treatment (sorption) significantly affects tungstate uptake, whereas an analogous effect on Co(II) sorption is not evident over the conditions examined.. Taken together, the sorption and desorption results demonstrate that Co(II) sorption pretreatment not only enhances tungstate uptake but also significantly reduces its sorption reversibility on boehmite at pH 7.5.

3.3.3. Powder XRD results

Powder XRD patterns of Co(II)-sorbed boehmite are compared with pure boehmite and CoAl LDH (Figure 3.3). CoAl LDH, synthesized as described above, shows an XRD pattern characteristic of LDH.[35] The assignment of peaks is well known in previous study.[35] The peak near 11.6° 2Θ corresponds to the basal spacing at ~7.63 Å, which higher-order basal peaks at 23.3 and 35°. The thickness of a brucite layer is about 4.8 Å, therefore the height of interlayer is ~2.83 Å. This interlayer distance is reasonable considering the ionic radius of water molecules and Cl⁻ which are expected to be the main interlayer species in our initial synthesis conditions.[40]

Co(II)-sorbed boehmite samples show the three major boehmite diffraction peaks in this scan range, with additional weak peaks in the 500 and 2000 µM Co(II)-sorbed boehmite patterns near 11.6°, 23.3°, and 35° 2Θ corresponding to CoAl LDH. These peaks confirm that CoAl LDH forms on the boehmite surface during reaction with Co(II) at the higher concentration range. We

cannot rule out the formation of CoAl LDH at 100 µM Co(II), because of limited sensitivity of powder XRD to minor phases. For the Co(II) concentrations used, the solution is oversaturated with respect to $Co(OH)_2$ at pH 7.5, and the peaks marked by an asterisk in Figure 3.3 correspond to the main peak of this phase, confiming its occurrence as a minor component. Co K-edge EXAFS results described in the following section provide more details of the Co(II) phases. The formation of CoAl LDH on boehmite agrees with previous studies documenting LDH formation on aluminum oxide mineral surfaces.[25, 31, 33]
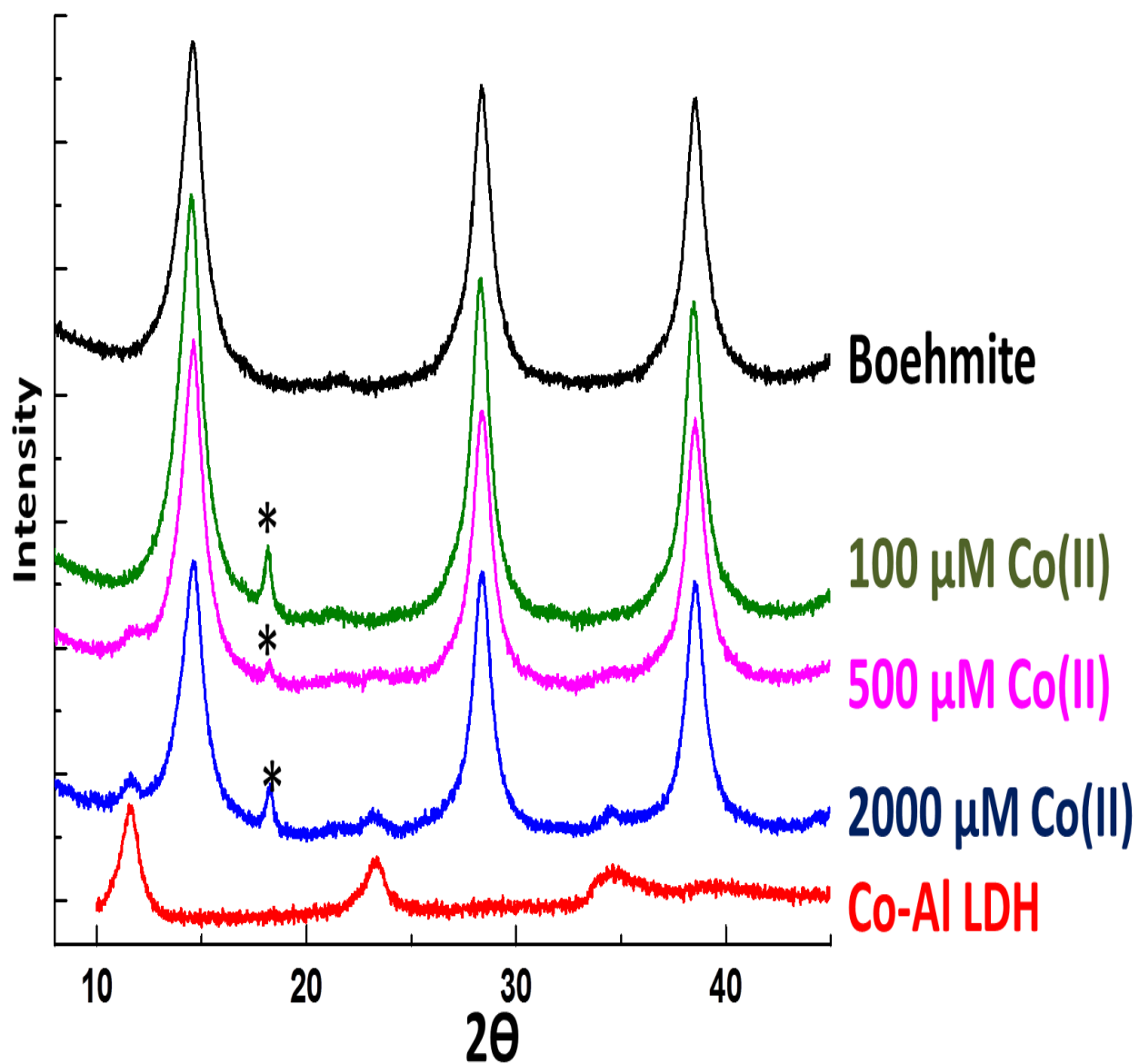
Figure 3. 3. Powder XRD patterns of CoAl LDH, Co(II) sorbed boehmite, and boehmite. The peaks marked by an asterisk correspond to the most intense peak for$Co(OH)_2$. Weak peaks for CoAl LDH are visible in the 500 and 2000 uM Co(II) samples.
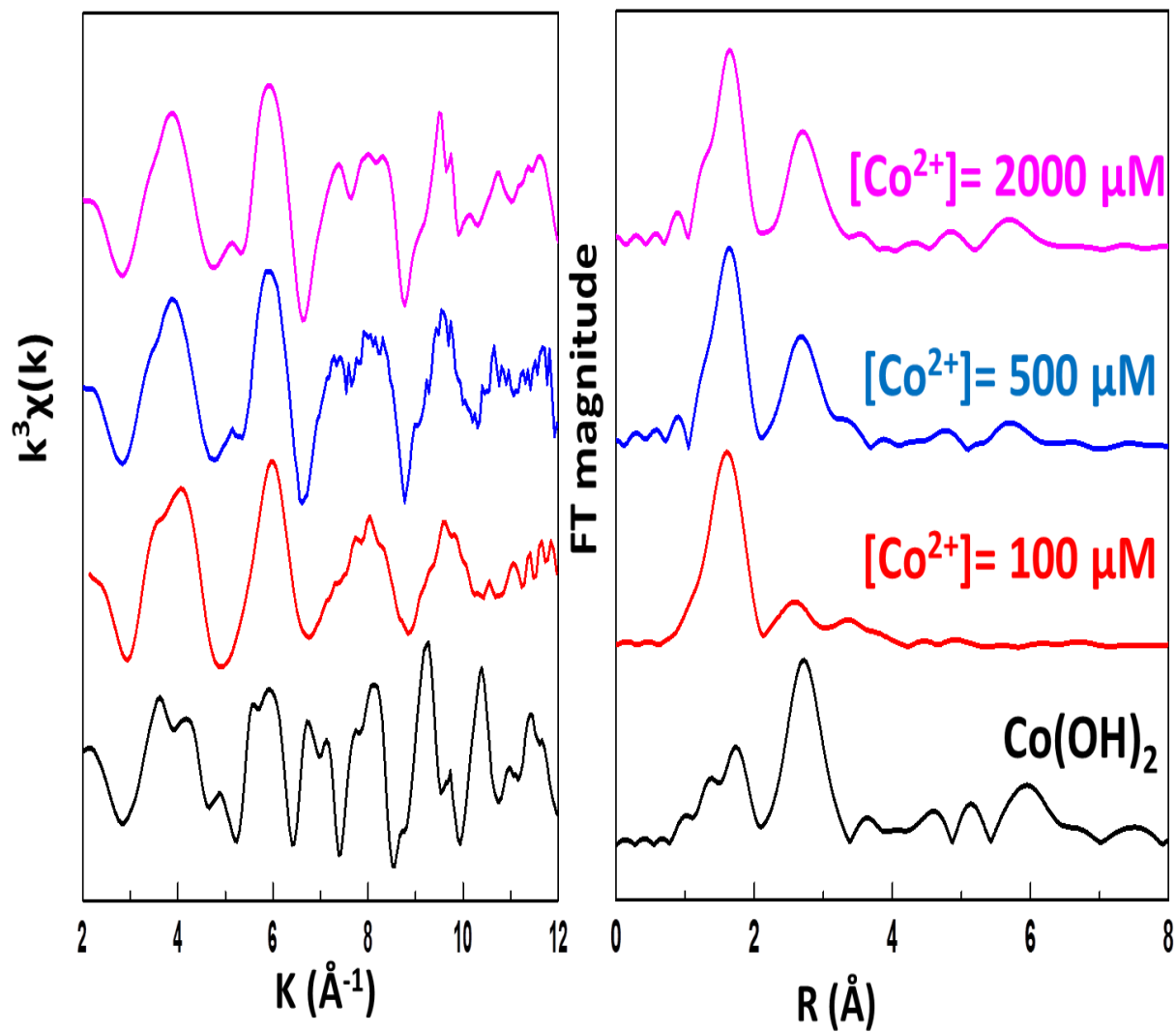
Figure 3. 4. Co K-edge EXAFS results for $Co(OH)_2$ and Co(II) sorption samples with 1000 μM tungstate on the boehmite.

3.3.4. Co K-edge EXAFS

Figure 3.4 shows Co K-edge EXAFS for boehmite reacted with Co(II) at three concentrations and then reacted with 1000 µM tungstate. A reference spectrum is shown for $Co(OH)_2$, which was determined to be a minor component by XRD. The chi functions (Figure 3.4, left) for the two higher concentration Co(II) sorption samples (500 and 2000 µM) are nearly identical, while the 100 µM Co(II) chi function displays some differences near 5 and 8 Å $^{-1}$. $Co(OH)_2$ displays a distinctly different beat pattern. The interesting feature among the spectra of the higher concentration sorption samples is the splitting of the feature centered near 8 Å $^{-1}$. This splitting has been reported as a signature of the LDH structure.[22]

The Fourier transform (FT) magnitude of the 100 uM Co(II) sorption sample is dominated by a single peak at 1.8 Å (not corrected for phase shift), with weaker peaks at 2.8 and 3.2 Å (Figure 3.4, right). The peak at 1.8 Å corresponds to the first-shell coordination by oxygen, and the weaker peaks at higher R result from backscattering from higher shells. The 1.8 Å peak appears in the FT magnitudes of the two higher concentration Co(II) sorption samples, along with a second intense peak at 2.8 Å (not corrected for phase shift). This latter peak is aligned exactly with the most intense peak in the FT magnitude for the $Co(OH)_2$ reference sample, and is consistent with the presence of a minor component of $Co(OH)_2$ in these two sorption samples as identified by XRD.

The FT magnitude for the $Co(OH)_2$ reference sample shows two prominent peaks, corresponding the published structure with the first-shell Co-O at 2.11 Å and Co-Co at 3.18 Å .[41] The distances obtained by fitting are 2.06 and 3.17 Å , respectively, in good agreement with the reported structure. In fitting the Co K-edge EXAFS of the sorption samples, we must recognize that two or more Co-containing phases are present, so that fit results may reflect a mixture of backscattering contributions dominated by the most abundant components. 100 µM Co(II)

sorption sample was fit with a W-O path at 2.06 Å and a Co-Co path at 3.11 Å. 500 and 2000 µM Co(II) sorption samples were fit with the same paths, but the fit obtained larger CN for the second shell. A Co-Al path was added in the fitting, but the results showed similar results without Co-Al. All Co(II) sorption samples were fit slightly a shorter Co-Co distance (3.11 Å) than Co(OH) (3.17 Å). This shorter Co-Co distance is characteristic in EXAFS spectra for metal cations forming LDH on aluminum oxide mineral surface, and this result is consistent to XRD results.[22, 31] These results are consistent with the XRD results that CoAl LDH forms on the boehmite surface. The absence of the significant $Co(OH)_2$ contribution at high Co(II) concentrations in Co K-edge EXAFS means CoAl LDH is the dominant Co(II) surface complex, although $Co(OH)_2$ feature was shown in XRD. The significant contributions of Co-W backscattering were not observed in Co K-edge EXAFS. The will be discussed later with W L_3-edge EXAFS results.

Table 3. 1. The fitting results of Co K-edge EXAFS for Co(II) sorption samples with 1000 µM tungstate.

Sample	Path	CN[a]	$R(Å)$[b]	$\sigma^2(Å^2)$[c]	$\Delta E0$ (eV)
100 µM Co(II)	Co-O	5.9	2.06	0.008	0.9
	Co-Co	1.7	3.11	0.008	
500 µM Co(II)	Co-O	5.9	2.08	0.007	0.2
	Co_Co	3.8	3.11	0.009	
2000 µM Co(II)	Co-O	6.0	2.06	0.008	0.5
	Co-Co	3.7	3.11	0.007	
Co(OH)	Co-O	6.0*	2.06	0.01	-2.3
	Co-Co	6.0*	3.17	0.01	

*: fixed in the fitting,

a : coordination number (±20%), b: distance in Å (±0.02 Å),

c : Debye-Waller factor
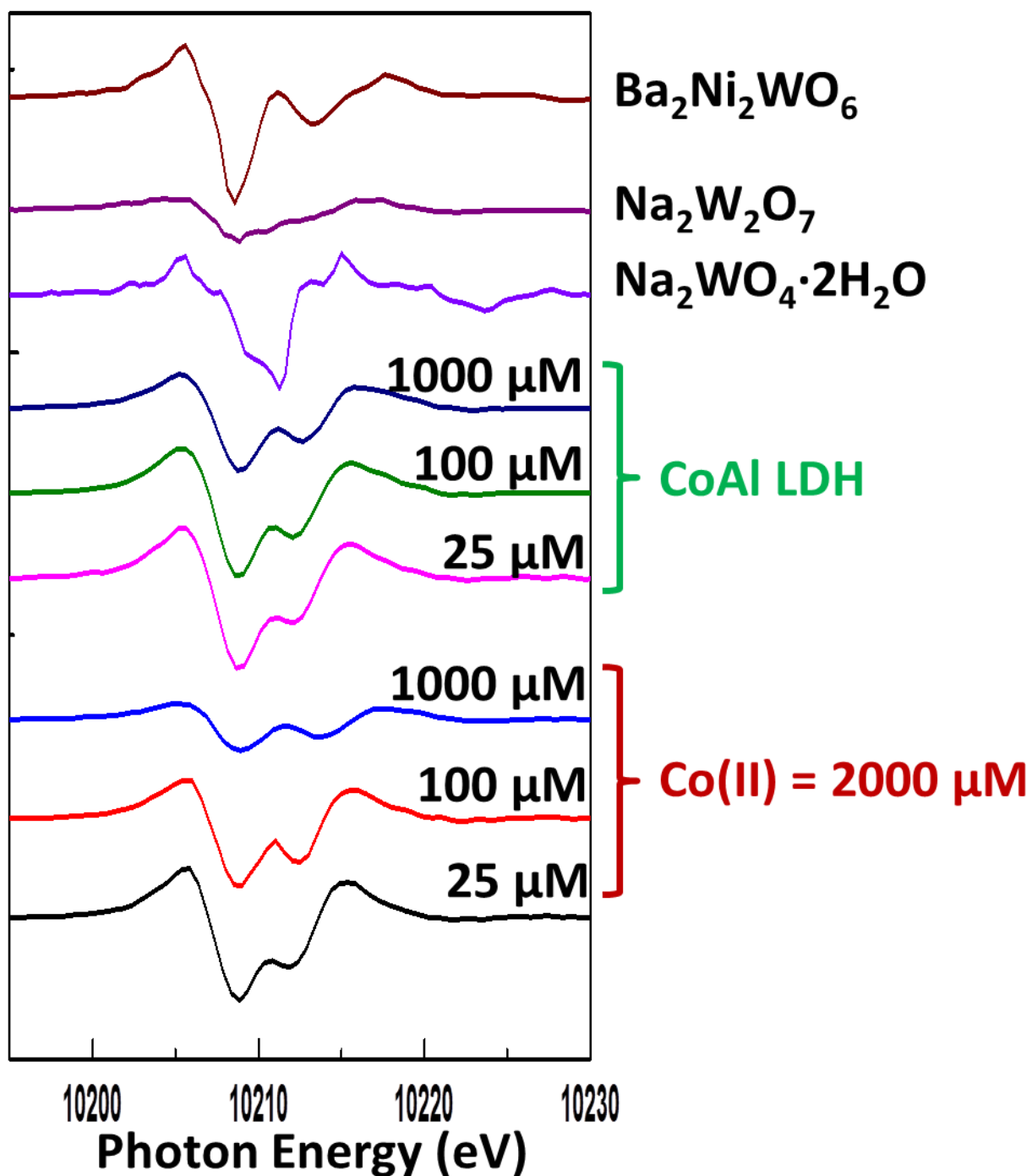
Figure 3. 5. Second derivatives of W L_3-edge XANES with tungstate sorption samples [Co(II)] = 2000 µM and selected model compounds. $Na_2WO_4 \cdot 2H_2O$ was selected for tetrahedral tungstate, and Ba_2NiWO_6 contains octahedral tungstate. $Na_2W_2O_7$ includes both tetra- and octahedral coordination.

3.3.5. W L₃-edge XANES

Tungsten L_3-edge XANES has been shown to be useful for distinguishing between tetrahedral and octahedral coordination environments of tungstate.[8, 42] The tungsten L_3-edge white line is attributed to the electron transition from 2p to vacant 5d orbitals.[42] Incipient splitting of the white line may occur as a result of ligand field splitting, and has been shown to reflect molecular symmetry of W(VI). This behavior is most readily observed in the second derivative of the XANES spectrum, in which a single minimum is found for tetrahedral coordination and two minima for octahedral coordination. Furthermore, the separation between minima is related to the degree of octahedral distortion.

Figure 3.5 shows second derivative spectra for three reference compounds and tungstate sorption samples after reaction with 2000 µM Co(II) co-sorbed boehmite and CoAl LDH. Tungstate in the reference compound $Na_2WO_4 \cdot 2H_2O$ is tetrahedrally coordinated; the second derivative spectrum exhibits a single minimum. In contrast, the octahedral coordination of W(VI) in Ba_2NiWO6 results in two distinct minima separated by 4.3 eV, similar to value reported in a previous study.[42] Second derivative spectra of all sorption samples display two distinct minima, indicating octahedral coordination. The interesting point here is that monotungstate is dominant in the solution at pH 7.5, so that a change in coordination occurs during interaction of dissolved WO_4^{2-} at the surface. In a separate study we observed a similar change in W(VI) coordination associated with sorption on boehmite at pH 8.[8] The separation values between the minima in the second derivatives are summarized in Table 2. These splitting values are 3.1, 3.5, and 5.0 eV for the 25, 100, and 1000 µM tungstate on the Co(II) treated boehmite surfaces respectively (Table 2). We also determined the energy separation of minima for tungstate-sorbed boehmite (Co-free) and for tungstate reacted with CoAl LDH (Table 2). The trend of increasing energy separation with increasing W concentration observed for the Co(II)-pretreated boehmite is nearly identical

to that observed for tungstate reacted with CoAl LDH, and different from that for the Co-free beohmite, which showed a nearly constant energy separation of 3.2-3.4 eV. The larger energy separation in the second derivative XANES with increasing tungstate concentration indicates that the octahedral coordination environment of W(VI) becomes more symmetric at the higher concentration.[42]

3.3.6. W L$_3$-edge EXAFS

Figure 3.6 shows the k^3-weighted W L$_3$-edge EXAFS data of tungstate sorbed on boehmite and Co(II) co-sorbed boehmite, and the corresponding Fourier transformation magnitudes. The chi functions are broadly similar for all samples (Figure 3.6, left), showing a split first oscillation and a sharp second oscillation from interference with a second or additional beat. Small differences in the 1000 µM sample for the Co(II) treated boehmite is observed near 9-10 Å^{-1}. FT magnitudes also show broadly similar features, but some differences are observed near 3–3.5 Å in FT magnitude of the 1000 µM sample (not corrected for phase shift). The broadly similar spectra for sorption samples imply the absence of significant contribution from W-Co backscattering, although the small difference observed near 9-10 Å^{-1} could be attributed to W-Co backscattering. This will be discussed later in this section about the fitting results. The positons of peak are identical for 25 µM sorption samples, but the Co(II) co-sorbed sample shows the broader first peak 1000 µM tungstate on Co(II) treated boehmite surface shows a broader first peak at 1.5 Å than 1000 µM on the pure boehmite surface. Furthermore, one small feature is shown at 3.2 Å (not corrected for phase shift) in 100 and 1000 µM tungstate on the Co(II) co-sorbed boehmite surface, while two distinct peaks appear near 3.2-3.5 Å (not corrected for phase shift) in the FT of the 1000 µM tungstate on boehmite sample.

Table 3. 2. The summary of energy gap between in W L_3-edge XANES second derivative

.

Name	Energy gap (eV) ±0.5
Co(II) pre-treated boehmite, [Co(II)]= 2000 µM, at pH 7.5	
25 µM WO_4^{2-}	3.1
100 µM WO_4^{2-}	3.5
1000 µM WO_4^{2-}	5.0
Pure boehmite at pH 8	
25 µM WO_4^{2-}	3.3
100 µM WO_4^{2-}	3.2
1000 µM WO_4^{2-}	3.4
CoAl layered double hydroxide at pH 7.5	
25 µM WO_4^{2-}	3.0
100 µM WO_4^{2-}	3.5
1000 µM WO_4^{2-}	5.0
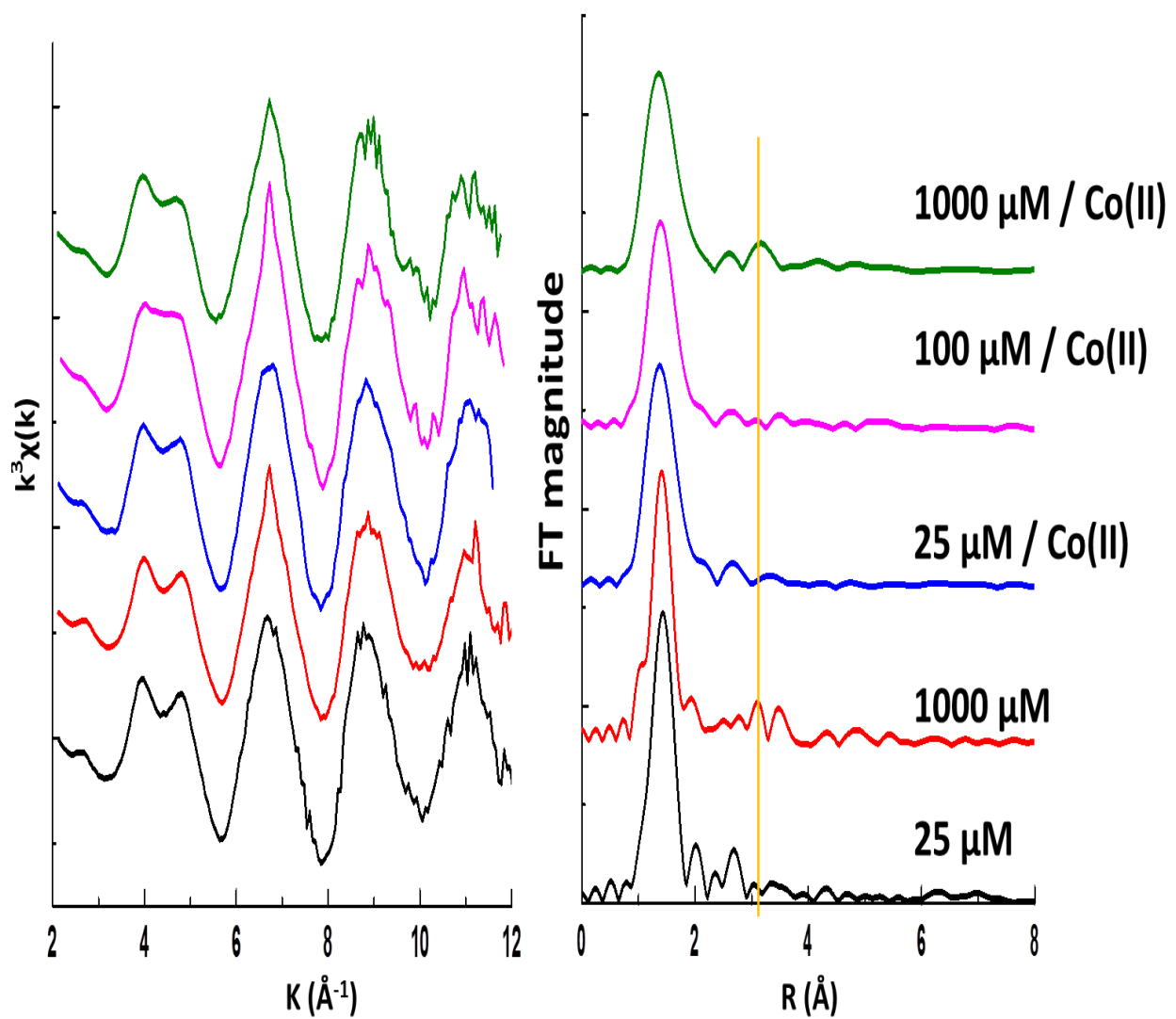
Figure 3. 6. The spectra of W L3-edge EXAFS with various combination of Co(II) and WO_4^{2-}

EXAFS data were fit using shell by shell approach in real space as described in section 2.4. Selected fits are shown Figure 3.7, and all fit results are summarized in table 3. Best fits for the 25 µM sorption samples were obtained using two W-O paths (1.75 and 2.16 Å) for the first shell with a combined coordination number (CN) of 5.9 (±1.2). The average W-O distance for the first shell is 1.96 Å, which is consistent with octahedral coordination of W(VI) and in agreement with the W L$_3$-edge XANES results. Based on previous studies, near-linear O-W-O path as a MS path was introduced to obtain a satisfactory fit of the first oscillation in the chi functions at 3–3.5 Å^{-1}.[39] (Chapter 2) The peak at 3.17 Å, which is unrealistically short for W-W or W-Co distances, was fit with a W-Al path. Moreover, W-W or W-Co backscattering paths could be ruled out with the identical EXAFS spectra for 25 µM sorption samples on the boehmite and Co(II) co-sorbed boehmite surface. The same fitting method was applied to the 100 µM sorption sample

For the 1000 µM sorption sample, two W-O paths (1.74 and 2.13 Å) were again used to obtain the best fit of the first peak in the FT. A W-Al path was introduced for the small feature near 2.5 Å (not corrected for phase shift) as in the lower concentration samples, which was found not to depend on the tungstate concentration. A MS path was again found to be necessary to fit the first oscillation in the chi function. Compared to tungstate sorbed on pure boehmite, the feature at 3.0-3.5 Å (not corrected for phase shift) was found to change as tungstate concentration increased. Fitting this peak alternately using W-W or W-Co backscattering paths showed that both paths resulted in satisfactory fits and reasonable distances. Therefore, we cannot distinguish between fits for this feature.
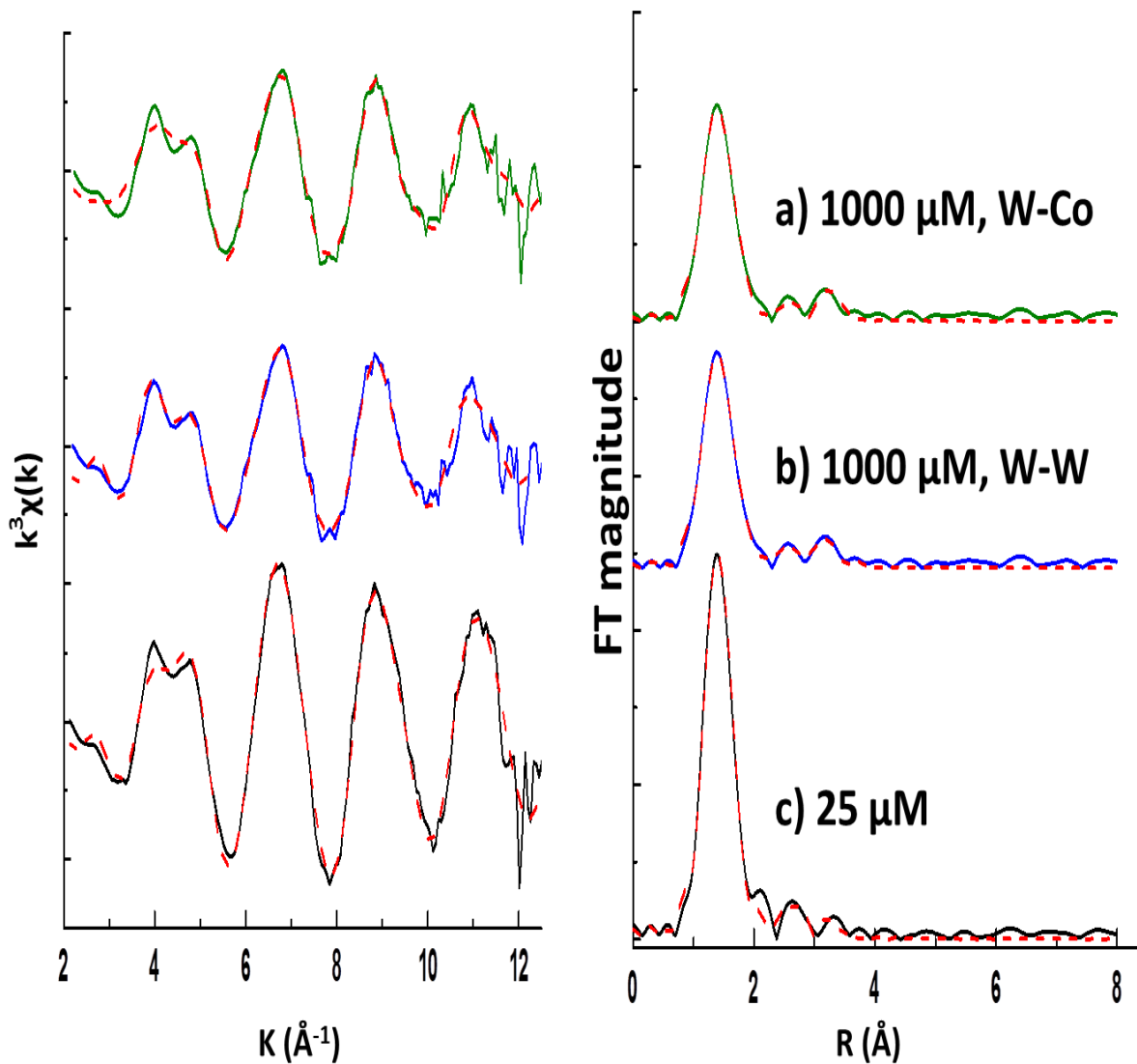
Figure 3. 7. The fit results of W L$_3$-edge EXAFS spectra for tungstate sorption samples with [Co(II)] = 2000 µM. The dotted lines are fits, and the solid lines are data. Using different paths to fit the 1000 µM sample are indicated in the figure.

Table 3. 3. The summary of the fit results for W L_3-edge EXAFS spectra of tungstate sorption samples with [Co(II)] = 2000 μM

Sample	Path	CN[a]	R (Å)[b]	σ^2 (Å^2)[c]	ΔE0 (eV)
25 μM	W-O1	3.1	1.76	0.002	2.4
	W-O2	3.2	2.16	0.01	
	W-Al	1.4	3.17	0.01	
100 μM	W-O1	3.1	1.76	0.002	1.8
	W-O2	3.2	2.14	0.01	
	W-Al	1.2	3.15	0.01*	
1000 μM	W-O1	2.9	1.74	0.005	
	W-O2	2.4	2.12	0.01	3.0
(W-W)	W-Al	1.3	3.13	0.01*	
	W-W	0.7	3.62	0.008*	
1000 μM	W-O1	2.7	1.77	0.004	
	W-O2	2.6	2.13	0.01	1.2
(W-Co)	W-Al	1.4	3.18	0.01*	
	W-Co	0.9	3.53	0.008*	

*: fixed in the fitting,

a : coordination number (±20%), b: distance in Å (±0.02 Å),

c : Debye-Waller factor

3.4. Discussion

Our findings demonstrate that tungstate sorption on boehmite at pH 7.5 is strongly enhanced by pre-treatment with Co(II). This results in formation of more stable surface complexes of tungstates, as demonstrated by the significant reduction in sorption reversibility on the boehmite surface. The significant finding is the relevance of tungstate uptake with Co(II) concentration. The tungstate uptake was largely increased with more Co(II) concentration on boehmite surface.

The formation of CoAl LDH leads us to the question of its role in enhanced tungstate uptake on the boehmite surface. Enhanced anion uptake may be associated with different mechanisms. For example, co-precipitation of anions with cations, pre-treatment to modify the surface (e.g., surface charge), and "lateral interaction (the formation of ternary surface complex)" are well documented for increasing uptake of anions.[9, 13, 15, 20, 21] In the present case, we can rule out precipitation of cobalt tungstate with no observed precipitate in our blank tests described in section 3.1. The calculation with thermodynamic data base using Phreeqc was not aware of any Co-tungstate precipitate within the concentration range used in this study at pH 7.5.[43] Moreover, the co-precipitation of Co(II) and tungstate could be ruled out with the absence of significant contributions in W L_3-edge and Co K-edge EXAFS spectra, although the precipitate could exist as a minor component which would not significantly affect tungstate sorption. The absence of substantial contribution in W L_3-edge EXAFS for sorption samples also rule out the formation of ternary surface complex.

The identical EXAFS spectra for 25 µM regardless of the CoAl presence imply that tungstate predominantly sorbed on the boehmite surface at this concentration. The PZC of boehmite is 8.7.[34] Therefore, large amount of tungstate could be sorbed on the boehmite surface. Furthermore, changes in PZC values resulting from cation sorption have been documented in

previous studies.[14, 15, 18] Co(II) sorption could shift the PZC of boehmite to a high pH value, resulting in increased tungstate uptake without any influence in W L_3-edge EXAFS spectra. Therefore, the enhanced tungstate uptake at low concentration could be mainly attribute the tungstate sorption on the Co(II) treated boehmite surface.

The speciation of Co(II) on the boehmite surface are a key to understand their roles in tungstate sorption and the mechanism of sorption enhancement. The thermodynamic calculation indicated $Co(OH)_2$ precipitation, and Figure 3.3 showed $Co(OH)_2$ feature (marked with stars). Co K-edge EXFAS and powder XRD results support that Co(II) mainly formed CoAl LDH on the boehmite surface, although $Co(OH)_2$ was precipitated as a minor phase. Co(II) sorption mechanisms on mineral surfaces containing Al have been extensively studied.[22, 31] Moreover, the formation of LDH at neutral and basic conditions on mineral surfaces containing Al or Si has been documented in previous studies[22] In this study, the Co(II) surface coverage (0.15mmole/g) in this study is much greater than the coverage at which Co(II) forms CoAl LDH on the boehmite surface (0.5 µmole/m^2 or 0.068 mmole/g).[30]

The intercalation of tungstate into CoAl LDH has the potential to be a significant mechanism for the enhanced tungstate uptake and more irreversible tungstate sorption reaction at higher tungstate concentrations. LDHs have large sorption capacity for anions.[44, 45] Previous study reported that the value of 2+ to 3+ metal cation ratio in LDH is important for controlling the preference of the anion exchange and surface adsorption.[46] In this study, CoAl LDH on boehmite surface would have a large Co(II) and Al(III) because of the low Al(III) concentration with the low solubility of boehmite at pH 7.5. A high Co(II)/Al(III) ratio favors intercalation of anions into the LDH interlayers.

The affinity of LDH for different anions has been reported to vary in the order $CO_3^{2-} >$ $SO_4^{2-} > Cl^- > NO_3^- >> I^-$. In the initial condition of our sorption experiments, the major anion is Cl^- in the LDH. Anions such as CO_3^{2-} (D_{3h}) and SO_4^{2-} (T_d), which possess symmetry compatible with the local symmetry of the interlayer sites in the LDH structure, show strong affinity to LDH. Intercalation of anions with greater charge is also favored to achieve charge compensation.[47] Our XAS results indicate octahedral tungstate which would not satisfy with respect to compatible symmetry. The intercalation of tungstate in the LDH could be driven by the higher negative charge of tungstate. Thus, the formation of CoAl LDH at the boehmite surface not only creates additional sites in which tungstate uptake would be favored, but also provides an explanation for the decreased sorption reversibility observed in our desorption experiments.

As we described in section 3.5, the energy separation of minima in tungstate L_3-edge XANES second derivative spectra provides evidence supporting intercalation of tungstate in CoAl LDH. Yamazoe et. al reported that the energy gap in W L_3-edge EXAFS is strongly linked to its geometry,[42] with the largest energy separation for symmetric octahedral (O_h) coordination of W(VI). The interesting finding in the present study is that energy separation values of second-derivative minima for tungstate sorbed onto Co(II)-pretreated boehmite increase with increasing tungstate concentration exactly as observed for tungstate reacted with CoAl LDH (Table 2). Furthermore, this trend in energy minima separation coincides with the expansion of CoAl LDH that would be expected for intercalation of tungstate in the interlayer. The shifting and broadening of XRD peaks for CoAl LDH with increasing tungstate concentrations are taken as evidence of tungstate intercalation between layers (Chpter 3)[45, 48] The greater separation of second derivative minima in the XANES with higher tungstate concentration would be consistent

with a more symmetric octahedral coordination of tungstate in the more expanded interlayer of the CoAl LDH. Taken together, these observations support the hypothesis that tungstate becomes intercalated into CoAL LDH that forms from Co(II) treatment. This represents a plausible explanation for the enhanced tungstate uptake on boehmite following treatment with Co(II), and further explains the decreased reversibility of tungstate sorption.

Our XAS results also demonstrate that tungstate undergoes coordination changes during interaction with Co(II)-treated boehmite. All of our sorption samples show two distinct minima in W L_3-edge XANES, indicating octahedral W(VI). Therefore, at near-neutral pH dissolved tungstate changes its coordination from tetrahedral (WO_4^{2-} in the solution) to octahedral following uptake on the surface. The second derivative W L_3-edge XANES further suggests that tungstates with different degrees of octahedral distortion exist depending on the tungstate concentration. Our EXAFS analysis of 25 µM sorption samples also confirm octahedral tungstate, which is most likely a monotungstate. . Kashiwabara et al reported octahedrally coordinated monomeric tungstate sorbed on birnessite (MnO_2) at basic pH.[8] Our previous study also suggests the occurrence of an octahedral monomeric tungstate sorbed onto boehmite at low W concentration and a polymeric tungstate at higher concentrations.(Our study) In W L_3-edge EXAFS, the clear difference in the second shell (3.2-3.8 Å, not corrected for phase shift) for 1000 µM sorption samples was observed(Figure 3.6). The EXAFS for the 1000 µM on Co(II)-treated boehmite was fit equally well by W-W and W-Co. We speculate that this is most likely to be W-Co backscattering in the light of our sorption, desorption, XANES results all supporting intercalation of tungstate into an LDH at higher tungstate concentrations.

Nevertheless, we cannot rule out some polymerization of tungstate on the surface, as reported in our previous study.(Chapter 2) The fit results using a W-W path shows reasonable fit

parameters. Furthermore, the absence of the backscattering between tungsten and metal atoms in LDH has been observed.[48, 49] If so, tungstate species on the Co(II) treated boehmite surface could be different from those on the boehmite surface.

The EXAFS results suggest that tungstate sorption reaction on the modified boehmite surface is favored at low tungstate concentration, while the combination of the PZC change and the LDH intercalation result in the enhanced tungstate uptake at higher tungstate concentration. The identical W EXAFS spectra for 25 µM sorption samples regardless of the CoAl LDH formation support the conclusion that enhanced tungstate sorption at the low concentration is driven by the change of PZC. The formation of CoAl LDH, resulting in greater tungstate uptake and less reversible reaction on the surface implies that CoAl LDH plays important roles for tungstate sorption mechanism.

3.5. Conclusion

It is important to control monotungstate at neutral and basic pH to limit mobility and its toxicity in natural environments. Our findings demonstrate that the existence of Co(II) as CoAl LDH results in enhanced tungstate uptake and more stable tungstate surface complex at neutral and basic pH conditions. Therefore, the mobility of tungstates may be effectively limited by the Co(II) presence on the boehmite surface. However, we still lack of understanding of tungstate species on the surface. Additionally, competitive sorption reaction of tungstate with other anions on mineral surface has been known in previous studies.[6] Other anions effects on tungstate sorption with co-existing cations would be important to evaluate the mobility and toxicity of tungstate in natural aqueous systems.

Acknowledgements

References

1.   Strigul, N., Does speciation matter for tungsten ecotoxicology? *Ecotox Environ Safe* **2010,** *73*, (6), 1099-1113.

2.   Dermatas, D.; Braida, W.; Christodoulatos, C.; Strigul, N.; Panikov, N.; Los, M.; Larson, S., Solubility, sorption, and soil respiration effects of tungsten and tungsten alloys. *Environ Forensics* **2004,** *5*, (1), 5-13.

3.   Strigul, N.; Koutsospyros, A.; Arienti, P.; Christodoulatos, C.; Dermatas, D.; Braida, W., Effects of tungsten on environmental systems. *Chemosphere* **2005,** *61*, (2), 248-258.

4.   Ringelberg, D. B.; Reynolds, C. M.; Winfield, L. E.; Inouye, L. S.; Johnson, D. R.; Bednar, A. J., Tungsten Effects on Microbial Community Structure and Activity in a Soil. *J Environ Qual* **2009,** *38*, (1), 103-110.

5.   Strigul, N.; Galdun, C.; Vaccari, L.; Ryan, T.; Braida, W.; Christodoulatos, C., Influence of speciation on tungsten toxicity. *Desalination* **2009,** *248*, (1-3), 869-879.

6.   Xu, N.; Christodoulatos, C.; Braida, W., Modeling the competitive effect of phosphate, sulfate, silicate, and tungstate anions on the adsorption of molybdate onto goethite. *Chemosphere* **2006,** *64*, (8), 1325-1333.

7.   Gustafsson, J. P., Modelling molybdate and tungstate adsorption to ferrihydrite. *Chem Geol* **2003,** *200*, (1-2), 105-115.

8.   Kashiwabara, T.; Takahashi, Y.; Marcus, M. A.; Uruga, T.; Tanida, H.; Terada, Y.; Usui, A., Tungsten species in natural ferromanganese oxides related to its different behavior from molybdenum in oxic ocean. *Geochim Cosmochim Ac* **2013,** *106*, 364-378.

9.   Li, W.; Xu, W. Q.; Parise, J. B.; Phillips, B. L., Formation of hydroxylapatite from co-sorption of phosphate and calcium by boehmite. *Geochim Cosmochim Ac* **2012,** *85*, 289-301.

10.   Sahai, N.; Lee, Y. J.; Xu, H. F.; Ciardelli, M.; Gaillard, J. F., Role of Fe(II) and phosphate in arsenic uptake by coprecipitation. *Geochim Cosmochim Ac* **2007,** *71*, (13), 3193-3210.

11. Taylor, R. W.; Bleam, W. F.; Ranatunga, T. D.; Schulthess, C. P.; Senwo, Z. N.; Ranatunga, D. R. A., X-ray Absorption Near Edge Structure Study of Lead Sorption on Phosphate-Treated Kaolinite. *Environ Sci Technol* **2009,** *43*, (3), 711-717.

12. Grafe, M.; Sparks, D. L., Kinetics of zinc and arsenate co-sorption at the goethite-water interface. *Geochim Cosmochim Ac* **2005,** *69*, (19), 4573-4595.

13. Tang, Y. Z.; Reeder, R. J., Uranyl and arsenate cosorption on aluminum oxide surface. *Geochim Cosmochim Ac* **2009,** *73*, (10), 2727-2743.

14. Li, W.; Zhang, S. Z.; Shan, X. Q., Surface modification of goethite by phosphate for enhancement of Cu and Cd adsorption. *Colloid Surface A* **2007,** *293*, (1-3), 13-19.

15. Mustafa, S.; Zaman, M. I.; Gul, R.; Khan, S., Effect of Ni2+ loading on the mechanism of phosphate anion sorption by iron hydroxide. *Sep Purif Technol* **2008,** *59*, (1), 108-114.

16. Yoon, S. J.; Helmke, P. A.; Amonette, J. E.; Bleam, W. F., X-ray absorption and magnetic studies of trivalent lanthanide ions sorbed on pristine and phosphate-modified boehmite surfaces. *Langmuir* **2002,** *18*, (26), 10128-10136.

17. Wang, K. J.; Xing, B. S., Adsorption and desorption of cadmium by goethite pretreated with phosphate. *Chemosphere* **2002,** *48*, (7), 665-670.

18. Wang, K. J.; Xing, B. S., Mutual effects of cadmium and phosphate on their adsorption and desorption by goethite. *Environ Pollut* **2004,** *127*, (1), 13-20.

19. Elzinga, E. J.; Kretzschmar, R., In situ ATR-FTIR spectroscopic analysis of the co-adsorption of orthophosphate and Cd(II) onto hematite. *Geochim Cosmochim Ac* **2013,** *117*, 53-64.

20. Spanos, N., Simultaneous deposition of W(VI) and Co(II) species on the gamma-alumina surface. *J Catal* **1999,** *183*, (2), 400-404.

21. Spanos, N., Simultaneous deposition of W(VI) species and Ni(II) ions on the gamma-alumina surface: Mechanistic model. *J Phys Chem B* **1999,** *103*, (11), 1890-1899.

22. Sparks, D. L., *Environmental soil chemistry*. Academic press: 2003.

23. Schenck, C. V.; Dillard, J. G.; Murray, J. W., Surface-Analysis and the Adsorption of Co(Ii) on Goethite. *J Colloid Interf Sci* **1983,** *95*, (2), 398-409.

24. Chisholmbrause, C. J.; Oday, P. A.; Brown, G. E.; Parks, G. A., Evidence for Multinuclear Metal-Ion Complexes at Solid Water Interfaces from X-Ray Absorption-Spectroscopy. *Nature* **1990,** *348*, (6301), 528-531.

25. Towle, S. N.; Bargar, J. R.; Brown, G. E.; Parks, G. A., Surface precipitation of Co(II)(aq) on Al2O3. *J Colloid Interf Sci* **1997,** *187*, (1), 62-82.

26. Katz, L. E.; Hayes, K. F., Surface Complexation Modeling .1. Strategy for Modeling Monomer Complex-Formation at Moderate Surface Coverage. *J Colloid Interf Sci* **1995,** *170*, (2), 477-490.

27. Katz, L. E.; Hayes, K. F., Surface Complexation Modeling .2. Strategy for Modeling Polymer and Precipitation Reactions at High Surface Coverage. *J Colloid Interf Sci* **1995,** *170*, (2), 491-501.

28. Oday, P. A.; Brown, G. E.; Parks, G. A., X-Ray-Absorption Spectroscopy of Cobalt(Ii) Multinuclear Surface Complexes and Surface Precipitates on Kaolinite. *J Colloid Interf Sci* **1994,** *165*, (2), 269-289.

29. Papelis, C.; Hayes, K. F., Distinguishing between interlayer and external sorption sites of clay minerals using X-ray absorption spectroscopy. *Colloid Surface A* **1996,** *107*, 89-96.

30. Boyle-Wight, E. J.; Katz, L. E.; Hayes, K. F., Macroscopic studies of the effects of selenate and selenite on cobalt sorption to gamma-Al2O3. *Environ Sci Technol* **2002,** *36*, (6), 1212-1218.

31. Boyle-Wight, E. J.; Katz, L. E.; Hayes, K. F., Spectroscopic studies of the effects of selenate and selenite on cobalt sorption to gamma-Al2O3. *Environ Sci Technol* **2002,** *36*, (6), 1219-1225.

32. Delacaillerie, J. B. D.; Kermarec, M.; Clause, O., Impregnation of Gamma-Alumina with Ni(Ii) or Co(Ii) Ions at Neutral Ph - Hydrotalcite-Type Coprecipitate Formation and Characterization. *J Am Chem Soc* **1995,** *117*, (46), 11471-11481.

33. Scheidegger, A. M.; Lamble, G. M.; Sparks, D. L., Spectroscopic evidence for the formation of mixed-cation hydroxide phases upon metal sorption on clays and aluminum oxides. *J Colloid Interf Sci* **1997,** *186*, (1), 118-128.

34. Li, W.; Feng, J.; Kwon, K. D.; Kubicki, J. D.; Phillips, B. L., Surface Speciation of Phosphate on Boehmite (gamma-AlOOH) Determined from NMR Spectroscopy. *Langmuir* **2010,** *26*, (7), 4753-4761.

35. Perez-Ramirez, J.; Mul, G.; Kapteijn, F.; Moulijn, J. A., In situ investigation of the thermal decomposition of Co-Al hydrotalcite in different atmospheres. *J Mater Chem* **2001,** *11*, (3), 821-830.

36. Ressler, T., WinXAS: a program for X-ray absorption spectroscopy data analysis under MS-Windows. *J Synchrotron Radiat* **1998,** *5*, 118-122.

37. Ressler, T., WinXAS: A new software package not only for the analysis of energy-dispersive XAS data. *J Phys Iv* **1997,** *7*, (C2), 269-270.

38. Zabinsky, S. I.; Rehr, J. J.; Ankudinov, A.; Albers, R. C.; Eller, M. J., Multiple-Scattering Calculations of X-Ray-Absorption Spectra. *Phys Rev B* **1995,** *52*, (4), 2995-3009.

39. Kuzmin, A.; Purans, J.; Benfatto, M.; Natoli, C. R., X-Ray-Absorption Study of Rhenium L3 and L1 Edges in Reo3 - Multiple-Scattering Approach. *Phys Rev B* **1993,** *47*, (5), 2480-2486.

40. Evans, J.; Pillinger, M.; Zhang, J. J., Structural studies of polyoxometalate-anion-pillared layered double hydroxides. *J Chem Soc Dalton* **1996**, (14), 2963-2974.

41. Pertlik, F., The distortion of the hexagonal close packing of oxygen atoms in Co (OH) 2 compared to isotypic brucite-type structures. *Monatshefte für Chemie/Chemical Monthly* **1999,** *130*, (9), 1083-1088.

42. Yamazoe, S.; Hitomi, Y.; Shishido, T.; Tanaka, T., XAFS study of tungsten L-1- and L-3-edges: Structural analysis of WO3 species loaded on TiO2 as a catalyst for photo-oxidation of NH3. *J Phys Chem C* **2008,** *112*, (17), 6869-6879.

43. Welch, A. H.; Szabo, Z.; Parkhurst, D. L.; VanMetre, P. C.; Mullin, A. H., Gross-beta activity in ground water: Natural sources and artifacts of sampling and laboratory analysis. *Appl Geochem* **1995,** *10*, (5), 491-503.

44. Khan, A. I.; O'Hare, D., Intercalation chemistry of layered double hydroxides: recent developments and applications. *J Mater Chem* **2002,** *12*, (11), 3191-3198.

45. Goh, K. H.; Lim, T. T.; Dong, Z., Application of layered double hydroxides for removal of oxyanions: A review. *Water Res* **2008,** *42*, (6-7), 1343-1368.

46. Ardau, C.; Frau, F.; Dore, E.; Lattanzi, P., Molybdate sorption by Zn-Al sulphate layered double hydroxides. *Appl Clay Sci* **2012,** *65-66*, 128-133.

47. Prasanna, S. V.; Kamath, P. V., Synthesis and characterization of arsenate-intercalated layered double hydroxides (LDHs): Prospects for arsenic mineralization. *J Colloid Interf Sci* **2009,** *331*, (2), 439-445.

48.   Vaysse, C.; Guerlou-Demourgues, L.; Demourgues, A.; Delmas, C., Thermal behavior of oxometalate (Mo,W)-intercalated layered double hydroxides: Study of the grafting phenomenon. *J Solid State Chem* **2002,** *167*, (1), 59-72.

49.   Vaysse, C.; Guerlou-Demourgues, L.; Demourgues, A.; Lazartigues, F.; Fertier, D.; Delmas, C., New (Ni, Co)-based layered double hydroxides with intercalated oxometalate (Mo, W) species, obtained by chimie douce reactions. *J Mater Chem* **2002,** *12*, (4), 1035-1043.

Chapter 4. The application of CoAl layered double hydroxide (LDH) for the removal of tungstate

Abstract

Tungstate sorption mechanisms on CoAl LDH were investigated as a function of tungstate concentrations at pH 8. Batch uptake experiments were conducted over the range of tungstate = 50-2000 μM. CoAl LDH showed a large sorption capacity to tungstate, and the anion exchange mechanism was suggested with the XRD results. The changes of the intensity, width, and position of peaks in XRD indicated the expansion of the interlayer space with the tungstate intercalation. W L_3-edge XANES implied that the coordination of tungsten changes from tetrahedral (solution) to octahedral (in CoAl LDH). However, exact tungstate species in CoAl LDH could not be determined with W L_3-edge EXAFS. Our results suggest the possible application of CoAl LDH for tungstate removal from aqueous media, but further studies about tungstate species and the competitive reaction with other anions are needed to evaluate the mobility, toxicity, and bioavailability of tungstate.

4.1. Introduction

Layered double hydroxides (LDHs) have received much attention recently for their wide range of applications related to a positive interlayer charge.[1-3] The structure of the LDHs is based on a stacking of brucite-like ($Mg(OH)_2$) layers.[4] A fraction of the divalent cations in a layer can be replaced with trivalent cations, giving positively charged sheets. The net positive charge is compensated by anions, which occupy the interlayer along with water molecules.[2] The octahedral M^{2+}/M^{3+} units share edges to form infinite sheets. These sheets are stacked on top of each other and are held together by hydrogen bonding.[2]

The significance of LDHs is based on their ability to retain anions and molecules in the interlayers. Layered double hydroxides have been well known for their large surface area,

flexible layer structure, and anion exchange reaction with various anions.[2, 3] These characteristics make LDHs good candidates for anion uptake. In general, three different mechanisms have been proposed for the removal of anions from aqueous solutions by the LDHs, namely surface adsorption, interlayer anion exchange, and reconstruction of calcined LDH precursors by memory effect.[5] The large surface areas provide more sorption sites for anions, and the anion adsorption on the LDH surface is dependent on pH. The anion exchange process of LDHs is mainly influenced by the layer charge density and its effect on intercalation of charge-balancing anions in the interlayer. Many studies reported on the application of LDHs for removal of various contaminants, including monoatomic anions, oxyanions, and organic molecules.[6-13] The reconstruction mechanism using memory effects is accompanied with the calcination procedure during LDH synthesis. As a result of it, LDHs obtain high surface area, small crystal size, and high stability. The calcination temperature is the key parameters to obtain proper properties for anion sorption.[2]

The advantage of LDHs for anion sorption is their stability and high sorption capacity of LDHs at neutral and basic conditions, where anion sorption onto many common sorbents is relatively low. The stability of sorbents is one of important factor for considering the practical application.[14] The dissolution of LDHs could result in the release of contaminants as well as potential health risks due to released metal cations from LDH. Ferreira et al. reported increased Mg^{2+} release from LDHs as pH decreased from 10 to 4.[15]

Dissolved tungstate, W(VI), is receiving attention recently as a more common contaminant that previously recognized, as a result of widespread industrial and military applications.[16, 17] Recently, Strigul et al. reported that toxicity of tungstate varies according to its speciation in solution, whereas tungsten metal and alloys are considered largely non-toxic.[16] This

study concluded that polymeric tungstate species are more toxic than monotungstate (WO_4^{2-}), although the latter are   more mobile in aquatic and soil systems.[16, 17] Therefore, the environmental fate of W ultimately depends on an accurate understanding of tungstate geochemistry.

Tungsten is in the same group with Cr and Mo (VIB). The oxyanions of these elements in their 6+ oxidation states form dimeric or polymeric species in solution under appropriate conditions of pH.[16, 18] The tendency for polymerization in the VIB group increases with increasing atomic number.[5] Polymerization reactions involving tungstate are generally the most complicated and least understood among this group. Formation of polymeric species of tungstate, , including $W_7O_{24}^{6-}$ and $H_2W_{12}O_{42}^{10-}$, is favored at acidic conditions and higher W concentrations, whereas monotungstate, WO_4^{2-}, is dominant at and above neutral pH values.[16, 17, 19]

Previous studies have shown that tungstate exhibits sorption behavior on mineral surfaces that is typical for anions, with maximum uptake at low pH.[20, 21] Only limited uptake is observed at neutral and basic pH conditions. Tungstate shows a strong affinity to mineral surfaces. The adsorption of tungstate is stronger than that of molybdate, whereas phosphate could displace tungstate on iron oxide surface.[21 20]

With its limited sorption at neutral and basic pH, tungstate is potentially a good candidate for anion exchange in LDHs. Anion exchange in LDHs is strongly influences by the symmetry and charge of anions.[14] Anions with compatible symmetries, such as D_{3h} and T_d, generally show significant exchange. Furthermore, more negatively charged anions have a strong tendency to replace similarly sized anions in LDH interlayers because of more effective charge compensation.[14].

In this study, we investigated the effectiveness of CoAl LDH for tungstate removal from aqueous media via anion exchange. We focus on slightly basic pH conditions (pH 8) because of the dominance of montungstate in solution and the overall stability of LDH. Batch reaction experiments with CoAl LDH were conducted as a function of tungstate concentration. Anion exchange resulting in layer expansion was studied using X-ray diffraction. Tungstate speciation was characterized using W L_3-edge X-ray absorption near edge spectroscopy (XANES) and extended X-ray absorption fine structure (EXAFS). The results provide new insight to the environmental behavior of tungstate and suggest potential remediation techniques.

4.2. Materials and experiments

4.2.1. CoAl LDH synthesis

The procedure for synthesizing CoAl LDH followed the method described by Perez-Ramierez et al.[22] Briefly, 0.02 M $CoCl_2$ (Acros) solution was added drop-wise into 0.02 M $AlCl_3$ (Fisher) solution under ambient conditions open to air. The pH was maintained at 9.5 by addition of 0.1 M NaOH using an auto-titrator. The cloudy pinkish suspension that formed was filtered, rinsed, and dried at 60 °C in a convection oven. XRD was used to confirm the identity of the LDH phase, with no other phase present (Figure 3.1). The dried LDH was used for sorption experiments without any further treatment. The possible anions in CoAl LDH are CO_3^{2-} dissolved from air and Cl^- from chemicals used for the synthesis.[23] This will be discussed in section 3.1 with XRD results.

4.2.2. Batch reactions

Tungstate sorption experiments were conducted at pH 8 as a function of tungstate concentration over the range 50-2000 μM. All sorption experiments were carried out with 1 g/L particle loading. Small amounts of 0.1 M NaOH or HCl was added to adjust pH. The CoAl LDH suspensions were equilibrated at pH 8 with 0.1 M NaCl as a background electrolyte at least 2

days prior to the addition of tungstate. In our preliminary kinetic experiments with $[WO_4^{2-}] = 200$ µM, tungstate uptake by CoAl LDH was found to be a rapid process, with 70% of tungstate sorbed within 1 h and 90% in 24 h. All our sorption experiments were equilibrated for 24 h based on this kinetic study. Designated amounts of 0.1 M $Na_2WO_4 \cdot 2H_2O$ were added to CoAl LDH suspensions and allowed to react for 24 h on a shaker table. A 5 mL aliquot of solution was extracted from selected samples, filtered using a 0.25 µM filter, and analyzed using inductively coupled plasma-atomic emission spectroscopy (ICP-AES) to calculate the amount of tungstate sorbed on CoAl LDH. The wet CoAl LDH pastes after reacting with tungstate were brought to the beamline to collect XAS data. XRD were measured with air-dried CoAl LDH recovered from experiments.

4.2.3. Powder XRD

Powder XRD was collected for synthesized and tungstate-sorbed CoAl LDHs. All samples were scanned from 5 to 45 in 2Θ with 0.2 degree/min rate with a Scintag Pad-X diffractometer using Cu Kα radiation. The peak position, width, and intensity were tracked as a function of tungstate concentration.

4.2.4. Tungsten L_3-edge X-ray absorption spectroscopy

XAS data for tungstate sorption samples and model compounds were collected at beamline X11A at the National Synchrotron Light Source (Brookhaven National Laboratory in Upton, NY) and beamline 12-BM at the Advanced Photon Source (Argonne National Laboratory, Argonne, IL). All model compounds and sorption samples were mounted in a Lucite sample holders and sealed with Kapton tape. Transmission mode was used to collect data for model compounds. Wet pastes of sorption samples were placed at 45° to the incident beam, and data were collected in fluorescence mode using a detector (Canberra 13-element Ge solid detector) was position at 90° to the incident beam. Si(111) crystals were used for the

monochrometer at these beamlines, and the beam was detuned 20-30 % for harmonic rejection. Energy calibration was performed with a Ga filter (K-edge, 10.367 keV) or a W metal foil for the W L_3-edge (10.207 keV).

Data analysis was performed with the EXAFS data analysis programs WinXAS [24, 25] and IFEFFIT[26]. Spectra were averaged to obtain proper signal to noise ratio after careful energy calibration. The $\chi(k)$ function was Fourier transformed using k^3 weighting, and shell-by-shell fitting was carried out in R-space. Theoretical paths were calculated using FEFF7 based on published structures.[26] A single threshold energy value (ΔE_0) was allowed to vary during fitting. The amplitude reduction factor was fixed at $S_0{}^2 = 0.9$ for all samples.

In fitting the model compounds, coordination numbers were fixed according to published structures. Fitting of model compounds was begun using only single scattering paths. In instances where like paths were close or overlapped one another, they were combined to minimize the number of paths necessary to obtain an acceptable fit. The significance of multiple scattering (MS) from linear chains, e.g., O-W-O, has been previously noted by Kuzmin et al.[27] Their study showed that the contribution of a MS path with 4 legs from near-linear O-W-O chains is most significant for EXAFS fitting. In the present study, fitting results were compared with and without this MS contribution.

In the fitting of W L_3-edge EXAFS spectra for sorption samples, no constraints were applied if the sum of the first-shell W-O coordination numbers (CN) was near 6. The octahedral coordination ofW(VI) was determined based on the W L_3-edge XANES, as described inSection 3.4. Debye-Waller factors were constrained with 0.01 Å^2 (in the typical range 0.005-0.015 Å^2) for the second shell and further distances. For the second shell, various combinations of W-W

and W-Co paths were attempted in the fitting. Based on previous studies and our fitting results

for model compounds, a MS path was included in fits for all sorption samples.

4.2.5. Reference Samples for X-ray absorption Spectroscopy

Reference samples were selected to reflect different coordination of W(VI) for

comparison with tungstate-reacted LDH and for validating XAFS fitting. The reagents were used

as obtained. $CaWO_4$ was selected to represent isolated tungstate tetrahedra exclusively. Distorted

octahedral coordination of W(VI) occurs in WO_3 (Sigma Aldrich), sharing all corners in a

perovskite-like structure. Ba_2NiWO_6 contains exclusively isolated tungstate octahedra (O_h

symmetry). Ba_2NiWO_6 was synthesized by the method described by Yamazoe, using $BaCO_3$

(Alfa Aesar), $NiCO_3$ (Alfa Aesar), WO_3 (Sigma Aldrich) reagents.[28] $Na_2W_2O_7$ contains both

tetrahedral and octahedral tungsten in a 1:1 ratio. $Na_2W_2O_7$ was synthesized by the method

described in previous studies.[29]
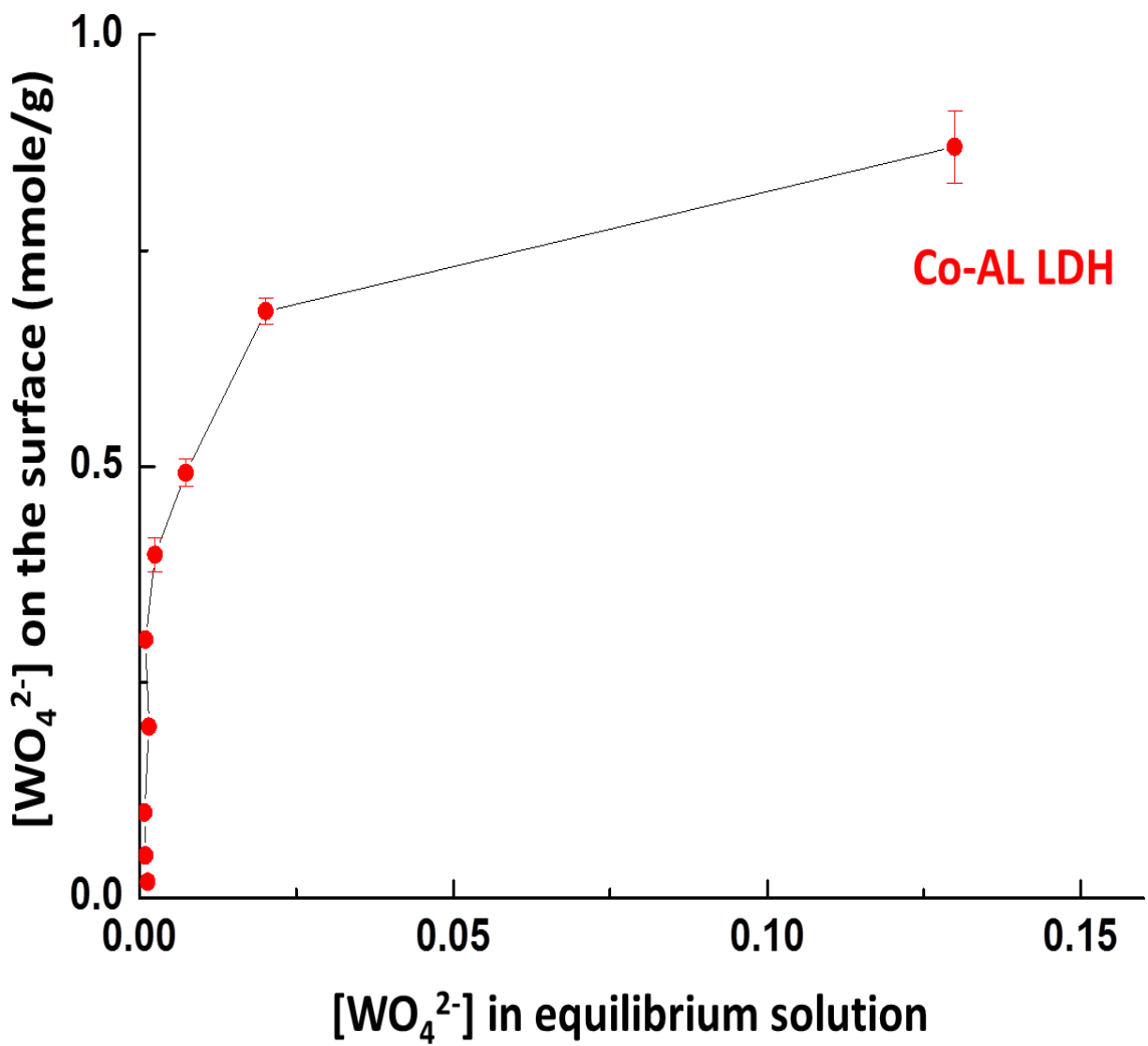
Figure 4. 1 The result of isotherm experiment as a function of tungstate concentration, 50-2000 μM at pH 8
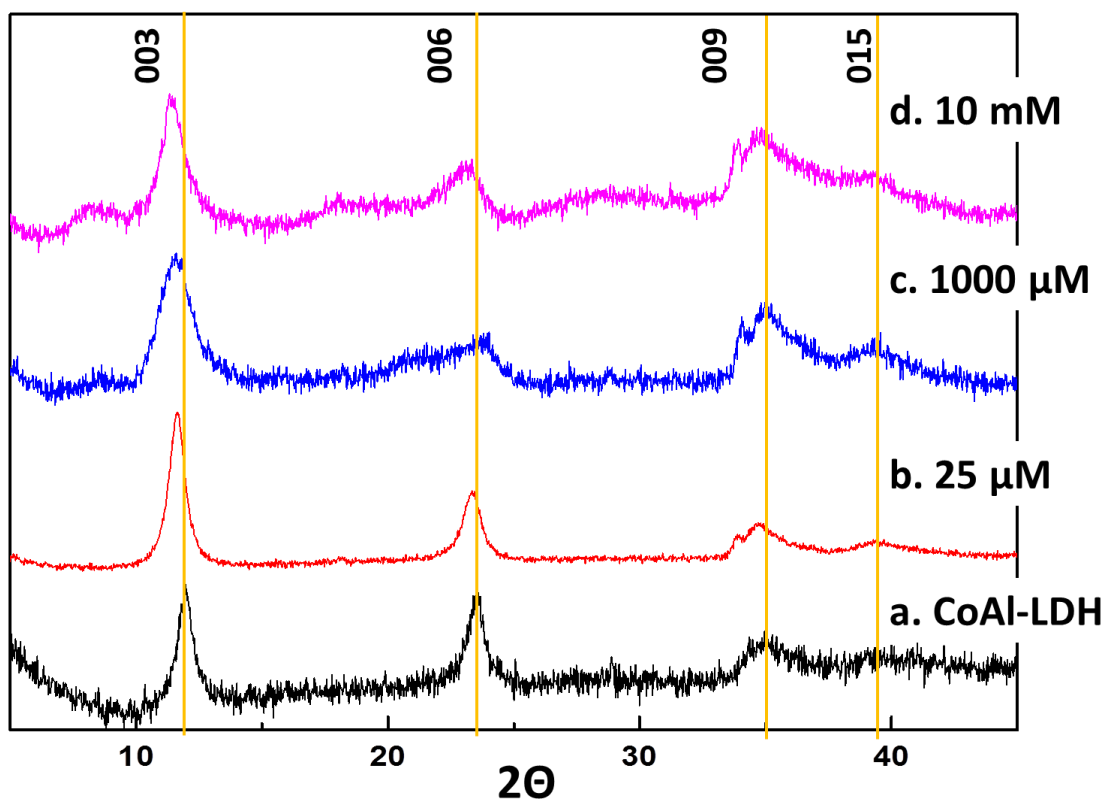
Figure 4. 2. XRD results of pure and tungstate-sorbed CoAl LDHs. Tungstate concentration indicated in the figure.

4.3. Results

4.3.1. Tungstate uptake experiments

Figure 4.1 shows the isotherm for tungstate uptake on CoAl LDH at pH 8 over the tungstate concentration range 50-2000 µM. The initial tungstate uptake increases steeply as tungstate concentration in the solution increases, followed by decreased slope at higher concentration. The tungstate coverage increased from 0.019 to 0.87 mmole/g for the concentration range studied. CoAl LDH shows a large sorption capacity for tungstate at pH 8, in agreement with previous studies indicating that LDHs are effective sorbents for anions.[2]

4.3.2. Tungstate intercalation into CoAl LDH

XRD data for synthesized CoAl LDH show typical patterns corresponding to the LDH phase.[22] The peaks at 11.6°, 23.3, and 35° 2-theta correspond to the (003), (006), and (009) basal planes. The corresponding interlayer distance for this synthetic CoAl LDH is 7.6 Å including the thickness of the layer, which is reasonable to consider Cl^- , CO_3^{2-}, and H_2O as the anion and molecule between layers in our initial condition.[2, 22, 23] After reaction with tungstate, systematic changes are observed in the XRD patterns, according to tungstate concentration (Figure 4.2). Most notably, a shift in the 003 peak to lower 2-theta is observed with increasing tungstate concentration, accompanied by peak broadening. A similar but smaller shift is observed for the 006 peak, however, the shift is obscured in the higher concentration samples because of asymmetry associated with the broadening. In addition, the higher concentration samples exhibit weak, broad features at 8 and 18 degrees. These shifts to lower 2-theta and the associated peak broadening indicate an expansion of the basal spacing, accompanied by some interlayer variation.[3] The progressive nature of the expansion with increasing tungstate concentration is consistent with increasing tungstate intercalation into the interlayers as tungstate concentration

136

increases in solution. The increase in broadening likely reflects variability in the degree of intercalation among layers.

4.3.4. L$_3$-edge XANES results

The W L$_3$-edge XANES are strongly linked to geometry and coordination of W(VI).[28] The white line feature in the W L$_3$-edge results from the electron transition from 2p to 5d orbital. Therefore, the number of peaks and their positions are sensitive to the ligand field splitting, which reflects the coordination geometry of W(VI). These details are best observed in the second derivative of the absorption edge, where subtle inflections correspond to one or more minima. Yamazoe showed that tetrahedral W(VI) compounds exhibit a single (sometimes asymmetric) minimum in the second derivative XANES, whereas octahedral W(VI) compounds exhibit two distinct minima. Furthermore, the energy separation between minima for octahedral coordination is correlated to the degree of octahedral distortion.

The second derivatives of W L$_3$-edge XANES for sorption samples and selected model compounds are shown in Figure 4.3, with energy separation values, where relevant, given in Table 1. Model compounds exhibit different numbers and shapes of minima in the second derivatives according to the W(VI) in each. Ba_2NiWO_6 and WO_3, both with octahedral coordination, show two distinct minima, while the tetrahedral W(VI) in $CaWO_4$ exhibits a single, slightly asymmetric minimum. One broad feature is seen in the spectrum of $Na_2W_2O_7$, which contains both octahedral and tetrahedral W(VI). More symmetric octahedra in Ba_2NiWO_6 result in a greater energy separation (4.5 eV) than the distorted octahedra in WO_3 with a 4.0 eV separation. These results are consistent with previous studies.[28, 30]

All tungstate-reacted LDH samples exhibit two distinct peaks in the second derivative XANES (Figure 4.3), indicating octahedral coordination. Close examination reveals that the energy separation of the minima increases progressively from 3.0 to 5.0 eV as tungstate

concentration increases. This indicates an increasingly symmetric octahedral environment of

W(VI) as tungstate concentration increases.

Table 4. 1 The energy gaps for sorption samples and model compounds in the second derivatives of W L$_3$-edge XANES

Name	Energy gap (eV)
CoAl layered double hydroxide at pH 7.5	
25 µM WO$_4^{2-}$	3.0
100 µM WO$_4^{2-}$	3.5
1000 µM WO$_4^{2-}$	5.0
Model compounds	
WO$_3$	3.3
Ba$_2$NiWO$_6$	4.5
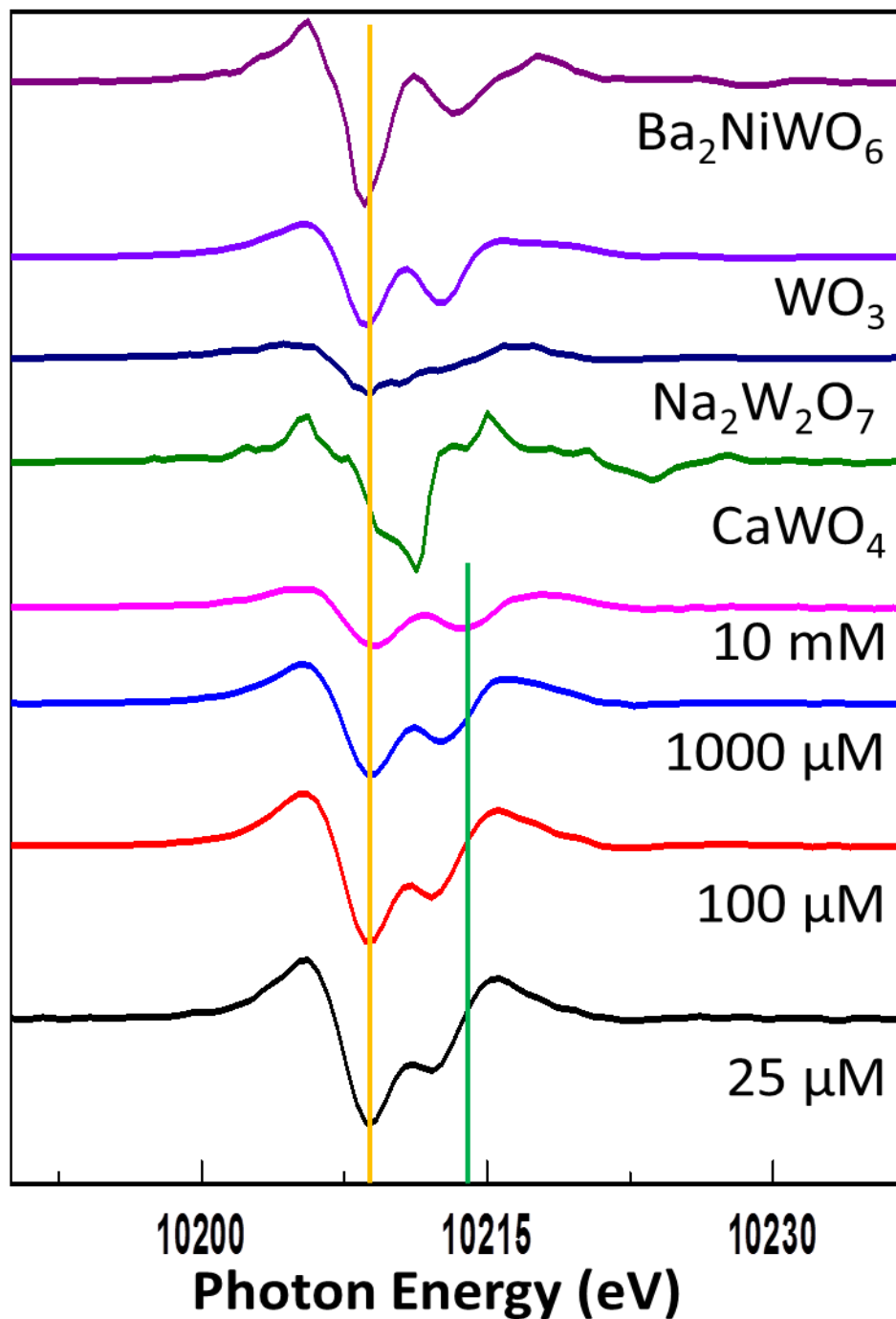
Figure 4. 3. Second derivatives of W L_3-edge XANES for sorption samples and model compounds. The number of peaks is related tungsten coordination.

4.3.5. L$_3$-edge EXAFS result and fitting

The W L$_3$-edge EXAFS and corresponding Fourier transform magnitudes of CoAl LDH reacted with tungstate at different concentrations are compared in Figure 4.4. Broadly, the chi functions and FT magnitudes are similar for all samples. The fitting results are summarized in table 2. Because the XANES analysis confirms octahedral coordination of W(VI), with varying degrees of distortion, the first peak in all spectra was fit using two W-O paths with the total CN near 6. For higher shells, various combinations of W-Co and W-W paths were used to fit the spectra. A MS path of a near-linear O-W-O chain was included to account for the distinct splitting of the first oscillation in the chi functions, in agreement with previous findings. [27]Best fits were obtained with two W-Co paths and a combination of W-Co (a shorter distance) and W-W (a longer distance) for higher shells. We did not obtain a satisfactory fit using a combination of W-W (a shorter distance) and W-Co (a longer distance) paths, or two W-W paths even with constrained Debye-Waller factor. W-Co distances at 3.3 and 3.6 Å are in the range expected for corner- or edge-sharing of tungsten and cobalt octahedral units. The W-W distance at ~3.7 Å could alternatively correspond to edge-sharing of W(VI) octahedra in a polytungstate.
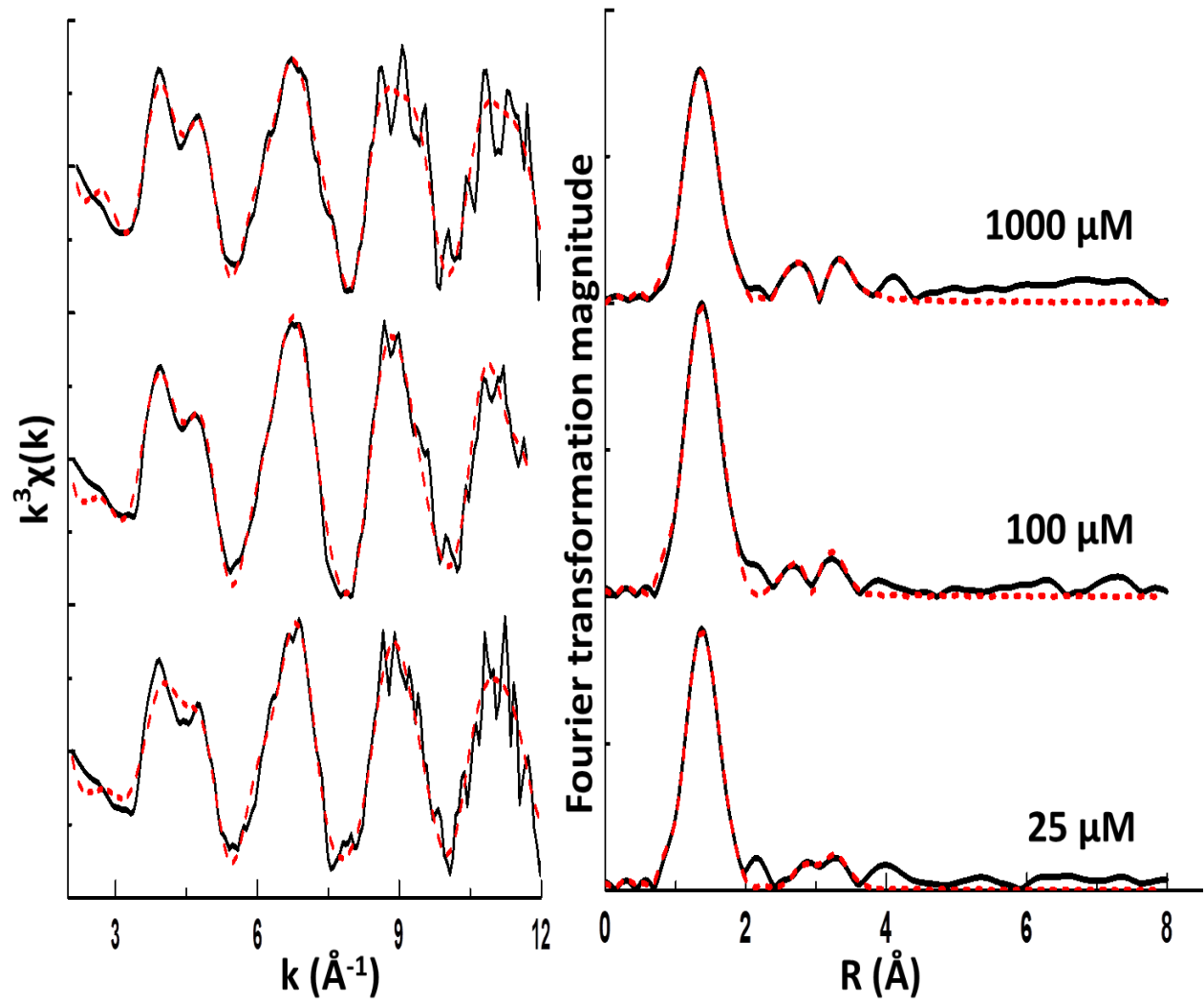
Figure 4. 4. W L$_3$-edge EXAFS spectra for sorption samples.

Table 4. 2 The summary of fitting results for sorption samples

Sample	Path	CN^a	$R\ (\text{Å})^b$	$\sigma^2\ (\text{Å}^2)^c$	$\Delta E0$ (eV)
1000 µM (2 W-Co)	W-O1	2.9	1.76	0.003	
	W-O2	1.8	2.08	0.01*	3.1
	W-Co	1.1	3.30	0.008	
	W-Co	1.9	3.69	0.007	
1000 µM (W-Co, W-W)	W-O1	2.9	1.77	0.003	
	W-O2	1.9	2.08	0.01*	3.9
	W-Co	0.9	3.30	0.005	
	W-W	1.6	3.77	0.01*	
100 µM (2 W-Co)	W-O1	3.8	1.76	0.004	
	W-O2	3.2	2.11	0.01*	0.3
	W-Co	1.2	3.28	0.006	
	W-Co	1.7	3.55	0.008*	
100 µM (W-Co, W-W)	W-O1	3.8	1.77	0.004	
	W-O2	3.2	2.11	0.01*	2.2
	W-Co	1.2	3.25	0.01*	
	W-W	3.3	3.68	0.01*	
25 µM (2 W-Co)	W-O1	3.1	1.77	0.003	
	W-O2	2.2	2.10	0.01*	2.6
	W-Co	1.0	3.37	0.01*	
	W-Co	1.4	3.59	0.01*	
25 µM (W-Co, W-W)	W-O1	3.0	1.77	0.003	
	W-O2	2.1	2.11	0.01*	2.4
	W-Co	0.6	3.43	0.01*	
	W-W	1.8	3.67	0.01*	

*: fixed in the fitting,

a : coordination number (±20%), b: distance in Å (±0.02 Å),

c : Debye-Waller factor

4.4. Discussion

The tungstate reactions with CoAl LDH described here document a large sorption capacity for tungstate at pH 8, a pH condition where uptake of tungstate and other oxyanions tends to be limited. This finding supports previous studies demonstrating that oxyanions, such as arsenate, vanadate, phosphate, and molybdate, can be effectively removed from near-neutral and basic solutions by LDH phases.[2] At pH 8, the dominant W(VI) aqueous species is tetrahedral, WO_4^{2-}, similar to the oxyanions mentioned above.[14]

Three possible mechanisms for the removal of oxyanions from aqueous solutions by LDHs include surface adsorption, anion exchange, and reconstruction of LDH precursors. In the latter two cases, anions are intercalated between metal layers. The reconstruction mechanism involves thermal treatment (calcination) and we do not consider it further here.[2]

The intercalation of tungstate via the anion exchange mechanism is supported by the XRD results, which showed progressive changes in the position and width of basal peaks of CoAl LDH.[2, 23] These observations demonstrated increasing interlayer expansion (from 7.6 Å to 11.1 Å) with increasing tungstate concentration. This is consistent with increasing exchange of tungstate for Cl$^-$, the dominant anion from synthesis, and possibly H_2O. The similar expansion of the interlayer space was observed by Ciocan et al. in molybdate intercalation study into MgAl LDH.[31] The XRD results showed broaden and asymmetric peaks, suggesting that the LDH phase is more or less disordered.

Although our findings support intercalation in the LDH via anion exchange, it is possible that adsorption onto surface sites is also operative in removing some tungstate from solution. In general, LDHs show large surface areas and high point of zero charge for CoAl LDH (pH 6.8-9.5).[32] Therefore, surface adsorption is expected to contribute to the overall sorption capacity of CoAl LDH for tungstate, even if only to a small extent.

Intercalation of tungstate in LDHs has been reported by previous workers. Mohapatra et. al reported intercalation of tungstate, into ZnY LDH, which they interpreted to be monomeric WO_4^{2-} on the basis of FT-IR.[33] Maciuca et al. concluded that a mixture of monomeric and polytungstates were present in anion exchange experiments with MgAl LDH.[34] Evans et al. also observed intercalation of Keggin-type polytungstate in MgAl LDH synthesized through a reconstitution mechanism.[35] These studies documented interlayer expansion using XRD resulting fromtungstate intercalation. The study by Maciuca et al. reported a similar basal spacing (10.46 Å) to our result (11.1 Å).[34] Therefore, we cannot rule out the possible existence of polytungstates into layers.

An interesting result from the W L_3-edge XANES is the presence of octahedral coordination for all of the tungstate-reacted CoAl LDH samples. Inasmuch as the dominant aqueous form of tungstate is monomeric WO_4^{2-} at pH 8, this result indicates that tungstate changes coordination from tetrahedral in the solution to octahedral in CoAl LDH.[16] This result is not entirely unexpected since our previous work has demonstrated that WO_4^{2-} undergoes a change in coordination during sorption on boehmite, where it is associated with polymerization. Furthermore, other studies have observed similar behavior during sorption.[30](Chapter 2)

Our W L_3-edge EXAFS results support the close proximity of tungstate with structural units of the CoAl LDH, but do not uniquely identify the location of the tungstate. Only minor differences were observed in the EXAFS results for the different tungstate concentrations. Fits of second and higher shell features (near 3-4 Å) in the FT magnitude support W-Co paths and/or the combination of W-Co and W-W paths, with W-Co and W-W distances comparable to those in model compounds. However, these distances do not necessarily distinguish intercalation from surface adsorption. Vaysse et al. reported the dimeric tungstate species in (Ni or Co)Al LDH

with the absence of the backscattering from Ni or Co in the host LDH.[36] Given our XRD evidence for intercalation of tungstate, we tentatively conclude that the EXAFS reflect the interlayer local environment, at least predominantly. Further experiment study, such as Raman or FT-IR, would be needed to provide additional constraints on the local structure.[23, 37]

4.5. Conclusion

Our present findings demonstrate the possible application of CoAl LDH for tungstate removal from aqueous media at pH 8, where more mobile tungstate exists. The large sorption capacity of CoAl LDH for tungstate is expected to effectively limit tungstate in aqueous systems via the anion exchange mechanism. However, the intercalation reaction into LDHs is sensitive to competitive anions such as CO_3^{2-}, $PO_4^{3-,}$ and SiO_4^{2-}.[2, 3, 5] We lack an understanding of the competitive sorption reaction of tungstate with other anions. Hence, further investigations of the tungstate sorption with other anions are needed to examine the prospective application of LDH for tungstate removal from aqueous systems. Strigul emphasized that tungstate species is significantly relevant to its toxicity.[16] Therefore, the determination of tungstate species is important to evaluate the toxicity and bioavailability. The stability of LDHs will be also needed to consider for the possible application of LDHs in the removal of contaminants.

Reference

1.   Khan, A. I.; O'Hare, D., Intercalation chemistry of layered double hydroxides: recent developments and applications. *J Mater Chem* 2002, *12*, (11), 3191-3198.

2.   Goh, K. H.; Lim, T. T.; Dong, Z., Application of layered double hydroxides for removal of oxyanions: A review. *Water Res* 2008, *42*, (6-7), 1343-1368.

3.   Carbajal Arizaga, G. G.; Satyanarayana, K. G.; Wypych, F., Layered hydroxide salts: Synthesis, properties and potential applications. *Solid State Ionics* 2007, *178*, (15-18), 1143-1162.

4.   Cavani, F.; Trifirò, F.; Vaccari, A., Hydrotalcite-type anionic clays: Preparation, properties and applications. *Catal Today* 1991, *11*, (2), 173-301.

5.   Feng, L.; Duan, X., Applications of layered double hydroxides. *Struct Bond* 2006, *119*, 193-223.

6.   Liu, M.; Yang, J. J.; Wu, G. Q.; Wang, L. Y., Performance and mechanism of Mg, Al layered double hydroxides and layered duble oxides for sulfide anion (S2-) removal. *Chinese J Inorg Chem* 2006, *22*, (10), 1771-1777.

7.   Lv, L.; He, J.; Wei, M.; Evans, D. G.; Duan, X., Factors influencing the removal of fluoride from aqueous solution by calcined Mg-Al-CO3 layered double hydroxides. *J Hazard Mater* 2006, *133*, (1-3), 119-128.

8.   Lv, L. A.; He, J.; Wei, M.; Evans, D. G.; Duan, X., Uptake of chloride ion from aqueous solution by calcined layered double hydroxides: Equilibrium and kinetic studies. *Water Res* 2006, *40*, (4), 735-743.

9.   Kang, M. J.; Chun, K. S.; Rhee, S. W.; Do, Y., Comparison of sorption behavior of I- and TcO4- on Mg/Al layered double hydroxide. *Radiochim Acta* 1999, *85*, (1-2), 57-63.

10.   Toraishi, T.; Nagasaki, S.; Tanaka, S., Adsorption behavior of IO3- by CO32-- and NO3--hydrotalcite. *Appl Clay Sci* 2002, *22*, (1-2), 17-23.

11.	Zhang, M.; Reardon, E. J., Removal of B, Cr, Mo, and Se from wastewater by incorporation into hydrocalumite and ettringite. *Environ Sci Technol* 2003, *37*, (13), 2947-2952.

12.	Wang, S. L.; Hseu, R. J.; Chang, R. R.; Chiang, P. N.; Chen, J. H.; Tzou, Y. M., Adsorption and thermal desorption of Cr(VI) on Li/Al layered double hydroxide. *Colloid Surface A* 2006, *277*, (1-3), 8-14.

13.	Yang, L.; Dadwhal, M.; Shahrivari, Z.; Ostwal, M.; Liu, P. K. T.; Sahimi, M.; Tsotsis, T. T., Adsorption of arsenic on layered double hydroxides: Effect of the particle size. *Ind Eng Chem Res* 2006, *45*, (13), 4742-4751.

14.	Prasanna, S. V.; Kamath, P. V., Synthesis and characterization of arsenate-intercalated layered double hydroxides (LDHs): Prospects for arsenic mineralization. *J Colloid Interf Sci* 2009, *331*, (2), 439-445.

15.	Ferreira, O. P.; de Moraes, S. G.; Duran, N.; Cornejo, L.; Alves, O. L., Evaluation of boron removal from water by hydrotalcite-like compounds. *Chemosphere* 2006, *62*, (1), 80-88.

16.	Strigul, N., Does speciation matter for tungsten ecotoxicology? *Ecotox Environ Safe* 2010, *73*, (6), 1099-1113.

17.	Koutsospyros, A.; Braida, W.; Christodoulatos, C.; Dermatas, D.; Strigul, N., A review of tungsten: From environmental obscurity to scrutiny. *J Hazard Mater* 2006, *136*, (1), 1-19.

18.	Fierro, J. L. G., *Metal Oxides: chemistry and applications*. CRC press: 2005.

19.	Cruywagen, J. J., Protonation, oligomerization, and condensation reactions of vanadate(V), molybdate(VI), and tungstate(VI). *Adv Inorg Chem* 2000, *49*, 127-182.

20.	Gustafsson, J. P., Modelling molybdate and tungstate adsorption to ferrihydrite. *Chem Geol* 2003, *200*, (1-2), 105-115.

21.	Xu, N.; Christodoulatos, C.; Braida, W., Modeling the competitive effect of phosphate, sulfate, silicate, and tungstate anions on the adsorption of molybdate onto goethite. *Chemosphere* 2006, *64*, (8), 1325-1333.

22.	Perez-Ramirez, J.; Mul, G.; Moulijn, J. A., In situ Fourier transform infrared and laser Raman spectroscopic study of the thermal decomposition of Co-Al and Ni-Al hydrotalcites. *Vib Spectrosc* 2001, *27*, (1), 75-88.

23. Vaysse, C.; Guerlou-Demourgues, L.; Demourgues, A.; Lazartigues, F.; Fertier, D.; Delmas, C., New (Ni, Co)-based layered double hydroxides with intercalated oxometalate (Mo, W) species, obtained by chimie douce reactions. *J Mater Chem* 2002, *12*, (4), 1035-1043.

24. Ressler, T., WinXAS: a program for X-ray absorption spectroscopy data analysis under MS-Windows. *J Synchrotron Radiat* 1998, *5*, 118-122.

25. Ressler, T., WinXAS: A new software package not only for the analysis of energy-dispersive XAS data. *Le Journal de Physique IV* 1997, *7*, (C2), C2-269-C2-270.

26. Zabinsky, S. I.; Rehr, J. J.; Ankudinov, A.; Albers, R. C.; Eller, M. J., Multiple-Scattering Calculations of X-Ray-Absorption Spectra. *Phys Rev B* 1995, *52*, (4), 2995-3009.

27. Kuzmin, A.; Purans, J.; Benfatto, M.; Natoli, C. R., X-Ray-Absorption Study of Rhenium L3 and L1 Edges in Reo3 - Multiple-Scattering Approach. *Phys Rev B* 1993, *47*, (5), 2480-2486.

28. Yamazoe, S.; Hitomi, Y.; Shishido, T.; Tanaka, T., XAFS study of tungsten L-1- and L-3-edges: Structural analysis of WO3 species loaded on TiO2 as a catalyst for photo-oxidation of NH3. *J Phys Chem C* 2008, *112*, (17), 6869-6879.

29. Sanchez, C.; Livage, J.; Launay, J. P.; Fournier, M., Electron Delocalization in Mixed-Valence Tungsten Polyanions. *J Am Chem Soc* 1983, *105*, (23), 6817-6823.

30. Kashiwabara, T.; Takahashi, Y.; Marcus, M. A.; Uruga, T.; Tanida, H.; Terada, Y.; Usui, A., Tungsten species in natural ferromanganese oxides related to its different behavior from molybdenum in oxic ocean. *Geochim Cosmochim Ac* 2013, *106*, 364-378.

31. Ciocan, C. E.; Dumitriu, E.; Cacciaguerra, T.; Fajula, F.; Hulea, V., New approach for synthesis of Mo-containing LDH based catalysts. *Catal Today* 2012, *198*, (1), 239-245.

32. Yang, L.; Shahrivari, Z.; Liu, P. K. T.; Sahimi, M.; Tsotsis, T. T., Removal of trace levels of arsenic and selenium from aqueous solutions by calcined and uncalcined layered double hydroxides (LDH). *Ind Eng Chem Res* 2005, *44*, (17), 6804-6815.

33. Mohapatra, L.; Parida, K.; Satpathy, M., Molybdate/Tungstate Intercalated Oxo-Bridged Zn/Y LDH for Solar Light Induced Photodegradation of Organic Pollutants. *J Phys Chem C* 2012, *116*, (24), 13063-13070.

34.   Maciuca, A. L.; Ciocan, C. E.; Dumitriu, E.; Fajula, F.; Hulea, V., V-, Mo- and W-containing layered double hydroxides as effective catalysts for mild oxidation of thioethers and thiophenes with H(2)O(2). *Catal Today* 2008, *138*, (1-2), 33-37.

35.   Evans, J.; Pillinger, M.; Zhang, J. J., Structural studies of polyoxometalate-anion-pillared layered double hydroxides. *J Chem Soc Dalton* 1996, (14), 2963-2974.

36.   Vaysse, C.; Guerlou-Demourgues, L.; Demourgues, A.; Delmas, C., Thermal behavior of oxometalate (Mo,W)-intercalated layered double hydroxides: Study of the grafting phenomenon. *J Solid State Chem* 2002, *167*, (1), 59-72.

37.   Maczka, M.; Hanuza, J.; Waskowska, A., Vibrational studies of alkali metal hexatungstates. *J Raman Spectrosc* 2003, *34*, (6), 432-437.

Chapter 5. Tungstate sorption and coprecipitation with hydroxyapatite

Abstract

The mechanisms of tungstate sorption and coprecipitation with hydroxyapatite (HAP) were investigated through batch uptake experiments combined with X-ray diffraction and X-ray absorption spectroscopy. Tungsten L_3-edge XANES analysis of W-doped HAP indicates octahedral coordination of tungsten in the structure. This is supported by fits of W L_3-edge EXAFS that yield an average W-O distance of 1.96 Å, consistent with octahedral coordination. These findings indicate that the coordination of tungstate changes, from tetrahedral in solution (at pH 8) to octahedral in the structure, during the incorporation process. Fits distances for W-Ca paths in higher shells are consistent with substitution of tungstate in phosphate sites, presumably accompanied by local distortion. Tungstate uptake experiments in HAP-equilibrated suspensions reveal that sorption behavior and mechanisms differ between pH 5.5 and pH 8. At pH 8, XANES analysis reveals that sorbed tungstate occurs in octahedral coordination, requiring a coordination change from solution conditions where it occurs as the tetrahedral WO_4^{2-} species. Additional studies are needed to fully identify tungstate surface complexes on HAP.

5.1. Introduction

Tungstate, W(VI), has recently received attention as a potential contaminant and health risk in water and soil systems. Tungstate is primarily derived from oxidative weathering and dissolution of tungsten metal and alloys, which have long been considered as non-toxic. With widespread applications of tungsten, ranging from daily household products to highly specialized components of modern technology, occurrences of tungstate in environmental settings are increasing reported.[1, 2] Some military and mining areas show high levels of tungstate concentration in the soil.[3-5] The possible relevance of tungstate to a Leukemia cluster in Fallon,

NV, has been studied.[4, 5] Moreover, eco-toxicological studies of tungstate are now becoming a focus of researchers.[1, 2] The U.S. Environmental Protection Agency (EPA) does not regulate tungsten in drinking water, but Russia is controlling tungsten levels in drinking water (0.05 mg/l) and in lakes and rivers used for fishing (0.008 mg/l).[1]

Mono- and polytungstates are different in mobility, toxicity, and bio-accessibility in environment. Recently, Strigul reported tungsten toxicity is strongly related to its speciation.[2] This study found that polytungstate is more toxic to fish than monotungstate. Different bioavailability properties for monotungstate and polytungstate were also reported in a recent experimental study with sunflowers.[6] In aqueous solution, the speciation of tungstate is linked to its concentration and pH conditions.[2, 7-9 7-10] Formation of polymeric species, with octahedral coordination of tungsten, is favored under acidic conditions, while monotungstate, with tetrahedral W coordination, is dominant at neutral and basic conditions.[10] Tungstate polymerization in the solution is fairly complicated and not fully understood because of its sluggish kinetics and the existence of several intermediate species during the polymerization process.[9]

Sorption mechanisms on mineral surfaces play an important role in controlling mobility, toxicity, and bioavailability of contaminants in natural aqueous and soil systems. Physical factors such as pH, mineral surface properties, and speciation of tungstate affect sorption mechanisms on mineral surfaces. Moreover, surface sorbed species can be susceptible for remobilization when solution conditions change, or as a result of competitive sorption of other naturally occurring oxyanions such as carbonate and phosphate. Under these conditions, tungstate coprecipitated with a sparingly soluble phase may be less likely to release tungstate and may

therefore be an alternative mechanism for long-term immobilization of tungstate in natural environments.

Hydroxyapatite (HAP), $Ca_{10}(PO_4)_6(OH)_2$, has been suggested as a common mineral for remediation of contaminants. It also shares structural and compositional similarities with natural bone tissue.[11] The structure of HAP is well-known for accommodating impurity species owing to its inherent flexibility. As a result, many studies have focused on incorporation of anions and cations in the structure. A wide range of divalent cations are known to substitute in one or both Ca sites in HAP.[12-14] Previous studies have also reported anion substitution in channel site normally occupied by OH^-, F^-, or Cl^- , as well as in the PO_4^{3-} site, including CO_3^{2-}, SiO_4^{2-}, SO_4^{2-}, AsO_4^{3-} and VO_4^{3-}.[12, 15-19] Incorporation into the structure effectively reduces the mobility of these anions through the formation of solid solutions.

The tetrahedral tungstate anion, WO_4^{2-}, is larger in size than the phosphate group (W-O = 1.76 Å ; P-O =1.53 Å), yet substitution of phosphate by larger tetrahedral oxyanions has been reported in previous studies.[12, 18] Understanding the structure and mode of tungstate incorporation is important to determine the extent of its incorporation into HAP, and the related effect on solubility and long-term stability, and therefore the potential remobilization of the contaminant. In this study, we compare results of tungstate batch uptake experiments in pre-equilibrated HAP suspensions with coprecipitation experiments that lead to incorporation during HAP formation. We use X-ray absorption spectroscopy to evaluate the local structure of tungstate and compare mechanisms of uptake.

5.2. Materials and methods

5.2.1 Synthesis of tungstate-doped HAP

Tungstate-doped HAP was synthesized using the method described by Lee et. al.[18] Briefly, 0.19 M KH_2PO_4 and 0.02 M Na_2WO_4 (Acros) solutions in separated syringes were added via syringe pumps at a rate of 0.25 mL/min and 0.1 mL/min, respectively, into a reaction vessel containing 50 mL of 0.2 M of $Ca(NO_3)$ with vigorous stirring. The pH was maintained at a value of 8.5 with an auto-titrator. The reaction temperature was maintained at 75–80 ℃ during the synthesis. In order to avoid precipitation of $CaWO_4$, the WO_4^{2-} concentration was maintained below saturation. A white precipitate was filtered using 0.3 µm membrane filters, and washed three times with DI water before drying. A portion of each sample was dissolved using nitric acid to analyze the W concentration in the HAP. DCP-AES analysis yielded concentrations of 700 and 1500 ppm W in two HAP samples. Powder X-ray diffraction (XRD) was used to confirm the identity of the HAP phase and the absence of any secondary precipitate (Figure 5.3). These W-doped HAP samples were mounted in Lucite sample holders and sealed with Kapton tape prior to X-ray absorption spectroscopy measurements.
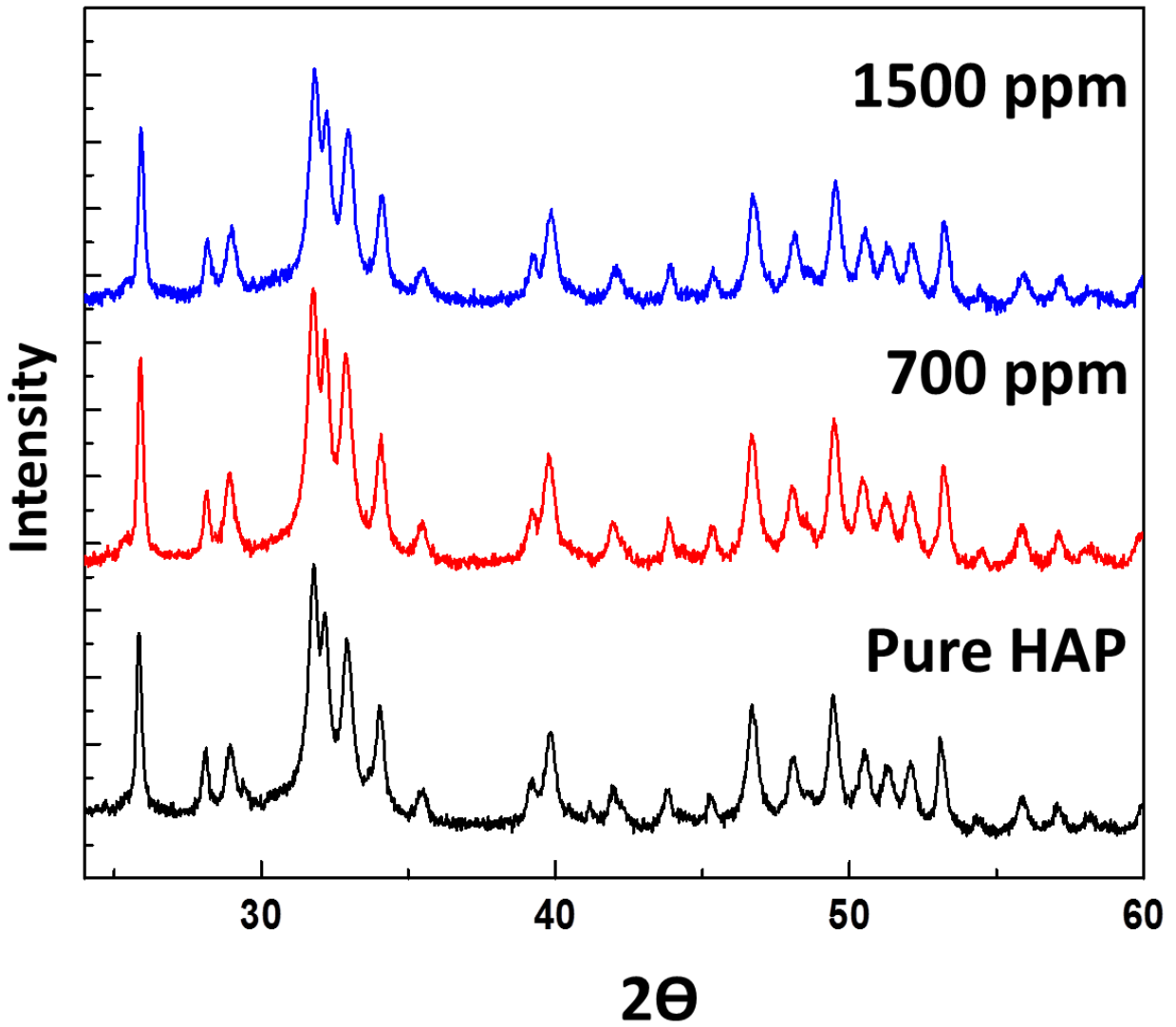
Figure 5. 1. XRD results of pure and W-doped HAP. Cu Kα radiation.

5.2.2 Tungstate batch sorption experiments on HAP

The HAP used for sorption experiments in this study is a precipitated reagent-grade tribasic calcium phosphate (J. T. Baker), with a surface area of 56 m^2/g.[18] XRD confirmed that it is HAP. HAP suspensions were pre-titrated to the target pH values and allowed to equilibrate for more than two weeks.[18] Suspensions were prepared with ionic strengths spanning the range 0.006-0.05 M. Freshly washed HAP was added to pre- equilibrated solutions to obtain final suspensions with a particle loading of 1 g/L for sorption experiments. Calculated amounts of 0.01 M Na_2WO_4 stock solution were added to suspensions. Small amounts of 0.1 M HCl or NaOH were used to make minor adjustments to pH. Sorption experiments with 50 µM tungstate were performed to determine the pH edge over the range pH 4.5-10. Isotherm experiments were conducted at pH 5.5 and 8 over a concentration range of 20-1000 µM W. Sorption suspensions were allowed to react for 24 h on a shaker table, after which 5 mL aliquots were taken from each suspension, filtered, and analyzed for tungsten concentration using DCP-AES to calculate the amount of tungstate sorbed on the surface. Selected samples were filtered to remove excess liquid and mounted as wet pastes in Lucite sample holders and sealed with Kapton tape for XAS data collection as described below.

5.2.3 W L_3-edge X-ray absorption spectroscopy

Tungsten L_3-edge XAS data were collected for selected samples and reference compounds at beamline X11B at the National Synchrotron Light Source (NSLS) at Brookhaven National Laboratory, and at sector 12BM at the Advanced Photon Source (APS) at Argonne National Laboratory. Model compounds ($CaWO_4$, WO_3, and TBA-W_6O_{19}) were mixed with boron nitride to obtain a proper edge step, and measured in transmission mode. EXAFS data from sorption samples were collected in fluorescence mode. A Si(111) monochromator was used with 10-30% detuning for harmonic rejection. Energy calibration was performed with a Ga filter

(K-edge, 10.367 keV) or a W metal foil for the L_3-edge (10.207 keV). The first inflection points in the absorption edge of a Ga filter or a W foil was assigned to the energy values, 10.367 keV or 10.207 keV. A PIPS detector (NSLS) and a 13-element Ge detector (APS) were used in fluorescence mode. Multiple XAS spectra were collected to obtain proper signal to noise ratio. Individual spectra were calibrated and averaged, and data analysis was performed with iFeffit and WinXAS.{Ressler, 1997 #28}{Zabinsky, 1995 #30} The $\chi(k)$ functions were extracted using cubic spline and were Fourier transformed with k^3 weighting over the k range 2.3-13 $\mathring{A}^{-1}$.

Theoretical phases shift and amplitudes were calculated by FEFF7 according to the published structures.[20] Shell-by-shell fitting was done in R-space. An amplitude reduction factor (S_0^2) was fixed with 0.9. No constraint was applied for fitting the first W-O shells. Coordination numbers (CN) for model compounds were fixed when values were known. Debye-Waller factors for higher shells for W-doped HAP were fixed at representative values ($0.008\mathring{A}^2$) when multiple nearby shells were present, and for weak backscattering atoms at high R values. For the second shell, various combinations of W-W and W-Ca paths were attempted in fitting. We did not add higher oxygen shells in the fitting because the good fitting result for model compounds was obtained without them.

5.2.4 XAS model compounds

XAS data were collected for several model compounds for comparison with the sorption and incorporated samples. Compounds were chosen to represent different W(VI) coordination environments, including isolated tetrahedra (scheelite, $CaWO_4$), octahedra (TBA-W_6O_{19}, WO_3), and a mixture of tetrahedral and octahedral ($Na_2W_2O_7$). TBA-W_6O_{19} contains polymeric W_6O_{19} units with all W atoms in octahedral coordination sharing edges. Tungsten occurs as distorted octahedra in WO_3, sharing all corners in a perovskite-like structure. $Na_2W_2O_7$ contains both tetrahedral and octahedral tungsten in a 1:1 ratio. TBA-W_6O_{19} (tetrabutyl-ammonium

hexatungstate) and $Na_2W_2O_7$ were synthesized by methods described in previous studies.[21, 22] Powder XRD confirmed the structures for model compounds without any impurity phases.

5.3. Results

5.3.1 Aqueous speciation and saturation state calculations

Tungstate species in the HAP-equilibrated solution at pH 5.5 and pH 8 were calculated with PhreeqC using a modified LLNL database.[23] Stability constants for polymeric tungstate species that were observed in previous studies and known to be stable were included in these calculations (Table 1).[9, 10] It is known, however, that formation of several polytungstate species is sluggish kinetically, with intermediate species present.[8] Tungstate speciation results and saturation indexes are summarized in Table 2. At pH 5.5 formation of polymeric species, including $H_2W_{12}O_{42}^{10-}$ and $W_7O_{24}^{6-}$ is favored, while monotungstate (WO_4^{2-}) is the dominant species at pH 8. Thermodynamic calculations show that HAP-equilibrated solutions are supersaturated with respect to $CaWO_4$ (scheelite) at total W concentrations greater than 50 (pH 5.5) and 200 µM (pH 8). Yet, no evidence for precipitation was observed in the sorption experiments, which is consistent with previous studies showing that extremely rapid uptake of tungstate reduces its concentration before any precipitation occurs.

Table 5. 1 Stability constants of polytungstate species used for simulation of aqueous speciation (at 298K)

Species	Solution Species Reaction	Stability Constant (log K)	Reference
Paratungstate A	$7\ WO_4^{2-} + 8\ H^+ <=> W_7O_{24}^{6-} + 4\ H_2O$	68.17	
Paratungstate B	$12\ WO_4^{2-} + 14\ H^+ <=> H_2W_{12}O_{41}^{10-} + 6\ H_2O$	118.00	9
a-Metatungstate	$12\ WO_4^{2-} + 18\ H^+ <=> H_2W_{12}O_{40}^{6-} + 8\ H_2O$	144.72	

Table 5. 2 Thermodynamic calculation of tungstate speciation and saturation state

| pH 8			
Concentration			% of total concentration
1000 µM	Speciation	WO_4^{2-}	99.637
		$CaWO_4(aq)$	0.36
	SI*		0.707, $CaWO_4(s)$
200 µM	Speciation	WO_4^{2-}	99.610
		$CaWO_4(aq)$	0.387
	SI*		0.040, $CaWO_4(s)$
50 µM	Speciation	WO_4^{2-}	99.604
		$CaWO_4(aq)$	0.393
	SI*		-0.556, $CaWO_4(s)$
pH 5.5			
1000 µM	Speciation	WO_4^{2-}	19.302
		$H_2W_{12}O_{42}^{10-}$	13.147
		$W_7O_{24}^{6-}$	66.409
		$CaWO_4(aq)$	3.065
	SI*		1.641, $CaWO_4(s)$
50 µM	Speciation	WO_4^{2-}	85.515
		$CaWO_4(aq)$	13.628
	SI*		0.9888, $CaWO_4(s)$

SI* : Saturation Index
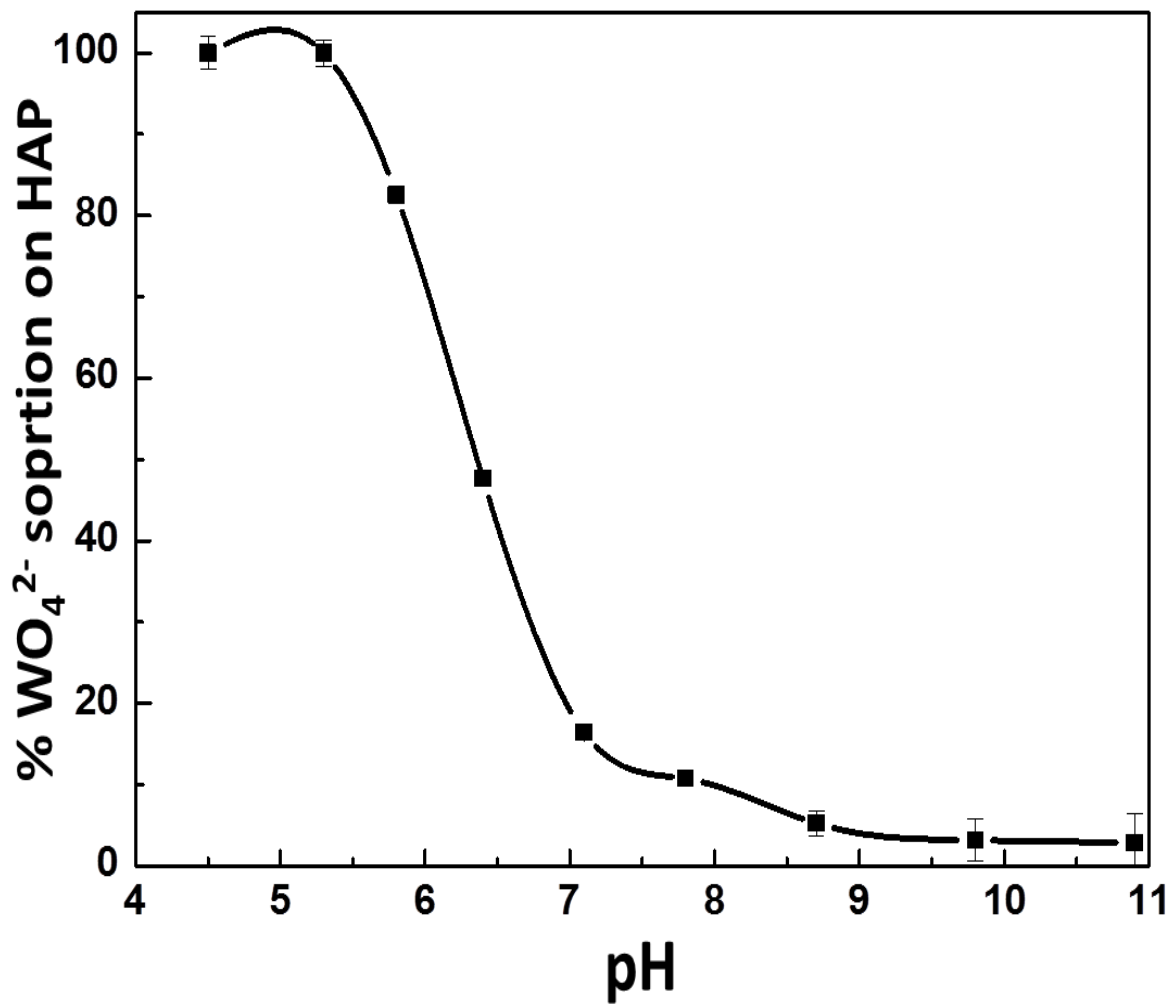
Figure 5. 2. The pH dependence of tungstate sorption on HAP. Initial $[WO_4^{2-}] = 50$ μM and 1 g/L particle loading.
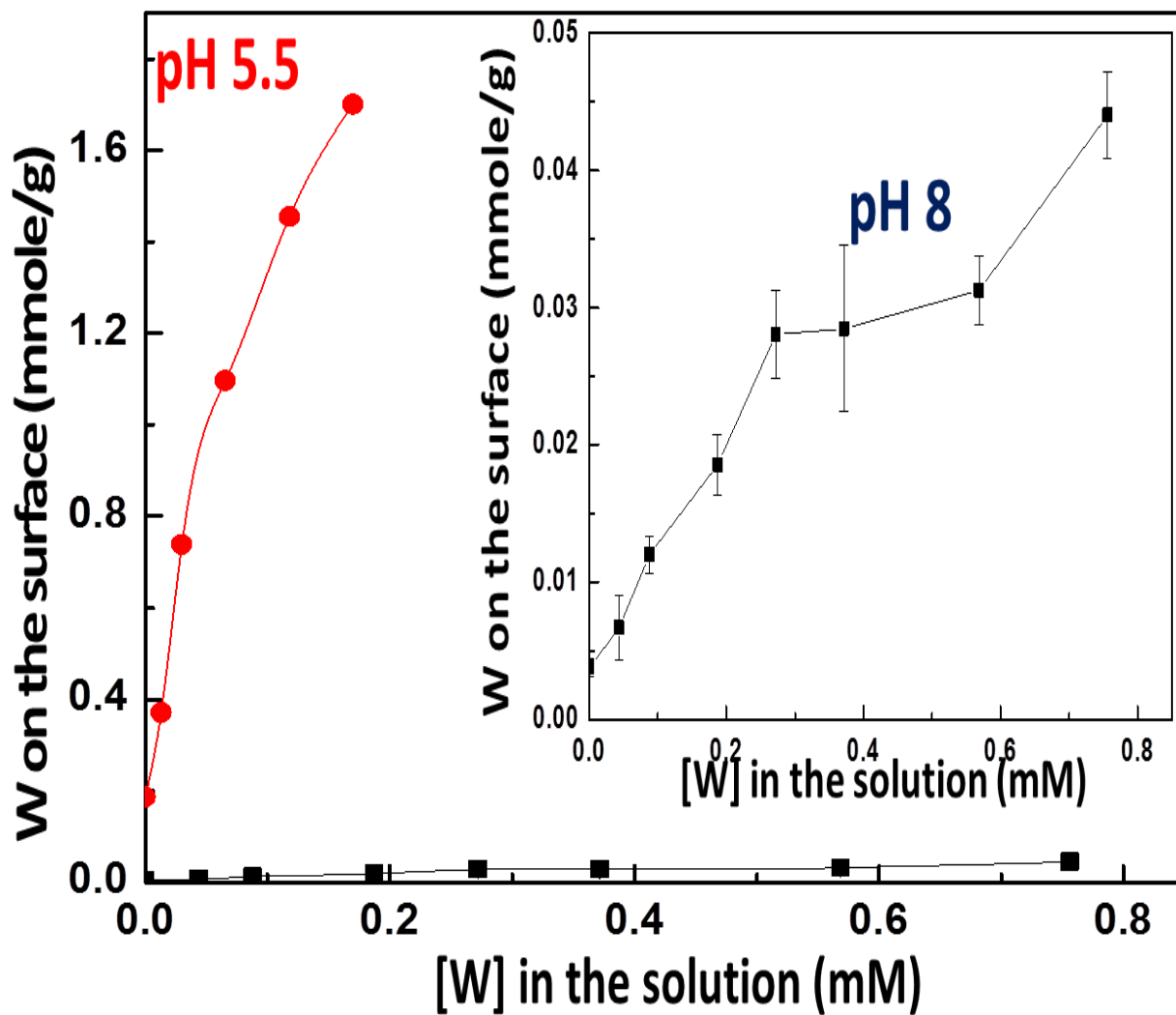
Figure 5. 3. Tungstate isotherm experiments on HAP over the concentration range 50-1000 µM at pH 5.5 and 8. The enlarged result of isotherm at pH 8 is inserted in the figure.

5.3.2 Tungstate batch uptake trends on HAP

The pH dependence of tungstate sorption on HAP at $[WO_4^{2-}] = 50$ µM is shown in Figure 1. Tungstate sorption behavior is typical for anion sorption. A maximum in uptake occurs near pH 5, with decreasing uptake as pH increases. 50 % sorption is observed at pH 6.5, near the point of zero charge (PZC) of HAP (6.9-8.5),[24] and 10 % or less sorption is observed above neutral pH conditions.

Subsequent uptake experiments were conducted at pH 5.5 and 8 over the concentration range 50-1000 µM to obtain isotherms. These pH conditions were chosen on the basis of pH edge results (Figure 1) and the tungstate speciation calculations. At both pH conditions, tungstate uptake increases as tungstate concentration in solution increases without reaching a maximum in the concentration range studied. Greater tungstate sorption occurs at pH 5.5, consistent with the pH edge results. The surface coverage of tungstate is 0.008-0.423 mmole/g and 0.004-0.034 mmole/g at pH 5.5 and 8, respectively. The greater tungstate uptake at pH 5.5 could be attributed to either the greater affinity of the HAP surface for anion species owing to its more positive surface charge or the greater formation of $CaWO_4$ precipitate (if such precipitation occurred). Tungsten L_3-edge XAS data were collected for selected sorption samples to identify mechanisms of uptake.

5.3.4 W L_3-edge XANES results

W L_3-edge XANES has proven useful for distinguishing W(VI) coordination environments.[25, 26] The number of minima in the second derivative of the XANES is strongly correlated to the coordination geometry (tetrahedral or octahedral), and the separation between minima reflects the degree of distortion in W(VI) octahedra. Second derivative spectra are shown in figure 4. $CaWO_4$ represents tetrahedral coordination with a single, asymmetric minimum, while octahedrally coordinated tungsten(VI) in WO_3 shows two well separated minima. The

second derivative for $Na_2W_2O_7$, which contains both tetrahedral and octahedral W(VI), exhibits a broad, asymmetric feature with a shoulder on the higher energy side. The two W-doped HAP samples (700 and 1500 ppm) show two minima with energy separations of 4 eV. This separation value indicates distorted octahedra for tungstate doped into the HAP structure.[25, 26] This finding therefore indicates that tungstate changed its coordination from tetrahedral (in solution) to octahedral (in the HAP) during coprecipitation.

Two well separated minima were observed for all sorption samples at pH 8 and for the lowest concentration sorption sample at pH 5.5 (Figure 4). This confirms that W(VI) in these sorption samples is dominantly (or exclusively) in octahedral coordination. This further confirms that $CaWO_4$ either did not precipitate in this suspension or that it was a very minor component, despite the aqueous speciation calculations which showed that the initial state was supersaturated. For the two higher concentration sorption samples at pH 5.5, one broad, slightly asymmetric minimum is found (Figure 4). These second derivative spectra are noticeably different than those for the other sorption sample. Aqueous speciation calculation indicated the initial state for these solutions were also supersaturated with respect to $CaWO_4$. However, the second derivative is dissimilar to that for the $CaWO_4$ reference sample, and more similar to that for the $Na_2W_2O_7$ sample, which contains a mixture of W(VI) octahedra and tetrahedra. W(VI) octahedral linked to W(VI) tetrahedra in this model compound. These results indicate different tungstate species exist on the HAP surface at pH 5.5 depending on tungstate concentration, with a distinct change between 50 and 100 uM.
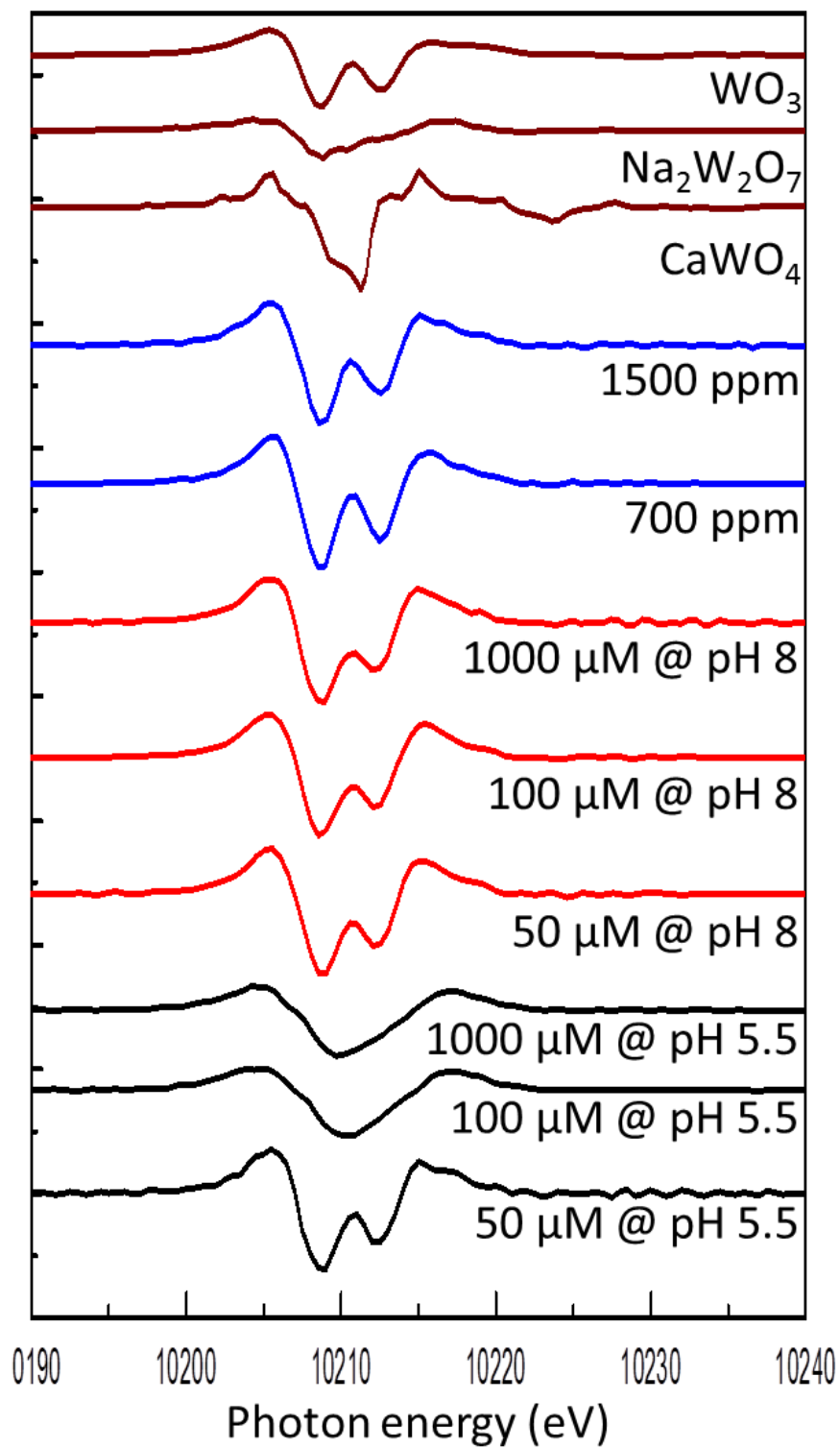
Figure 5. 4. W L_3-edge second derivative XANES spectra showing differences that distinguish tetrahedral and octahedral coordination of W(VI).

5.3.5 W L$_3$-edge EXAFS fitting results

Figure 5 shows W L$_3$-edge EXAFS chi functions and corresponding Fourier transforms (FT) for selected model compounds and W-doped HAP. TBA-W$_6$O$_{19}$ and WO$_3$ were chosen for edge- and corner-shared W(VI) octahedra, respectively. TBA-W$_6$O$_{19}$ shows a strong peak in the FT magnitude at ~3 Å (not corrected for phase shift), while the FT for WO$_3$ exhibits a peak at ~3.5 Å (not corrected for phase shift). CaWO$_4$ has exclusively tetrahedral coordination of W(VI).

For fitting the model compounds, CN was constrained to the known values from published structures. In the fitting for all model compounds, a multiple scattering (MS) contribution with a near linear O-W-O chain was included to obtain satisfactory fit results for the split feature near 3.5-5 Å^{-1} in chi functions.{Kuzmin, 1993 #36} All fitting results for model compounds are summarized in Table 3. CaWO$_4$ is well fit with 4 first-shell oxygen atoms at 1.78 Å, and 4 oxygen atoms from a second shell at 2.94 Å. Eight Ca atoms are located at 3.78 Å. WO$_3$ was fit with six oxygen atoms in three shells (2 each at 1.78, 1.93, and 2.14 Å), reflecting the distorted octahedral environment. W-W distances occur at 3.7 and 3.9 Å in the exclusively corner-sharing structure. TBA-W$_6$O$_{19}$ also contains distorted W(VI) octahedra. The first shell was fit with one oxygen atom at 1.71 Å, four oxygen atoms at 1.92 Å, and one oxygen atom at 2.32 Å. The W(VI) octahedra in TBA-W$_6$O$_{19}$ are edge-sharing, with W-W distances at 3.3 Å.
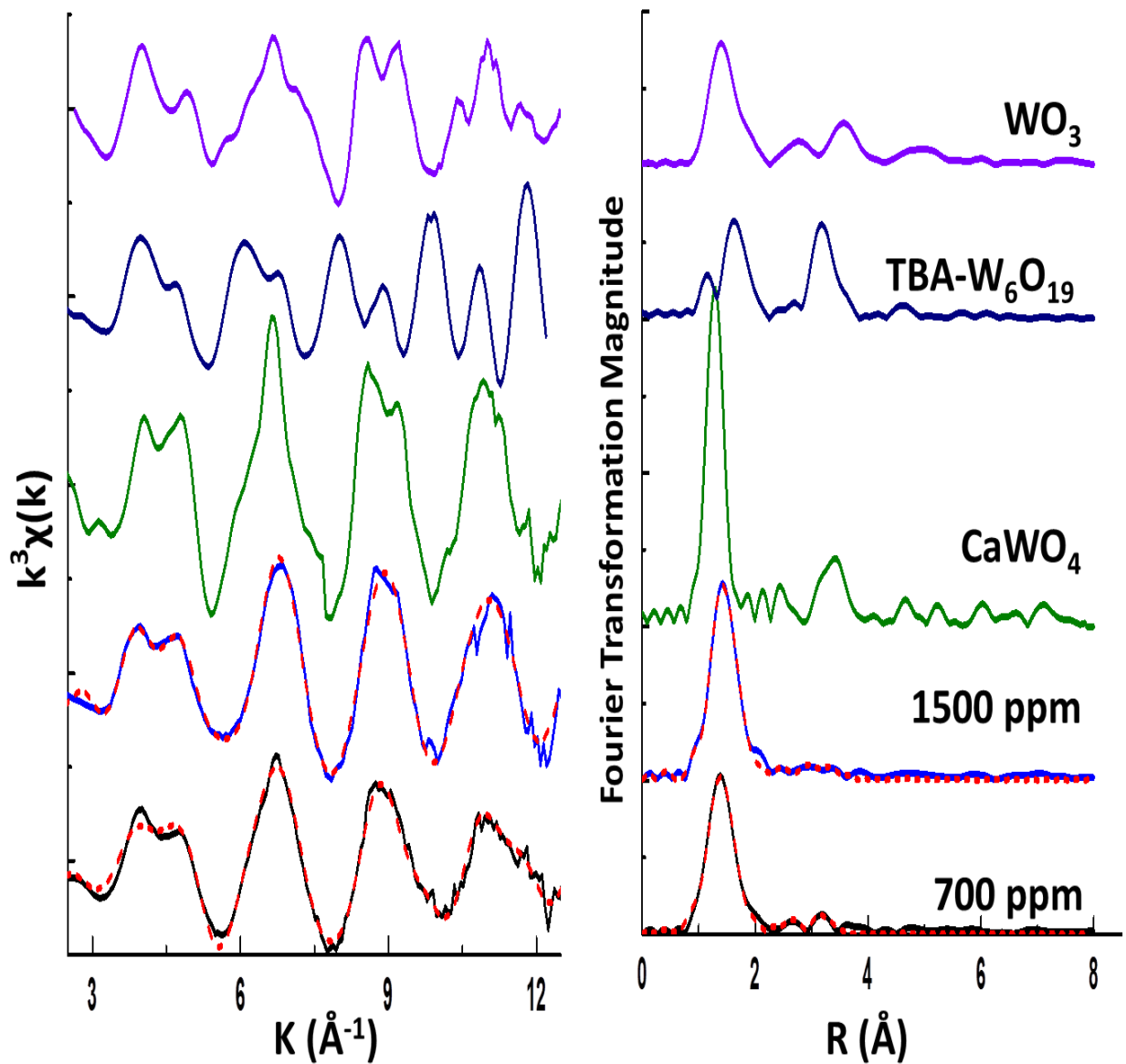
Figure 5. 5. W L_3-edge EXAFS chi functions (left) and corresponding Fourier transform magnitudes (right, not corrected for phase shifts) for W-doped HAP (700 and 1500 ppm) and selected model compounds. Dotted lines in the figure indicate the fitting results. The results are summarized in Table 4.

Table 5. 3 Summary of W L$_3$-edge EXAFS fitting results of model compounds

Sample	Path	CN^a	R(Å)^b	σ^2(Å^2)^c	ΔE0 (eV)
CaWO$_4$	W-O1	4*	1.78	0.004	3.5
	W-O2	4*	2.94	0.012	
	W-Ca	8*	3.78	0.02	
TBA-W$_6$O$_{19}$	W-O1	1.0*	1.71	0.002	0.5
	W-O2	4.0*	1.92	0.003	
	W-O3	1*	2.32	0.004	
	W-W1	4.0*	3.30	0.004	
WO$_3$	W-O1	2*	1.78	0.001	1.3
	W-O2	2*	1.93	0.007	
	W-O3	2*	2.14	0.004	
	W-W	2*	3.78	0.002	
	W-W	4*	3.9	0.006	

*: fixed in the fitting,

a : coordination number (±20%), b: distance in Å (±0.02 Å),

c : Debye-Waller factor,

EXAFS spectra for selected sorption samples are shown in Figure 6. Data for $CaWO_4$ are also shown for comparison. EXAFS chi functions and FT magnitudes for all sorption samples are clearly different from those for $CaWO_4$, confirming that this phase was not a (significant) precipitate in the suspensions even though the initial solution was supersaturated in most cases, and consistent with the XANES results. Differences between pH 5.5 and 8 sorption samples are observed in the first (split) oscillation and also near 7 and 9 $Å^{-1}$ in the chi functions. In the FT magnitudes, pH 8 sorption samples show distinctly more intensive first peaks (corresponding to the first oxygen shell) compared to the pH 5.5 sorption samples. For the pH 8 samples, the intensity of the first peak decreases as tungstate concentration increases. All sorption samples at pH 5.5 exhibit similar features in higher shells of the FT magnitude, while 1000 µM sample at pH 8 shows distinct higher shell compared to the 50 and 100 µM samples.

5.3.6 EXAFS fitting results for W-doped HAP

In fitting the EXAFS from the W-doped HAP, it was necessary to account for the likely substitution of tungstate in the tetrahedral phosphate site of HAP, the possible precipitation of $CaWO_4$ (with its tetrahedral coordination), and the contrasting XANES analysis indicating octahedral W(VI) coordination. Consequently, fitting was attempted using alternately tetrahedral and octahedral coordination for the two W-doped samples. Best fit results are shown in Figure 5 and summarized in Table 4. Fitting with tetrahedral coordination did not yield satisfactory results for either samples (700 and 1500 ppm W), even when constraining the CN to 4. Hence, we quickly ruled out tetrahedral coordination of W(VI), or any measureable fraction of it, in the W-doped HAP. As with the model compounds, all fits includes a MS path from a near-linear O-W-O chain. The 1500 ppm W-doped HAP was best fit with two W-O distances (1.77 and 2.13 $Å$) for the first peak with a total CN of 7.6 (± 1.5). The average W-O distance for the first shell is 1.97 $Å$, consistent with the XANES result indicating octahedral coordination. For fitting higher

shells, W-W paths were introduced in fitting, but we could not obtain any reasonable parameters. Instead, we attempted to use a single W-Ca path to fit the broad peak near 3.2 Å, under the assumption that tungstate replaced phosphate in the structure. This gave a Debye-Waller factor of 0.03 Å^2, which was considered unrealistically large. We found that the best fit was obtained using three W-Ca paths at 3.23, 3.43, and 3.61 Å with a summed CN of 9.4. The 700 ppm W-doped HAP was also fit with octahedral coordination for the first oxygen shell based on the XANES results. Two W-O distances (1.75 and 2.14 Å) were used to fit the first peak with a total CN 6.7 (± 1.5). Higher shells were fit with two W-Ca paths (3.34 and 3.57 Å). In both fitting results, the W-Ca distances are longer than P-Ca distances in the HAP structure.
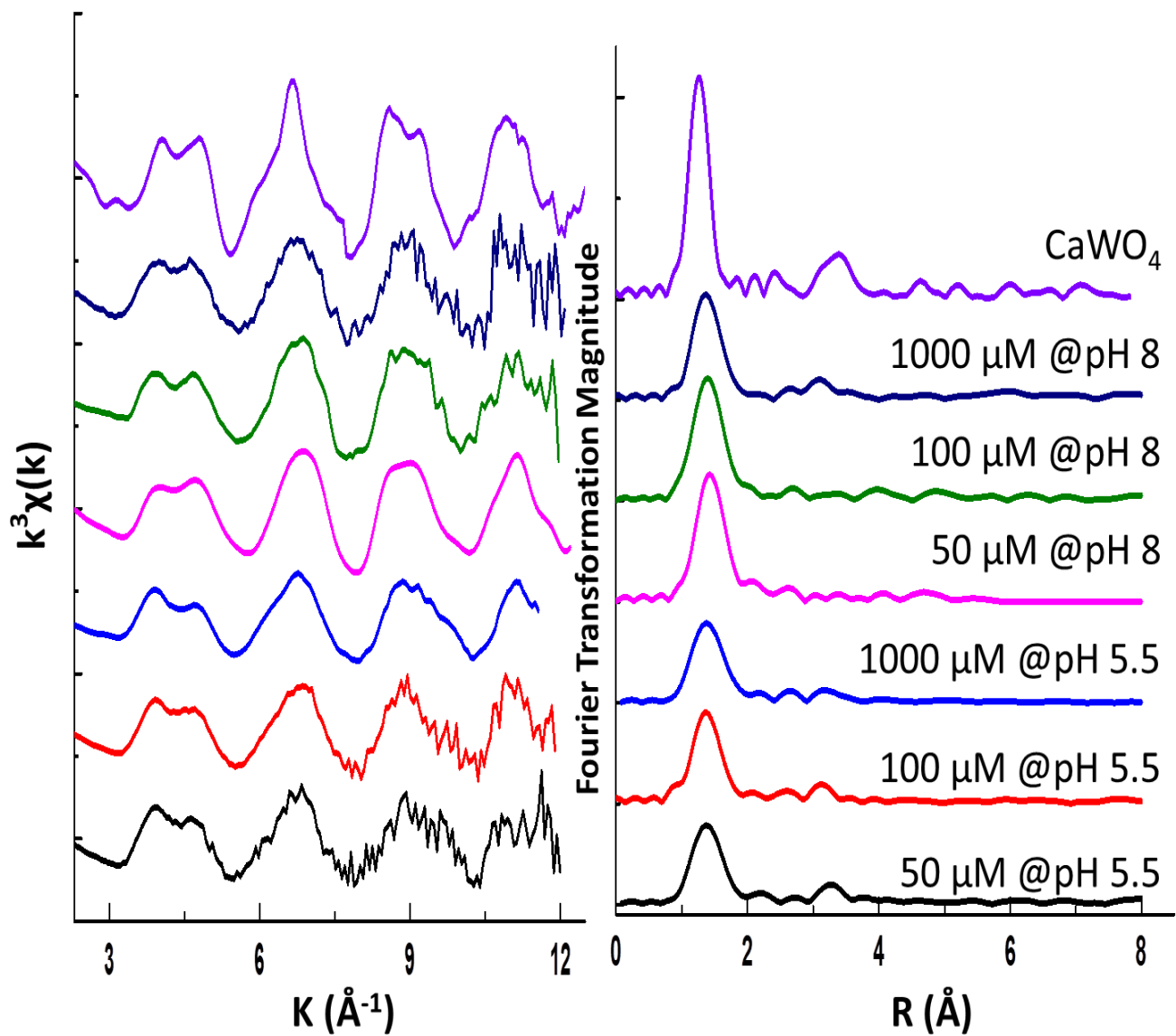
Figure 5. 6. W L_3-edge EXAFS results for $CaWO_4$ and sorption samples on HAP.

Table 5. 4 Summary of W L$_3$-edge EXAFS fitting results of two W-doped HAP samples

Sample	Path	CN[a]	R(Å)[b]	σ^2(Å^2)[c]	ΔE0
1500 ppm	W-O1	3.4	1.77	0.002	5.26
	W-O2	4.2	2.13	0.01*	
	W-Ca	2.4	3.23	0.008*	
	W-Ca	3.9	3.43	0.008*	
	W-Ca	3.1	3.61	0.008*	
700 ppm	W-O1	3.4	1.75	0.004	2
	W-O2	3.3	2.14	0.01*	
	W-Ca	2.0	3.34	0.008*	
	W-Ca	2.5	3.57	0.008*	

*: fixed in the fitting,

a : coordination number (±20%), b: distance in Å (±0.02 Å),

c : Debye-Waller factor,

5.4. Discussion

5.4.1 W doped HAP

Our present results provide new insight to interactions of dissolved tungstate with HAP for two conditions relevant for understanding its mobility in natural systems, with possible applications for remediation strategies. The sorption experiments are most relevant for solutions that are equilibrated with HAP, so that no net dissolution or precipitation of this phase is expected. In contrast, the coprecipitation experiments specifically relate to dynamic conditions where HAP is precipitating in the presence of dissolved tungstate. Our findings reveal some common aspects in the uptake mechanisms for these different conditions, but with distinctly different final states.

For the tungstate coprecipitation experiments, our EXAFS results indicate that tungstate substitutes in the phosphate site in the HAP structure. While this conclusion might be anticipated based on the many previous studies of oxyanion substitution for phosphate in HAP, it is complicated by the XANES and EXAFS fit results, both of which show that the W(VI) has octahedral coordination. The EXAFS fit for the first oxygen shell gives an average W-O distance of 1.96 A, consistent with octahedral geometry, and the second derivative XANES shows the two split minima that are distinctive of distorted octahedral coordination. Yet octahedral coordination for W(VI) is seemingly inconsistent with the tetrahedral coordination of phosphate. The EXAFS fit result for more distant shells indicates 5-9 Ca atoms at an average distance of 3.46 A. This distance is greater than the corresponding average P-Ca distance (3.35 A) in HAP, and is consistent with an overall expansion of the local environment around W(VI), which is presumably a strongly distorted site. Previous studies of As-doped HAP also reported longer As(or Se)-Ca distances.[18] The phosphate groups are surrounded by 9 Ca atoms in HAP. The fit results for the two W-doped HAP samples give different total coordination numbers W-Ca shells:

4.5 (± 0.9) and 9.4 (± 1.9) for 700 and 1500 ppm samples, respectively. Although the total CN values for W-Ca shell differ, the distances of the fitted Ca shells are nevertheless similar for both samples.

A significant finding is the coordination change of tungsten during coprecipitation with HAP, from tetrahedral (in solution) to octahedral (in HAP). This is unexpected since the dominant tungstate species in solution at the synthesis pH (8) is tetrahedral WO_4^{2-} , and the possible precipitate ($CaWO_4$), which did not form, is also tetrahedral. Although Ba_2NiWO_6 contains isolated tungstate octahedra, we are not aware of isolated tungstate octahedra in any other compounds that contain Ca and W without any other metal elements.

5.4.2 Tungstate sorption mechanism on HAP

The tungstate uptake behavior in the HAP-equilibrated suspensions shows a strong dependence on pH, with significantly great uptake at pH 5.5 compared to pH 8. This is consistent with the behavior typically observed for anion sorption. The tungstate isotherm at pH 5.5 showed a rapid increase in sorption as tungstate concentration increased, without any maximum being reached. This behavior is sometimes interpreted as indicating formation of tungstate precipitates. Moreover, the speciation calculations indicated the initial solutions were supersaturated with respect to $CaWO_4$ at this pH. Yet, the W L_3-edge XANES and EXAFS results are unlike those found for CaWO4, suggesting that it did not precipitate. The W L_3-edge XANES results, however, do indicate notable differences in sorption mechanism at pH 5.5 depending on tungstate concentration. The 50 µM sorption sample at pH 5.5 shows octahedral coordination of tungsten. The 100 and 1000 µM samples at pH 5.5 show distinctly different XANES second derivatives that are suggestive of a mixture of tetrahedral and octahedral coordination. The EXAFS results of sorption samples at pH 5.5 do not show any similarity to the $CaWO_4$ chi function. These limited observations would suggest that tungstate forms surface

complexes containing both octahedral and tetrahedral coordination. However, non-unique fits raise questions that will require further study.

The adsorption of tungstate on the HAP surface at pH 8 could be major sorption mechanism based on the results of XAS and isotherm experiments, while a $CaWO_4$ precipitate was expected by tungstate speciation calculation at pH 8. The PZC values of HAP reported in previous studies varies from pH 6.5 to 8.4.[24] Considering the $CaWO_4$ precipitation predicted by theoretical calculation results at higher tungstate concentration, much less tungstate uptake was observed at pH 8. Furthermore, XAS results indicate $CaWO_4$ was not formed on the surface or in the solution. XANES results suggest octahedral coordination of tungsten on the HAP surface, and EXAFS results for sorption samples at pH 8 do not show any similar features to $CaWO_4$. Therefore, tungstate uptake on the HAP surface at pH 8 can be attributed to the formation of octahedral surface complexes.

An important to question reaming is whether we can distinguish between W-doped into the HAP structure and tungstate sorbed at the surface. The combination of EXAFS and XAENS results would be useful to distinguish them at pH 5.5. However, we need to be careful to differentiate W-doped HAP from tungstate sorbed on the surface. Both W-doped HAP and tungstate sorbed on the surface at pH 8 contain W(VI) octahedral and exhibit broadly similar spectra in chi function, but small difference observed in second shell in FT magnitude. In FT magnitude, the trend toward a little shorter distance of the first shell (W-O) with higher tungstate concentrations is observed, whereas W-doped HAP show the same distance. Therefore, it would be useful to utilize complementary techniques as well as XAS to distinguish surface sorption and coprecipitation of tungstate with HAP.

5.5 Conclusion

A combination of XRD and XAS analyses were used to examine tungstate interaction with HAP for two environmentally relevant conditions: adsorption and coprecipitation. For tungstate coprecipitation into HAP, EXAFS fitting results show that an octahedral tungstate substitutes in the phosphate site. This is expected to be accompanied by local distortion owing to the large size and different coordination geometry compared to phosphate. The incorporation of trace elements into HAP and HAP-like minerals has a considerable influence the mechanical and physio-chemical properties of the crystals and significantly affects their reactivity and solubility.[12, 19] The impact of such a defect site on the properties of HAP is unknown and deserves further study.

In HAP-equilibrated suspensions, tungstate forms octahedral surface complexes at pH 8, whereas multiple coordination environments are observed at pH 5.5, including possible surface precipitation. Exact details of local structure of tungstate require further study. Overall, the findings indicate that tungstate has a high affinity for HAP at low pH, with decreasing affinity as pH increases. For certain environmental settings HAP may be useful in remediation strategies where dissolved tungstate is present. Further work is needed to address the effectiveness of HAP at higher pH conditions.

Reference

1. Koutsospyros, A.; Braida, W.; Christodoulatos, C.; Dermatas, D.; Strigul, N., A review of tungsten: From environmental obscurity to scrutiny. *J Hazard Mater* 2006, *136*, (1), 1-19.

2. Strigul, N., Does speciation matter for tungsten ecotoxicology? *Ecotox Environ Safe* 2010, *73*, (6), 1099-1113.

3. Clausen, J. L.; Bostick, B. C.; Bednar, A.; Sun, J.; Landis, J. D. *Tungsten Speciation in Firing Range Soils*; DTIC Document: 2011.

4. Mullen Jr, F., Scientists Say Tungsten a Promising Clue to Leukemia Cluster. The Reno Gazette Journal. In.

5. Rubin, C. S.; Holmes, A. K.; Belson, M. G.; Jones, R. L.; Flanders, W. D.; Kieszak, S. M.; Osterloh, J.; Luber, G. E.; Blount, B. C.; Barr, D. B.; Steinberg, K. K.; Satten, G. A.; McGeehin, M. A.; Todd, R. L., Investigating childhood leukemia in Churchill County, Nevada. *Environ Health Persp* 2007, *115*, (1), 151-157.

6. Johnson, D.; Inouye, L.; Bednar, A.; Clarke, J.; Winfield, L.; Boyd, R.; Ang, C.; Goss, J., Tungsten bioavailability and toxicity in sunflowers (Helianthus annuus L.). *Land Contamination & Reclamation* 2009, *17*, (1), 141-151.

7. Barre, T.; Arurault, L.; Sauvage, F. X., Chemical behavior of tungstate solutions. Part 1. A spectroscopic survey of the species involved. *Spectrochim Acta A* 2005, *61*, (4), 551-557.

8. Maczka, M.; Hanuza, J.; Waskowska, A., Vibrational studies of alkali metal hexatungstates. *J Raman Spectrosc* 2003, *34*, (6), 432-437.

9. Smith, B. J.; Patrick, V. A., Quantitative determination of sodium metatungstate speciation by W-183 NMR spectroscopy. *Aust J Chem* 2000, *53*, (11-12), 965-970.

10. Walanda, D. K.; Burns, R. C.; Lawrance, G. A.; von Nagy-Felsobuki, E. I., Electrospray mass spectrometry of aqueous solutions of isopolyoxotungstates. *J Clust Sci* 2000, *11*, (1), 5-28.

11. Jarcho, M., Calcium-Phosphate Ceramics as Hard Tissue Prosthetics. *Clin Orthop Relat R* 1981, (157), 259-278.

12. Pan, Y. M.; Fleet, M. E., Compositions of the apatite-group minerals: Substitution mechanisms and controlling factors. *Rev Mineral Geochem* 2002, *48*, 13-49.

13. Sutter, B.; Ming, D. W.; Clearfield, A.; Hossner, L. R., Mineralogical and chemical characterization of iron-, manganese-, and copper-containing synthetic hydroxyapatites. *Soil Sci Soc Am J* 2003, *67*, (6), 1935-1942.

14. Tang, Y. Z.; Chappell, H. F.; Dove, M. T.; Reeder, R. J.; Lee, Y. J., Zinc incorporation into hydroxylapatite. *Biomaterials* 2009, *30*, (15), 2864-2872.

15. Kreidler, E. R.; Hummel, F. A., The crystal chemistry of apatite: Structure fields of fluor- and chlorapatite. *Am Mineral* 1970, *55*, (1-2), 170-184.

16. Mason, H. E.; Kozlowski, A.; Phillips, B. L., Solid-state NMR study of the role of H and Na in AB-type carbonate hydroxylapatite. *Chem Mater* 2008, *20*, (1), 294-302.

17. Comodi, P.; Liu, Y.; Stoppa, F.; Woolley, A. R., A multi-method analysis of Si-, S- and REE-rich apatite from a new find of kalsilite-bearing leucitite (Abruzzi, Italy). *Mineral Mag* 1999, *63*, (5), 661-672.

18. Lee, Y. J., Spectroscopic investigation of arsenate and selenate incorporation into hydroxylapatite. *Curr Appl Phys* 2010, *10*, (1), 158-163.

19. Lee, Y. J.; Stephens, P. W.; Tang, Y.; Li, W.; Phillips, B. L.; Parise, J. B.; Reeder, R. J., Arsenate substitution in hydroxylapatite: Structural characterization of the Ca-5(PxAs1-xO4)(3)OH solid solution. *Am Mineral* 2009, *94*, (5-6), 666-675.

20. Zabinsky, S. I.; Rehr, J. J.; Ankudinov, A.; Albers, R. C.; Eller, M. J., Multiple-Scattering Calculations of X-Ray-Absorption Spectra. *Phys Rev B* 1995, *52*, (4), 2995-3009.

21. Sanchez, C.; Livage, J.; Launay, J. P.; Fournier, M., Electron Delocalization in Mixed-Valence Tungsten Polyanions. *J Am Chem Soc* 1983, *105*, (23), 6817-6823.

22. Liu, S. J.; Chen, Q. Y.; Zhang, P. M., Thermodynamic properties of Na2W2O7(s) and Na2W4O13(S) in the temperature range 298.15-1000 K. *Thermochim Acta* 2001, *371*, (1-2), 7-11.

23. Parkhurst, D. L., User's guide to PHREEQC: A computer program for speciation, reaction-path, advective-transport, and inverse geochemical calculations. 1995.

24. Lee, Y. J.; Elzinga, E. J.; Reeder, R. J., Sorption mechanisms of zinc on hydroxyapatite: Systematic uptake studies and EXAFS spectroscopy analysis. *Environ Sci Technol* 2005, *39*, (11), 4042-4048.

25.   Yamazoe, S.; Hitomi, Y.; Shishido, T.; Tanaka, T., XAFS Study of Tungsten L1-and L3-Edges: Structural Analysis of WO3 Species Loaded on TiO2 as a Catalyst for Photo-oxidation of NH3. *The Journal of Physical Chemistry C* 2008, *112*, (17), 6869-6879.

26.   Kashiwabara, T.; Takahashi, Y.; Marcus, M. A.; Uruga, T.; Tanida, H.; Terada, Y.; Usui, A., Tungsten species in natural ferromanganese oxides related to its different behavior from molybdenum in oxic ocean. *Geochim Cosmochim Ac* 2013, *106*, 364-378.

Chapter 6. Conclusions

Through this thesis, we have investigated the role of tungstate speciation on sorption onto various mineral surfaces, which are environmentally relevant. In this study, we first consider tungstate speciation in aqueous solution using reported stability constants of known tungstates, combined with XAS and ESI-MS. Tungstate favors to polymerize under acidic condition, while monotungstate is a major component at neutral and basic conditions.

Batch uptake experiments were carried out to investigate tungstate sorption behavior on mineral surfaces over a range of environmentally relevant conditions such as pH, tungstate concentration, and ionic strength. Tungstate showed strong affinity to the mineral surfaces, used in this study, and XAS results suggested various sorption mechanisms such as surface sorption accompanied polymerization (boehmite), intercalation (Co(II) treated boehmite and CoAl LDH), and coprecipitation (HAP).

In Chapter 2, tungstate sorption on the boehmite surface was investigated with systematic batch uptake studies and XAS. Tungstate has been shown to adsorb as polymeric complexes on the boehmite surface, even when monotungstate is the dominant solution species. The polymeric tungstates on the surface were inferred from the W-W distance at near 3.3 and 3.75 Å of typical the edge and corner sharing octahedra found in polytungstates at high tungstate concentration, while monomeric tungstate with octahedral coordination was suggested at low concentration both pH 4 and 8. We suggested the tungstate polymerization driven by the mineral surface, although the role of the mineral surface remains unclear.

179

We determined the effect of Co(II) present on the boehmite surface on tungstate sorption at near-neutral pH, where more mobile tungstate (monotungstate) exits, in Chapter 3. Sorption studies showed enhanced tungstate uptake is strongly related to the CoAl LDH formation on the bohemite surface. The intercalation mechanism for enhanced tungstate uptake at higher tungstate concentration was supported by desorption experiments and the XANES results. W L_3-edge EXAFS suggested the surface sorption of tungstate as a main mechanism at low tungstate concentration.

The interaction mechanism of tungstate on CoAl LDH was suggested for the tungstate uptake mechanism (Chapter 4). Batch uptake experiments at pH 8 revealed a large sorption capacity of CoAl LDH for tungstate. XRD results confirmed the expansion of the layer space with tungstate intercalation. This study suggest the possible application of CoAl LDH for tungstate removal form aqueous systems, although the exact tungstate spices in CoAl LDH could not be determined with W L_3-edge EXAFS.

For the long-term sequestration of tungstate from environmental systems, the coprecipitation of tungstate in HAP structure was investigated in Chapter 5. Phosphate sites in HAP were replaced with octahedral tungstate, confirmed with XAS results. W L3-edge EXAFS results revealed that tungstates form defects site, resulting in structural distortion in HAP. The effects of the defect sites created by tungstate substitution on the properties of HAP are unknown, and are needed further studies. Tungstate showed strong affinity for HAP at low pH, with decreasing affinity as pH increases. Further work in needed to evaluate the effectiveness of HAP at higher pH conditions.

This study finds that tungstate is effectively limited in aqueous systems by sorption reactions on mineral surfaces. However, the exact tungstate species on mineral surfaces are still remained unclear. Moreover, we lack an understanding the mechanisms of the surface-driven polymerization of tungstate and the coordination change of tungsten from tetrahedral (in solution at pH 8) to octahedra (on mineral surfaces or in structures). Further studies should be undertaken to understand tungstate mobility, toxicity, and bioavailability, which are strongly related to its spcies. This work will provide a foundation for subsequent studies of tungstate sorption on other solids as well as other oxyanion species, such as molybdates and vanadates, which show similar behavior in solution. The findings also have possible implications for tungsten toxicity in natural environments.

Chapter 7. References

[1]   ACGIH, Documentation 7th edition (2001).

[2]   M.T. Aide, M.F. Cummings, Soil Sci 162 (1997) 599.

[3]   A.L. Ankoudinov. Relativistic Spin-dependent X-ray Absorption Theory. University of Washington, 1996.

[4]   Y. Arai, Environ Sci Technol 44 (2010) 8491.

[5]   C. Ardau, F. Frau, E. Dore, P. Lattanzi, Appl Clay Sci 65-66 (2012) 128.

[6]   H. Aritani, T. Tanaka, T. Funabiki, S. Yoshida, K. Eda, N. Sotani, M. Kudo, S. Hasegawa, J Phys Chem-Us 100 (1996) 19495.

[7]   R. Arnek, Y. Sasaki, Acta Chem Scand A A 28 (1974) 20.

[8]   J. Aveston, Inorg Chem 3 (1964) 981.

[9]   J.C. Bailar, A.F. Trotman-Dickenson, Comprehensive inorganic chemistry. Pergamon Press, 1973.

[10]   S.R. Bare, G.E. Mitchell, J.J. Maj, G.E. Vrieland, J.L. Gland, J Phys Chem-Us 97 (1993) 6048.

[11]   T. Barre, L. Arurault, F.X. Sauvage, Spectrochim Acta A 61 (2005) 551.

[12]   N.J. Barrow, J.W. Bowden, A.M. Posner, J.P. Quirk, Aust J Soil Res 18 (1980) 395.

[13]   A. Bednar, J.L. Clausen, J. Sun, B.C. Bostick, J.D. Landis, in: (Ed.)^(Eds.); ENGINEER RESEARCH AND DEVELOPMENT CENTER HANOVER NH, 2011.

[14]   A. Bednar, R. Kirgan, D. Johnson, A. Russell, C. Hayes, C. McGrath, Land Contamination & Reclamation 17 (2009) 129.

[15]   A.J. Bednar, R.E. Boyd, W.T. Jones, C.J. McGrath, D.R. Johnson, M.A. Chappell, D.B. Ringelberg, Chemosphere 75 (2009) 1049.

[16]   A.J. Bednar, W.T. Jones, R.E. Boyd, D.B. Ringelberg, S.L. Larson, J Environ Qual 37 (2008) 229.

[17]   E.J. Boyle-Wight, L.E. Katz, K.F. Hayes, Environ Sci Technol 36 (2002) 1212.

[18]   E.J. Boyle-Wight, L.E. Katz, K.F. Hayes, Environ Sci Technol 36 (2002) 1219.

[19]   V. Briois, P. Sainctavit, G.J. Long, F. Grandjean, Inorg Chem 40 (2001) 912.

[20]   A. Butler, V. Medina, S. Larson, C. Nestler, Land Contamination & Reclamation 17 (2009) 153.

[21]   G.G. Carbajal Arizaga, K.G. Satyanarayana, F. Wypych, Solid State Ionics 178 (2007) 1143.

[22]   X. Carrier, E. Marceau, H. Carabineiro, V. Rodriguez-Gonzalez, M. Che, Phys Chem Chem Phys 11 (2009) 7527.

[23]   W.H. Casey, Chem Rev 106 (2006) 1.

[24]   F. Cavani, Catal Today 41 (1998) 73.

[25]   F. Cavani, F. Trifiro, A. Vaccari, Catal Today 11 (1991) 173.

[26]   F. Cavani, F. Trifirò, A. Vaccari, Catal Today 11 (1991) 173.

[27]   M. Che, K. Mori, H. Yamashita, P Roy Soc a-Math Phy 468 (2012) 2113.

[28]   Y.G. Chen, J. Gong, L.Y. Qu, Coordin Chem Rev 248 (2004) 245.

[29]   C.J. Chisholmbrause, P.A. Oday, G.E. Brown, G.A. Parks, Nature 348 (1990) 528.

[30]   M.C. Ciardelli, H.F. Xu, N. Sahai, Water Res 42 (2008) 615.

[31]   C.E. Ciocan, E. Dumitriu, T. Cacciaguerra, F. Fajula, V. Hulea, Catal Today 198 (2012) 239.

[32]   J.L. Clausen, N. Korte, Sci Total Environ 407 (2009) 2887.

[33]   P. Comodi, Y. Liu, F. Stoppa, A.R. Woolley, Mineralogical Magazine 63 (1999) 661.

[34]   J.J. Cruywagen, Adv Inorg Chem 49 (2000) 127.

[35]   J.J. Cruywagen, I.F.J. Vandermerwe, J Chem Soc Dalton (1987) 1701.

[36]   J.B.D. Delacaillerie, M. Kermarec, O. Clause, Journal of the American Chemical Society 117 (1995) 11471.

[37]   D. Dermatas, W. Braida, C. Christodoulatos, N. Strigul, N. Panikov, M. Los, S. Larson, Environ Forensics 5 (2004) 5.

[38]   J.L. Domingo, Biol Trace Elem Res 88 (2002) 97.

[39]   E.J. Elzinga, R. Kretzschmar, Geochim Cosmochim Ac 117 (2013) 53.

[40]   D.G. Evans, D.A. Xue, Chem Commun (2006) 485.

[41]   J. Evans, J.F.W. Mosselmans, J Phys Chem-Us 95 (1991) 9673.

[42]   J. Evans, M. Pillinger, J.J. Zhang, J Chem Soc Dalton (1996) 2963.

[43]   J.W. Fellowes, R.A.D. Pattrick, J.R. Lloyd, J.M. Charnock, V.S. Coker, J.F.W. Mosselmans, T.C. Weng, C.I. Pearce, Nanotechnology 24 (2013).

[44]   L. Feng, X. Duan, Struct Bond 119 (2006) 193.

[45]   O.P. Ferreira, S.G. de Moraes, N. Duran, L. Cornejo, O.L. Alves, Chemosphere 62 (2006) 80.

[46]   J. Fierro, Metal Oxides: chemistry and applications. CRC press, 2006.

[47]   G. Furrer, B.L. Phillips, K.U. Ulrich, R. Pothig, W.H. Casey, Science 297 (2002) 2245.

[48]   H. Gecol, E. Ergican, P. Miakatsindila, J Colloid Interf Sci 292 (2005) 344.

[49]   G.N. George, W.E. Cleland, J.H. Enemark, B.E. Smith, C.A. Kipke, S.A. Roberts, S.P. Cramer, Journal of the American Chemical Society 112 (1990) 2541.

[50]   K.H. Goh, T.T. Lim, Z. Dong, Water Res 42 (2008) 1343.

[51]   M. Grafe, D.L. Sparks, Geochim Cosmochim Ac 69 (2005) 4573.

[52]   F. Granados-Correa, J. Jimenez-Becerril, J Hazard Mater 162 (2009) 1178.

[53]   J.P. Gustafsson, Chem Geol 200 (2003) 105.

[54]   J.J. Hastings, O.W. Howarth, J Chem Soc Dalton (1992) 209.

[55]   F. Hilbrig, H.E. Gobel, H. Knozinger, H. Schmelz, B. Lengeler, J Phys Chem-Us 95 (1991) 6973.

[56]   S. Himeno, M. Takamoto, T. Ueda, B Chem Soc Jpn 78 (2005) 1463.

[57]   K. Hollenstein, M. Comellas-Bigler, L.E. Bevers, M.C. Feiters, W. Meyer-Klaucke, P.L. Hagedoorn, K.P. Locher, J Biol Inorg Chem 14 (2009) 663.

[58]   J.A. Horsley, Abstr Pap Am Chem S 191 (1986) 167.

[59]   J.A. Horsley, Abstr Pap Am Chem S 191 (1986) 167.

[60]   J.A. Horsley, I.E. Wachs, J.M. Brown, G.H. Via, F.D. Hardcastle, J Phys Chem-Us 91 (1987) 4014.

[61]   J.M. Hughes, J. Rakovan, Rev Mineral Geochem 48 (2002) 1.

[62]   M. Jarcho, Clin Orthop Relat R (1981) 259.

[63]   M. Jelikic-Stankov, S. Uskokovic-Markovic, I. Holclajtner-Antunovic, M. Todorovic, P. Djurdjevic, J Trace Elem Med Bio 21 (2007) 8.

[64]   Y.F. Jia, L.Y. Xu, Z. Fang, G.P. Demopoulos, Environ Sci Technol 40 (2006) 3248.

[65]   D. Johnson, L. Inouye, A. Bednar, J. Clarke, L. Winfield, R. Boyd, C. Ang, J. Goss, Land Contamination & Reclamation 17 (2009) 141.

[66]   M.J. Kang, K.S. Chun, S.W. Rhee, Y. Do, Radiochim Acta 85 (1999) 57.

[67]   M. Karki, H. Araujo, J. Magolan, Abstr Pap Am Chem S 244 (2012).

[68] T. Kashiwabara, Y. Takahashi, M.A. Marcus, T. Uruga, H. Tanida, Y. Terada, A. Usui, Geochim Cosmochim Ac 106 (2013) 364.

[69] T. Kashiwabara, Y. Takahashi, M. Tanimizu, A. Usui, Geochim Cosmochim Ac 75 (2011) 5762.

[70] L.E. Katz, K.F. Hayes, J Colloid Interf Sci 170 (1995) 491.

[71] L.S. Keith, D.B. Moffett, Z.A. Rosemond, D.W. Wohlers, Toxicol Ind Health 23 (2007) 347.

[72] S. Kelly, D. Hesterberg, B. Ravel, Methods of soil analysis. Part 5 (2008) 387.

[73] A.I. Khan, D. O'Hare, J Mater Chem 12 (2002) 3191.

[74] D. Koningsberger, R. Prins, (1988).

[75] D. Koningsberger, R. Prins, (1988).

[76] A. Koutsospyros, W. Braida, C. Christodoulatos, D. Dermatas, N. Strigul, J Hazard Mater 136 (2006) 1.

[77] E.R. Kreidler, F.A. Hummel, Am Mineral 55 (1970) 170.

[78] A. Kuzmin, J. Purans, Radiat Meas 33 (2001) 583.

[79] A. Kuzmin, J. Purans, M. Benfatto, C.R. Natoli, Phys Rev B 47 (1993) 2480.

[80] F. Lagarde, M. Leroy, Met Ions Biol Syst 39 (2002) 741.

[81] E. Lassner, W.-D. Schubert, Tungsten: properties, chemistry, technology of the elements, alloys, and chemical compounds. Springer, 1999.

[82] E.J. Lede, F.G. Requejo, B. Pawelec, J.L.G. Fierro, J Phys Chem B 106 (2002) 7824.

[83] Y.J. Lee, Curr Appl Phys 10 (2010) 158.

[84] Y.J. Lee, E.J. Elzinga, R.J. Reeder, Environ Sci Technol 39 (2005) 4042.

[85] Y.J. Lee, P.W. Stephens, Y. Tang, W. Li, B.L. Phillips, J.B. Parise, R.J. Reeder, Am Mineral 94 (2009) 666.

[86] A. Ler, R. Stanforth, Environ Sci Technol 37 (2003) 2694.

[87] W. Li, J. Feng, K.D. Kwon, J.D. Kubicki, B.L. Phillips, Langmuir 26 (2010) 4753.

[88] W. Li, X.H. Feng, Y.P. Yan, D.L. Sparks, B.L. Phillips, Environ Sci Technol 47 (2013) 8308.

[89] W. Li, W.Q. Xu, J.B. Parise, B.L. Phillips, Geochim Cosmochim Ac 85 (2012) 289.

[90] W. Li, S.Z. Zhang, X.Q. Shan, Colloid Surface A 293 (2007) 13.

[91] M. Liu, J.J. Yang, G.Q. Wu, L.Y. Wang, Chinese J Inorg Chem 22 (2006) 1771.

[92] S.J. Liu, Q.Y. Chen, P.M. Zhang, Thermochim Acta 371 (2001) 7.

[93] E. Lopezsalinas, Y. Ono, Microporous Mater 1 (1993) 33.

[94] L. Lv, J. He, M. Wei, D.G. Evans, X. Duan, J Hazard Mater 133 (2006) 119.

[95] L.A. Lv, J. He, M. Wei, D.G. Evans, X. Duan, Water Res 40 (2006) 735.

[96] A.L. Maciuca, C.E. Ciocan, E. Dumitriu, F. Fajula, V. Hulea, Catal Today 138 (2008) 33.

[97] M. Maczka, J. Hanuza, A. Waskowska, J Raman Spectrosc 34 (2003) 432.

[98] T. Mahmood, S.U. Din, A. Naeem, S. Mustafa, M. Waseem, M. Hamayun, Chem Eng J 192 (2012) 90.

[99] N.M. Markovic, T.J. Schmidt, B.N. Grgur, H.A. Gasteiger, R.J. Behm, P.N. Ross, J Phys Chem B 103 (1999) 8568.

[100] H.E. Mason, A. Kozlowski, B.L. Phillips, Chemistry of Materials 20 (2008) 294.

[101] J.A. Meima, R.N.J. Comans, Environ Sci Technol 32 (1998) 688.

[102] C.T.J. Mensch, J.A.R. Vanveen, B. Vanwingerden, M.P. Vandijk, J Phys Chem-Us 92 (1988) 4961.

[103] L. Mohapatra, K. Parida, M. Satpathy, J Phys Chem C 116 (2012) 13063.

[104] F. Mullen Jr, in: (Ed.)^(Eds.).
[105] S. Mustafa, M.I. Zaman, R. Gul, S. Khan, Sep Purif Technol 59 (2008) 108.
[106] W.A. Neiwert, J.J. Cowan, K.I. Hardcastle, C.L. Hill, I.A. Weinstock, Inorg Chem 41 (2002) 6950.
[107] M. Newville, J Synchrotron Radiat 8 (2001) 322.
[108] NIOSH, Publication No. 77-127 (1997).
[109] J. Nordin, P. Persson, E. Laiti, S. Sjoberg, Langmuir 13 (1997) 4085.
[110] J.P. Nordin, D.J. Sullivan, B.L. Phillips, W.H. Casey, Geochim Cosmochim Ac 63 (1999) 3513.
[111] P.A. Oday, G.E. Brown, G.A. Parks, J Colloid Interf Sci 165 (1994) 269.
[112] C.A. Ohlin, Chem-Asian J 7 (2012) 262.
[113] T. Okuhara, N. Mizuno, M. Misono, Appl Catal a-Gen 222 (2001) 63.
[114] K. Osseoasare, Jom-J Min Met Mat S 32 (1980) 75.
[115] Y. Pan, M.E. Fleet, Reviews in Mineralogy and Geochemistry 48 (2002) 13.
[116] Y.M. Pan, M.E. Fleet, Rev Mineral Geochem 48 (2002) 13.
[117] C. Papelis, Abstr Pap Am Chem S 209 (1995) 153.
[118] C. Papelis, K.F. Hayes, Colloid Surface A 107 (1996) 89.
[119] M.J. Pardus, J.K. Sueker, T.E. Gass, Abstr Pap Am Chem S 230 (2005) U1730.
[120] D.L. Parkhurst, (1995).
[121] G.Y. Peng, J.F. Luhr, J.J. McGee, Am Mineral 82 (1997) 1210.
[122] J.E. Penner-Hahn, eLS (2004).
[123] J. Perez-Ramirez, G. Mul, F. Kapteijn, J.A. Moulijn, J Mater Chem 11 (2001) 821.
[124] P. Persson, G.A. Parks, G.E. Brown, Langmuir 11 (1995) 3782.
[125] F. Pertlik, Monatshefte für Chemie/Chemical Monthly 130 (1999) 1083.
[126] F.J. Peryea, J.A. Kittrick, Clay Clay Miner 36 (1988) 391.
[127] M.T. Pope, Y. Jeannin, M. Fournier, Heteropoly and isopoly oxometalates. Springer-Verlag Berlin, 1983.
[128] M.T. Pope, A. Muller, Angew Chem Int Edit 30 (1991) 34.
[129] S.V. Prasanna, P.V. Kamath, J Colloid Interf Sci 331 (2009) 439.
[130] R. Radhakrishnan, C. Reed, S.T. Oyama, M. Seman, J.N. Kondo, K. Domen, Y. Ohminami, K. Asakura, J Phys Chem B 105 (2001) 8519.
[131] J. Rakovan, R.J. Reeder, Am Mineral 79 (1994) 892.
[132] A.F. Redkin, G.V. Bondarenko, J Solution Chem 39 (2010) 1549.
[133] J.J. Rehr, R.C. Albers, Rev Mod Phys 72 (2000) 621.
[134] T. Ressler, J Phys Iv 7 (1997) 269.
[135] T. Ressler, Le Journal de Physique IV 7 (1997) C2.
[136] T. Ressler, J Synchrotron Radiat 5 (1998) 118.
[137] J.T. Rhule, C.L. Hill, D.A. Judd, Chem Rev 98 (1998) 327.
[138] D.B. Ringelberg, C.M. Reynolds, L.E. Winfield, L.S. Inouye, D.R. Johnson, A.J. Bednar, J Environ Qual 38 (2009) 103.
[139] C.L. Rollinson, The chemistry of chromium, molybdenum and tungsten. Pergamon Press, 1975.
[140] G.M. Rozantsev, O.I. Sazonova, Russ J Coord Chem+ 31 (2005) 552.
[141] C.S. Rubin, A.K. Holmes, M.G. Belson, R.L. Jones, W.D. Flanders, S.M. Kieszak, J. Osterloh, G.E. Luber, B.C. Blount, D.B. Barr, K.K. Steinberg, G.A. Satten, M.A. McGeehin, R.L. Todd, Environ Health Persp 115 (2007) 151.

[142] N. Sahai, Y.J. Lee, H.F. Xu, M. Ciardelli, J.F. Gaillard, Geochim Cosmochim Ac 71 (2007) 3193.
[143] C. Sanchez, J. Livage, J.P. Launay, M. Fournier, Journal of the American Chemical Society 105 (1983) 6817.
[144] D.E. Sayers, E.A. Stern, F.W. Lytle, Physical Review Letters 27 (1971) 1204.
[145] K.G. Scheckel, A.C. Scheinost, R.G. Ford, D.L. Sparks, Geochim Cosmochim Ac 64 (2000) 2727.
[146] A.M. Scheidegger, G.M. Lamble, D.L. Sparks, J Colloid Interf Sci 186 (1997) 118.
[147] C.V. Schenck, J.G. Dillard, J.W. Murray, J Colloid Interf Sci 95 (1983) 398.
[148] R.L. Seiler, K.G. Stollenwerk, J.R. Garbarino, Appl Geochem 20 (2005) 423.
[149] Sheppard, Environ Health Persp 120 (2012) A57.
[150] P.R. Sheppard, G. Ridenour, R.J. Speakman, M.L. Witten, Appl Geochem 21 (2006) 152.
[151] P.R. Sheppard, R.J. Speakman, G. Ridenour, M.L. Witten, Environ Health Persp 115 (2007) 715.
[152] B.J. Smith, V.A. Patrick, Aust J Chem 53 (2000) 965.
[153] I.K. Song, R.B. Shnitser, J.J. Cowan, C.L. Hill, M.A. Barteau, Inorg Chem 41 (2002) 1292.
[154] N. Spanos, J Catal 183 (1999) 400.
[155] N. Spanos, J Phys Chem B 103 (1999) 1890.
[156] D.L. Sparks, Environmental soil chemistry. Academic press, 2003.
[157] E. Stern, Contemporary Physics 19 (1978) 289.
[158] E. Stern, S. Heald, Handbook of synchrotron radiation 1 (1983).
[159] T.J. Strathmann, S.C.B. Myneni, Environ Sci Technol 39 (2005) 4027.
[160] N. Strigul, Ecotox Environ Safe 73 (2010) 1099.
[161] N. Strigul, C. Galdun, L. Vaccari, T. Ryan, W. Braida, C. Christodoulatos, Desalination 248 (2009) 869.
[162] N. Strigul, A. Koutsospyros, P. Arienti, C. Christodoulatos, D. Dermatas, W. Braida, Chemosphere 61 (2005) 248.
[163] N. Strigul, A. Koutsospyros, C. Christodoulatos, Ecotox Environ Safe 73 (2010) 164.
[164] N. Strigul, A. Koutsospyros, C. Christodoulatos, Ecotox Environ Safe 73 (2010) 164.
[165] T.Z. Su, X.H. Guan, G.W. Gu, J.M. Wang, J Colloid Interf Sci 326 (2008) 347.
[166] S. Sugiyama, Y. Kanda, H. Ishizuka, K.I. Sotowa, J Colloid Interf Sci 320 (2008) 535.
[167] B. Sutter, D.W. Ming, A. Clearfield, L.R. Hossner, Soil Sci Soc Am J 67 (2003) 1935.
[168] Y. Tajima, Biol Pharm Bull 24 (2001) 1079.
[169] Y. TAJIMA, Biomedical research 24 (2003) 39.
[170] Y. Tajima, Microbiol Immunol 47 (2003) 207.
[171] Y. Tajima, H. Amagai, N. Okamura, Thromb Res 55 (1989) 329.
[172] Y. Tajima, Z. Nagasawa, J. Tadano, Microbiol Immunol 37 (1993) 695.
[173] Y. Tajima, Z. Nagasawa, I. Tanabe, K. Kusaba, J. Tadano, Microbiol Immunol 38 (1994) 639.
[174] Y. Tajima, Z. Nagasawa, I. Tanabe, K. Kusaba, J. Tadano, Res Microbiol 147 (1996) 279.
[175] S. Takenaka, T. Tanaka, T. Funabiki, S. Yoshida, J Phys Chem B 102 (1998) 2960.
[176] Y.Z. Tang, H.F. Chappell, M.T. Dove, R.J. Reeder, Y.J. Lee, Biomaterials 30 (2009) 2864.
[177] Y.Z. Tang, J. McDonald, R.J. Reeder, Environ Sci Technol 43 (2009) 4452.

[178] Y.Z. Tang, R.J. Reeder, Environ Sci Technol 43 (2009) 4446.

[179] Y.Z. Tang, R.J. Reeder, Geochim Cosmochim Ac 73 (2009) 2727.

[180] R.W. Taylor, W.F. Bleam, T.D. Ranatunga, C.P. Schulthess, Z.N. Senwo, D.R.A. Ranatunga, Environ Sci Technol 43 (2009) 711.

[181] B.-K. Teo, P. Lee, Journal of the American Chemical Society 101 (1979) 2815.

[182] E. Tombacz, A. Dobos, M. Szekeres, H.D. Narres, E. Klumpp, I. Dekany, Colloid Polym Sci 278 (2000) 337.

[183] T. Toraishi, I. Farkas, Z. Szabo, I. Grenthe, J Chem Soc Dalton (2002) 3805.

[184] T. Toraishi, S. Nagasaki, S. Tanaka, Appl Clay Sci 22 (2002) 17.

[185] T. Toraishi, S. Nagasaki, S. Tanaka, Radiochim Acta 90 (2002) 671.

[186] S.N. Towle, J.R. Bargar, G.E. Brown, G.A. Parks, J Colloid Interf Sci 187 (1997) 62.

[187] G.B. van der Voet, T.I. Todorov, J.A. Centeno, W. Jonas, J. Ives, F.G. Mullick, Mil Med 172 (2007) 1002.

[188] J.W. Vanput, Int J Refract Met H 13 (1995) 61.

[189] C. Vaysse, L. Guerlou-Demourgues, A. Demourgues, C. Delmas, J Solid State Chem 167 (2002) 59.

[190] C. Vaysse, L. Guerlou-Demourgues, A. Demourgues, F. Lazartigues, D. Fertier, C. Delmas, J Mater Chem 12 (2002) 1035.

[191] D.K. Walanda, R.C. Burns, G.A. Lawrance, E.I. von Nagy-Felsobuki, J Clust Sci 11 (2000) 5.

[192] K.J. Wang, B.S. Xing, Chemosphere 48 (2002) 665.

[193] K.J. Wang, B.S. Xing, Environ Pollut 127 (2004) 13.

[194] S.L. Wang, R.J. Hseu, R.R. Chang, P.N. Chiang, J.H. Chen, Y.M. Tzou, Colloid Surface A 277 (2006) 8.

[195] L.E. Wasylenki, C.L. Weeks, J.R. Bargar, T.G. Spiro, J.R. Hein, A.D. Anbar, Geochim Cosmochim Ac 75 (2011) 5019.

[196] B.M. Weckhuysen, I.E. Wachs, R.A. Schoonheydt, Chem Rev 96 (1996) 3327.

[197] A.H. Welch, Z. Szabo, D.L. Parkhurst, P.C. VanMetre, A.H. Mullin, Appl Geochem 10 (1995) 491.

[198] G.R. Williams, A.J. Norquist, D. O'Hare, Chem Commun (2003) 1816.

[199] N. Xu, C. Christodoulatos, W. Braida, Chemosphere 64 (2006) 1325.

[200] S. Yamazoe, Y. Hitomi, T. Shishido, T. Tanaka, J Phys Chem C 112 (2008) 6869.

[201] S. Yamazoe, Y. Hitomi, T. Shishido, T. Tanaka, The Journal of Physical Chemistry C 112 (2008) 6869.

[202] L. Yang, M. Dadwhal, Z. Shahrivari, M. Ostwal, P.K.T. Liu, M. Sahimi, T.T. Tsotsis, Ind Eng Chem Res 45 (2006) 4742.

[203] L. Yang, Z. Shahrivari, P.K.T. Liu, M. Sahimi, T.T. Tsotsis, Ind Eng Chem Res 44 (2005) 6804.

[204] J. Yano, V.K. Yachandra, Photosynth Res 102 (2009) 241.

[205] S.J. Yoon, P.A. Helmke, J.E. Amonette, W.F. Bleam, Langmuir 18 (2002) 10128.

[206] S.I. Zabinsky, J.J. Rehr, A. Ankudinov, R.C. Albers, M.J. Eller, Phys Rev B 52 (1995) 2995.

[207] M. Zhang, E.J. Reardon, Environ Sci Technol 37 (2003) 2947.

Appendix

EXAFS spectra for tungsten model compounds

XAS data were collected for several tungstate-containing model compounds, which were chosen to represent a range of W(VI) coordination environments, including isolated tetrahedra and octahedra and polymeric forms. The detailed structures of these model compounds were described in section 1.4.6 and shown in Figure 1.11 (Chapter 1). $Na_2WO_4 \cdot 2H_2O$ and $CaWO_4$ contain isolated W(VI) tetrahedra, whereas Ba_2NiWO_6 contains isolated W(VI) octahedra. Polymeric tungstate reference compounds include $Na_2W_2O_7$ (tetrahedra and octahedra), WO_3, TBA-W_6O_{19}, sodium metatungstate, and phosphotungstic acid. Each model compound is distinctive in its chi function. Multiple scattering (MS) paths were introduced to fit the splitting of the first oscillation in the chi function for all model compounds. On this basis, MS paths were also used in fitting the W L_3-edge EXAFS data of sorption samples (Figure A1, left). The model compounds with distorted W(VI) octahedra such as phosphotungstic acid, TBA-W_6O_{19}, sodium metatungstate, and WO_3, showed a broad or split first peak in the FT magnitudes (Figure A1, right). The peaks in the range 3.3-3.8 Å in the FT magnitudes are consistent with edge- and corner-sharing of tungstate octahedra, and confirmed by fitting reference compounds. These peaks were used to distinguish monomeric and polymeric tungstates for sorption samples on the boehmite surface.
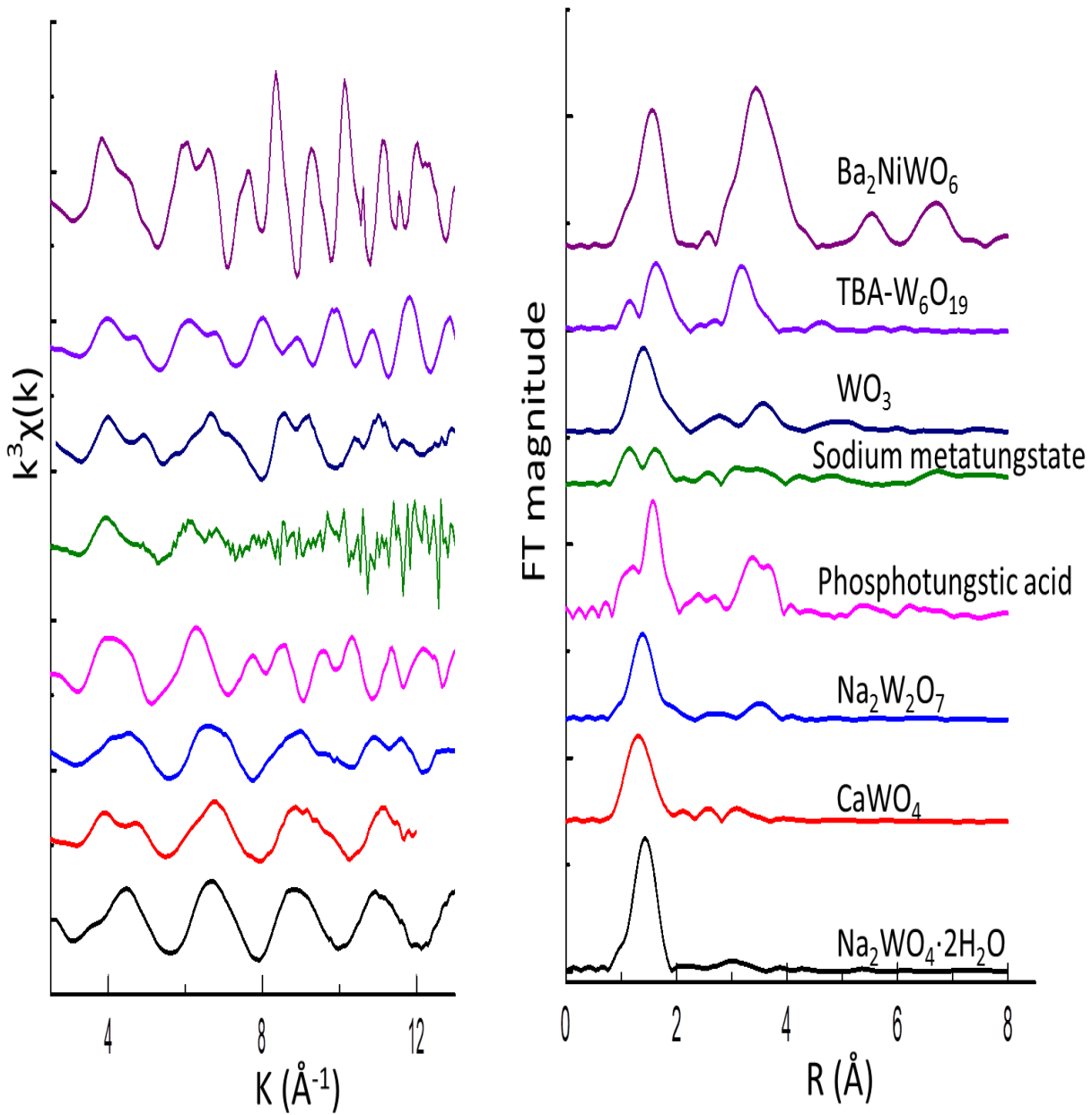
Figure A1. Tungsten L_3-edge EXAFS chi functions (left) and corresponding Fourier transform magnitudes (right, not corrected for phase shifts) for selected model compounds.

Tungsten L$_1$-edge XANES spectra for model compounds

The pre-edge feature in W L$_1$-edge XANES is senstive to the local symmetry and the geometry of W in the structures. The electron transition from a 2s→ 5d is dipole-forbidden for regular octahedral symmetry. However, it is partially allowed for a distorted octahedral structure, which gives rise to the absence of an inversion symmetry because the p orbitals are mixed with 5d orbitals. Simplified tungstate structures and corresponding XANES spectra are shown in Figure A2. Tungsten tetrahedra, as in $Na_2WO_4 \cdot 2H_2O$ and $CaWO_4$, exhibit large pre-edge areas in W L$_1$-edge XANES, while tungsten octahedra, including WO_3, $FeWO_4$, and Ba_2NiWO_6, show weak features in the pre-edge region depending on the degree of distortion.
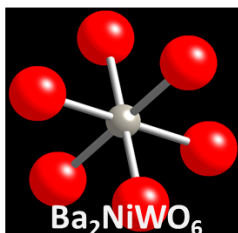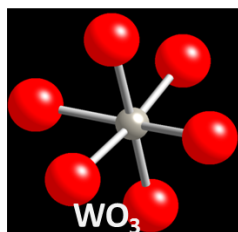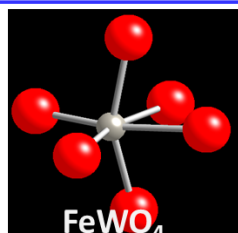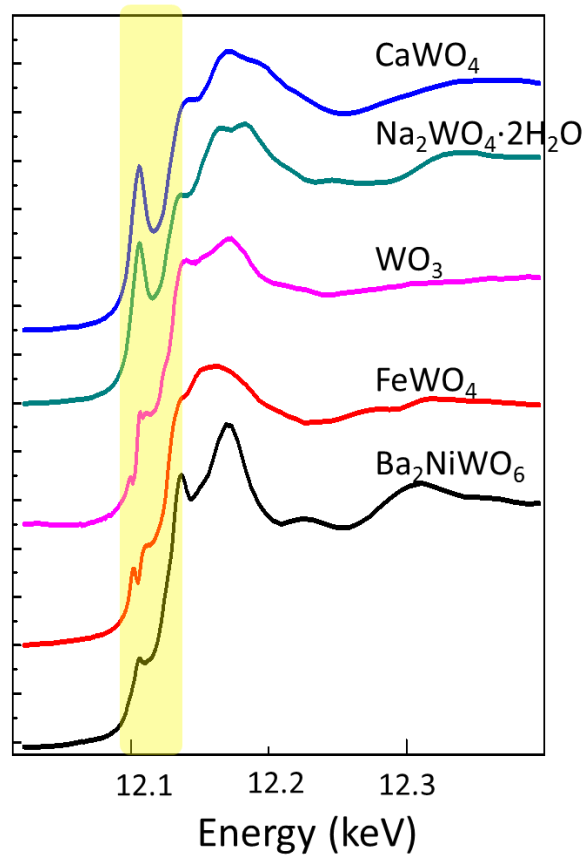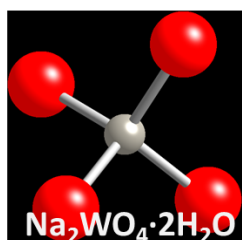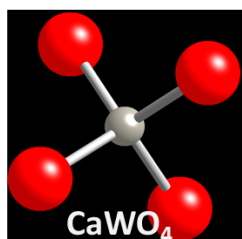
Figure A2. W L$_1$-edge XANES spectra for selected model compounds (right). Panels at left show simplified tungsten structures in reference compounds. Model compounds with octahedral coordination exhibit different pre-edge features depending on the degree of the distortion.

Tungsten L$_3$-edge XANES spectra for model compounds

The L$_3$-edge white lines, caused by the 2p → 5d transition, reflect the electronic states of the vacant d orbitals of the W atom. The splitting of the white lines depends on the symmetry of the W unit because the splitting corresponds to ligand field splitting of the d orbitals. Therefore, W L$_3$-edge XANES provides direct structural information for W units via splitting of the white line. Figure A3 shows XANES (left) and the corresponding second derivative spectra (right) for selected model compounds. Na$_2$WO$_4$·2H$_2$O and CaWO$_4$ with tetrahedral coordination show a single minimum value in second derivatives. Reference compounds with W(VI) octahedra show broader white line in W L$_3$-edge XANES, and corresponding second derivative spectra exhibit two minima. The energy gap between two minima is dependent on the degree of octahedral distortion. Ba$_2$NiWO$_6$, with perfect octahedral symmetry around W(VI), shows the greatest energy gap (4.5 eV).
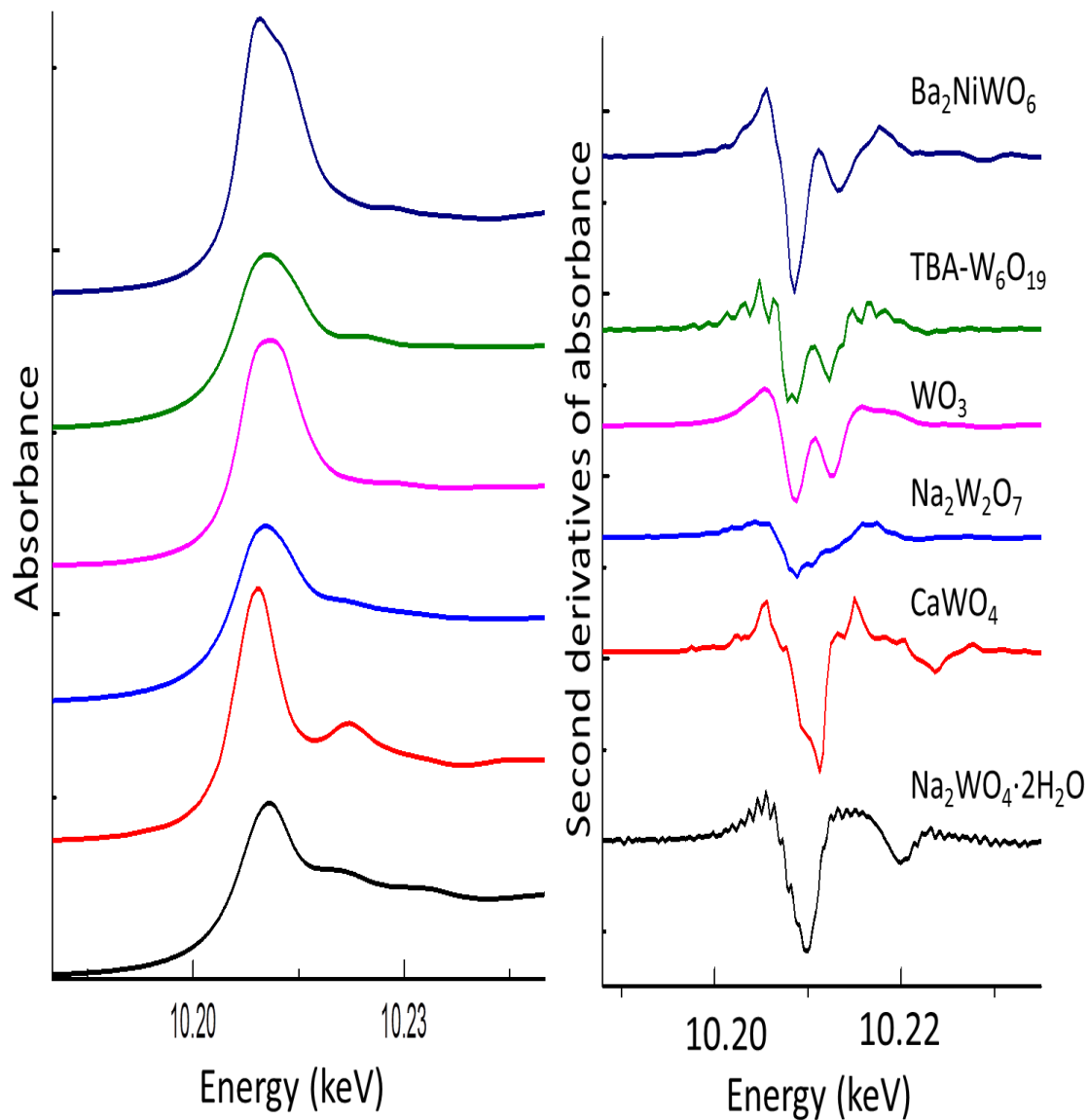
Figure A3. XANES (left) and second derivative spectra of W L_3-edge XANES (right) for selected model compounds showing differences that distinguish tetrahedral and octahedral coordination of W(VI).